A THESIS

FOR THE DEGREE OF MASTER OF SCIENCE

Molecular dissection of Cystatin B and C from big-belly seahorse and Cyclooxygenase 2 from red-spotted grouper reveals their implications in host immune defense mechanisms

Ms. KODAGODA YASARA KAVINDI

DEPARTMENT OF MARINE LIFE SCIENCES
GRADUATE SCHOOL
JEJU NATIONAL UNIVERSITY
REPUBLIC OF KOREA

FEBRUARY 2023

Molecular dissection of Cystatin B and C from big-belly seahorse and Cyclooxygenase 2 from red-spotted grouper reveals their implications in host immune defense mechanisms

Miss. Kodagoda Yasara Kavindi
(Supervised by Professor Jehee Lee)

A thesis submitted in partial fulfillment of the requirement for the degree of

MASTER OF SCIENCE

February 2023

This thesis has been examined and approved by

…….

Thesis Director, **Chulhong Oh (Ph.D.),** Professor, Department of Ocean Science,
University of Science and Technology

…….

Sukkyoung Lee (Ph.D.), Research Professor
Marine Science Institute of Jeju National University

……..

Jehee Lee (Ph.D.), Professor of Marine Life Sciences,
School of Marine Biomedical Sciences, Jeju National University

2022.12.08
Date

DEPARTMENT OF MARINE LIFE SCIENCES
GRADUATE SCHOOL
JEJU NATIONAL UNIVERSITY
REPUBLIC OF KOREA

TABLE OF CONTENTS

SUMMARY V
ACKNOWLEDGEMENT IX
LIST OF TABLES XI
LIST OF FIGURES XII
BACKGROUND 12
1.1. Aquaculture 13
1.2. Big-belly seahorse (*Hippocampus abdominalis*) 14
1.3. Red-spotted grouper (*Epinephelus akaara*) 17
CHAPTER 1 19
2.1. Introduction 20
2.2. Materials and methodology 24
2.2.1. Identification and bioinformatics analysis of *HaCSTB* and *HaCSTC* 24
2.2.2. Experimental fish, tissue distribution, and immune challenge experiments 25
2.2.3. Total RNA isolation and cDNA synthesis 26
2.2.4. Analysis of spatial and temporal expression by quantitative real-time PCR (qPCR) 27
2.2.5. Cloning and construction of *HaCSTB* and *HaCSTC* expression vectors 28
2.2.6. Overexpression and purification of recombinant HaCSTB (rHaCSTB) and HaCSTC (rHaCSTC) proteins 33
2.2.7. Maintenance of FHM cell line and transfection 34
2.2.8 Subcellular localization of HaCSTB 34
2.2.9. Functional assays 35
2.2.9.6. Flow cytometry analysis of apoptotic cell percentage 38
2.3. Results 39
2.3.1. Identification and bioinformatics analysis of *HaCSTB* and *HaCSTC* 39
2.3.2. Spatial and temporal expression analysis of *HaCSTB* and *HaCSTC* 45
2.3.3. Overexpression and protein purification 48
2.3.4. Subcellular localization of HaCSTB 50
2.3.5. Functional assays 50
2.3.5.1 Papain inhibitory activity assay 50
2.3.5.2. Effect of pH and temperature effect on papain inhibitory activity 52

2.3.5.3. HaCSTB and HaCSTC overexpression protects FHM cells against VHSV infection **52**

2.3.5.4. HaCSTB and HaCSTC overexpression suppresses VHSV gene expression **53**

2.3.5.5. HaCSTB and HaCSTC overexpression reduces VHSV-induced apoptosis **56**

2.4. Discussion **60**

2.5. Conclusion **70**

CHAPTER 2 ..... **72**

3.1. Introduction **73**

3.2. Materials and methods **75**

3.2.1. Identification and *in-silico* analysis of EaCOX2 ..... **75**

3.2.2. Fish husbandry **76**

3.2.3. Immune challenge experiment and tissue collection **76**

3.2.4. RNA isolation and cDNA synthesis **77**

3.2.5. EaCOX2 transcription analysis by quantitative real-time PCR (qPCR) **77**

3.2.6. Construction of recombinant *EaCOX-2* expression vectors, cell culture, and transfection **78**

3.2.7. Functional assays **80**

3.2.7.1. Determination of cell viability by WST-1 assay **80**

3.2.7.3. Determination of macrophage polarization **81**

3. 3. Results **83**

3.3.1. Identification and sequence characterization of EaCOX2 ..... **83**

3.3.2. Spatial expression pattern of *EaCOX2* **87**

3.3.3. Temporal expression of *EaCOX2* after immune challenge **88**

3.3.4. the effect of EaCOX2 overexpression on FHM cell viability **89**

3.3.5. The effect of EaCOX2 overexpression on apoptosis **90**

3.3.6. The effect of EaCOX2 overexpression on macrophage polarization **92**

3.3.7. The effect of EaCOX2 overexpression on NO production **92**

3.4. Discussion **94**

3.5. Conclusion **97**

References **98**

SUMMARY

Aquaculture has emerged as a vital fish production practice, overtaking the captive fisheries due to insufficient wild capture to meet the rising demand for fish over the past few decades. It contributes to a substantial impact on global food security as the cheapest source of human nutrition and providing livelihood. Nevertheless, aquaculture has been combatted due to frequent outbreaks of pathogen infections. Therefore, it is important to have a deep insight into fish immune defense mechanisms, and the overall objective of the current study is to perceive the immune defense mechanisms of teleosts and thereby foster sustainable aquaculture through disease prevention. In the present study, I have identified and characterized two Cystatin homologs from big-belly seahorse and Cyclooxygenase 2 from red-spotted grouper and elucidated their roles in the innate immune system of teleost.

Big-belly seahorse (*Hippocampus abdominalis*) is the largest seahorse species, naturally inhabited in shallow coastal areas, such as seagrass beds and natural estuaries. They have good commercial value for the aquarium trade and Chinese traditional medicine, albeit they are highly vulnerable 0to their natural habitat loss and overexploitation due to many human interventions. Therefore, seahorse aquaculture has emerged as a good solution to overcome consumer demand while conserving the wild population. However, there are some shortcomings in seahorse aquaculture such as their high sensitivity towards the varying culture conditions and the frequent outbreak of pathogen infections.

Red spotted grouper (*Epinephelus akaara*) is an ideal research model and a perfect candidate for extensive aquaculture owing to its high nutritional value, rapid growth, and high market demand. However, the frequent outbreak of viral diseases, especially, Nervous Necrosis Virus, are the major drawbacks in grouper aquaculture that has been creating a huge economic loss annually.

Cystatins are natural inhibitors of lysosomal cysteine proteases, including cathepsins B, L, H, and S. Cystatin B (CSTB) is a member of the type 1 cystatin family and found to be involved in numerous pathophysiological conditions. Cystatin C (CSTC) is a member of the type 2 cystatin family and is an essential biomarker in the prognosis of several diseases. In this study, the 297-bp cystatin B (HaCSTB) and 390-bp cystatin C (HaCSTC) cDNA from big-belly seahorse were cloned and characterized by screening the pre-established cDNA library. Based on similarities in sequence, HaCSTB is a homolog of the teleostean type 1 cystatin family. HaCSTC is a homolog of the teleost type 2 cystatin family with putative catalytic cystatin domains, signal peptides, and disulfide bonds. *HaCSTB* and *HaCSTC* transcripts were ubiquitously expressed in all tested big-belly seahorse tissues, with the highest expression in blood and ovaries respectively. Immune challenge with lipopolysaccharides, polyinosinic:polycytidylic acid, *Edwardsiella tarda*, and *Streptococcus iniae* caused significant upregulation in both *HaCSTB* and *HaCSTC* transcript levels. Using a pMAL-c5X expression vector, the 10.80-kDa of recombinant HaCSTB protein (rHaCSTB) and 14.29-kDa of recombinant HaCSTC protein (rHaCSTC) were expressed in *Escherichia coli* BL21

(DE3), and its protease inhibitory activity against papain cysteine protease was determined with the aid of a protease substrate. Papain was competitively blocked by both rHaCSTB and rHaCSTC in a dose-dependent manner. In response to viral hemorrhagic septicemia virus (VHSV) infection, both HaCSTB and HaCSTC overexpression significantly ($p < 0.05$) decreased the expression of VHSV transcripts, pro-inflammatory cytokines, and pro-apoptotic genes; while increasing the expression of anti-apoptotic genes in fathead minnow (FHM) cells. Furthermore, both HaCSTB and HaCSTC overexpression protected VHSV-infected FHM cells against VHSV-induced apoptosis and increased cell viability.

Cyclooxygenases (COXs) are major biosynthetic enzymes of prostaglandins, which play a key role in the generation of inflammatory response by acting on specific cellular receptors. There are two types of COX isomers, COX-1, and COX-2. COX-1 is constitutively expressed as house-keeping gene whereas COX-2 is highly inducible in response to various external stimuli. COX-2 is the most comprehensively studied mammalian dioxygenase and commonly used in anti-inflammatory drug therapies. The cDNA sequence of COX-2 with 1827 bp length, encoding 608 amino acid sequence, was cloned from Epinephelus akaara and designated as EaCOX-2. According to in silico analysis EaCOX-2 is a teleostean homolog of myeloperoxidase superfamily with prostaglandin endoperoxide synthase domain and a membrane-binding domain. The 3D structure of EaCOX-2 was a homodimer with heme binding sites at the center of the catalytic domains. The results of pairwise alignment disclosed

that *EaCOX-2* possessed 99% of the highest identity and 99% of similarity with Epinephelus lanceolatus. *EaCOX-2* transcripts were ubiquitously expressed in all tested, red-spotted grouper tissues, with significantly ($p<0.05$) the highest expression in gills. Immune challenge with lipopolysaccharides, polyinosinic:polycytidylic acid, and nervous necrosis virus caused significant ($p<0.05$) upregulation in *EaCOX-2* transcript levels at 12 h and 24 h post-infection in gills. The overexpression of *EaCOX-2* exhibited pro-inflammatory effect through reducing FHM cell viability, activation of classical M1 type macrophage polarization and increased nitric oxide (NO) production in murine macrophage cells (RAW264.7). Collectively, our findings imply the profound roles of Cystatins and Cyclooxygenase 2 against pathogen infections in teleosts by modulating fish immune responses.

ACKNOWLEDGEMENT

Foremost, I would like to extend my sincere gratitude to my research supervisor Professor Jehee Lee, who gave me this opportunity to commence my post-graduate studies at Marine Molecular Genetics Lab, Jeju National University, Republic of Korea, and for his patience, motivation, guidance, advice, and support to me for successful completion of my thesis.

I would like to thank the rest of my thesis committee, Prof. Chulhong Oh, Department of Marine Biology, University of Science and Technology, and Dr. Sukkyoung Lee, Marine Science Institute of Jeju National University, Republic of Korea, for insightful comments and encouragement. Further, I would like to thanks all the Professors and Doctors in my department for their patience and conductive comments during my coursework. I am highly obliged to take the opportunity to sincerely thanks Dr. Omeka, who introduced me to the professor, assisted when I arrived at Jeju, shared her knowledge and taught me new skills, and Dr. Dileepa Liyanage, who advised me whenever necessary, shared his knowledge and reviewed my manuscripts.

I extend my sincere thanks to Genomic selection team members: Dr. Sukkyoung Lee, Dr. Taehyug Jeong, Dr. Dileepa Liyanage, Dr. Malithi Omeka, Dr. Viraj Udayantha, Ms. Chaehyeon, Ms. Gaeun Kim, Ms. Jeongeun Kim, Mr. Jihun Lee, and, Mr. Chanuka Hanchapola for their support and encouragement to achieve great

accomplishment together. Further, I would like to thank all the past and present lab members who helped me in various situations.

My sincere thanks to all the funding authorities (Ministry of Oceans and Fisheries, Jeju National University, Korea) for providing research grants to accomplish the lab experiments.

I also acknowledge with a deep sense of reverence, my gratitude towards my teacher, Prof. C.V.L Jayasinghe (Dean, Faculty of Livestock, Fisheries and Nutrition, Wayamba University of Sri Lanka) for her consistent faith on me and endless support, advising me whenever I encounter any hardship. Last but not least I would like to thank my parents (Mr. A. Kodagoda and Mrs. Mallika Pathirana), and family members who have always supported me and always be my side.

LIST OF TABLES

Table 1: Details of the gene-specific primers used in this study 30

Table.2. Pairwise identity (I%) and similarity (S%) of the big-belly seahorse HaCSTB protein with selected orthologs at the amino acid level. 43

Table 3: Sequences of primers used in this study 80

LIST OF FIGURES

Fig.1. World capture fisheries and aquaculture production..... 13

Fig.2. Big-Belly Seahorse (*Hippocampus abdominalis*) 15

Fig.3. Big-belly seahorse worldwide distribution..... 16

Fig.4. Red-spotted grouper (*Epinephelus akaara*)..... 18

Fig.5. Nucleotide and deduced amino acid sequences of (A). HaCSTB and (C) HaCSTC..... 41

Fig.6. Multiple sequence alignment of (A). HaCSTB and (B). HaCSTC with known cystatin orthologs in other species. 44

Fig.7. The phylogenetic tree of (A). cystatin superfamily members and (B). cystatin family 2 members from different species 45

Fig.8. Tissue-specific mRNA expression of (A). HaCSTB and (B). HaCSTC in different tissues and temporal mRNA expression of (C). HaCSTB and (D). HaCSTC in the blood after immune challenge..... 46

Fig.9. Analysis of purified MBP fused rHaCSTB (A) and rHaCSTC (B) protein by SDS PAGE..... 49

Fig.10. *In vitro* papain inhibitory activity of rHaCSTB and rHaCSTC at different (A). protein concentrations, (B). temperature, and (C). pH. 51

Fig.11. (A) The effect of (A). HaCSTB and (B). HaCSTC overexpression on FHM epithelial cell viability 24 h after VHSV (1×10^{-4} MOI) infection in empty pcDNA™ 3.1(+) and HaCSTB- or HaCSTC- pcDNA™ 3.1(+) transfected FHM cells..... 54

Fig.12. The relative mRNA expression levels of VHSV genes VHSV_NV, VHSV_N, VHSV_M and VHSV_RdRp at 24 and 48 h after VHSV (1×10^{-4} MOI) infection in empty pcDNA™ 3.1(+) and HaCSTB- or HaCSTC- pcDNA™ 3.1(+) transfected FHM cells. 55

Fig. 13. The relative mRNA expression levels of FHM_Bcl2, FHM_Bax, and the ratio of Bax/Bcl-2 expression levels at 24 and 48 h after VHSV (1×10^{-4} MOI) infection in empty pcDNA™ $3.1^{(+)}$ or HaCSTB- and HaCSTC- pcDNA™ $3.1^{(+)}$ transfected FHM cells. 56

Fig.14. (A) Morphological changes in the nuclei of Hoechst 33342-stained FHM cells 24 h post-VHSV infection; (B) Flow cytometry analysis of apoptotic cells at 24 h post-VHSV infection. 59

Fig.15. (A). EaCOX2 protein domain architecture, (B). the predicted three-dimensional structure of EaCOX2 protein..... 85

..... 86

Fig.16. (A). Multiple sequence alignment of EaCOX2 with other vertebrate orthologs. (B). The phylogenetic tree of EaCOX2 and other COX2 orthologs..... 87

Fig.17. The spatial transcriptional analysis of *EaCOX2* in different tissues of *E. akaara*. 88

Fig.18 Temporal expression of *EaCOX2* in gills of *E. akaara*, upon immune stimulation. 89

Fig.19. The cell survival rate of FHM cells transfected with EaCOX2-pcDNA and pcDNA 3.1(+) after 24 h lipopolysaccharide (LPS)-treatment..... 90

Fig.20. Flow cytometry analysis of apoptotic cells percentage. 91

Fig.21. Fluorescent microscopy images of RAW 264.7 cells transfected with EaCOX2-pcDNA and pcDNA 3.1(+). 92

Fig.22. NO production by empty pcDNA™3.1(+) (control) and EaCOX2-pcDNA™3.1(+) transfected RAW264.7 cells after 12 h lipopolysaccharide (LPS)-treatment. 93

BACKGROUND

1.1. Aquaculture

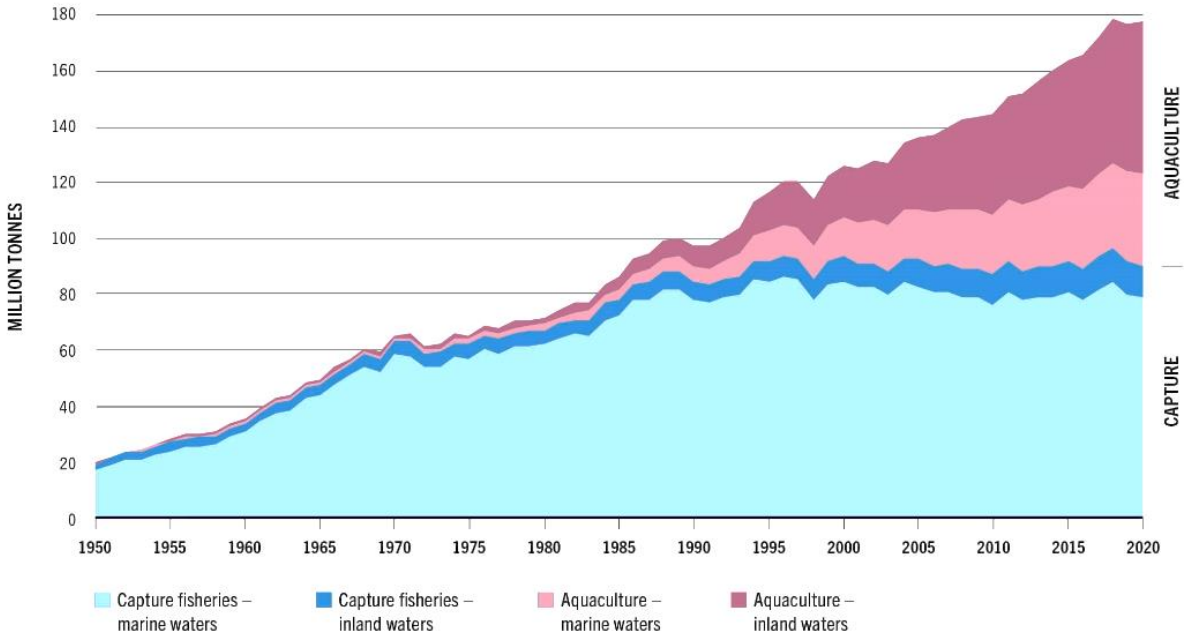

Fig.1. World capture fisheries and aquaculture production[1]

Global fisheries and aquaculture production has been acknowledged for their great contribution to global food security and nutrition in the present century. Aquatic food consumption has been increasing over the past few decades as the cheapest source of global protein supply. Global aquatic production was estimated to be 178 million tonnes in 2020 with 90 million tons (51%) of contribution from capture fisheries and 88 million tonnes (49%) of contribution from aquaculture (Figure 1). Capture fisheries comprise a real value of USD 141 billion in global production whereas aquaculture comprises a real value of USD 265 billion ("Global fisheries and aquaculture at a glance," 2022). Aquaculture production has been overtaking capture fisheries

[1] https://www.fao.org/3/cc0461en/online/sofia/2022/world-fisheries-aquaculture.html

production since 2016 due to insufficient wild capture to meet the rising demand for fish (Boyd et al., 2022). Overfishing, pollution, and the inability to restore the ecosystem to a productive state are the major challenges that may lead to a decline in fishery resources ("Global fisheries and aquaculture at a glance," 2022). Hence, a sustainable aquaculture system is a great approach to nourishing the world's growing population while safeguarding the ecosystems, protecting biodiversity, and minimizing pollution. However, aquaculture has certain drawbacks compared to terrestrial animal husbandry, especially, frequent disease outbreaks because pathogen infections can be easily transmitted through open water in aquatic systems with high fish density (Gudding and Van Muiswinkel, 2013). Therefore, several preventive measures are undertaken to combat the pathogen outbreaks such as the use of antibiotics, chemotherapeutics and vaccinations (Gudding and Van Muiswinkel, 2013).

1.2. Big-belly seahorse (*Hippocampus abdominalis*)

The big-belly seahorse (*Hippocampus abdominalis)* is the largest seahorse species in the Syngnathidae family; it grows up to 35 cm in length (Woods, 2000). Seahorses are exploited and traded for traditional Chinese medicine because of their medicinal value, including immunostimulatory, reno-protective, and anti-tumorigenic properties (K Kumaravel et al., 2012). The global demand for seahorses is increasing owing to their uses in traditional medicine and the ornamental fish industry. In Chinese and Chinese-derived traditional medicine, seahorses are believed to be therapeutic for various ailments, such as arthritis, inflammation, asthma, infertility, dermatitis, goiter,

and kidney malfunction (K. Kumaravel et al., 2012). Their unique horse-like curvaceous body structure, prehensile tail, and vertical swimming behavior are causes for curiosity and result in their high demand in the aquarium trade (Luo et al., 2016). The majority of seahorses are obtained as by-catch in non-selective fishing gear such as shrimp trawls. Despite the significant proportion of discards, over 25 million seahorses are annually exchanged for medicinal and ornamental use (Baum et al., 2003; Foster and Vincent, 2004; Salin and Mohanakumaran, 2006).

Fig.2. Big-Belly Seahorse (*Hippocampus abdominalis*)[2]

Seahorses are generally characterized by low fecundity, monogamy, extensive parental care, and a low population density (Foster and Vincent, 2004; Sadovy, 2001). Wild seahorses are highly vulnerable to the degradation of their natural inshore habitats and overexploitation (Lin et al., 2016). The low mobility and site fidelity of seahorses make it challenging for them to relocate after habitat loss (Foster and Vincent, 2004). Big-belly seahorses are included in Appendix II of the Convention for the International

[2] https://www.zoochat.com/community/media/pot-bellied-seahorse.389286/

Trade in Endangered Species of Wild Fauna and Flora (CITES) and have been described as species of least concern in the Red List of the International Union for Conservation of Nature (IUCN) since 2004 (Koldewey and Martin-Smith, 2010).

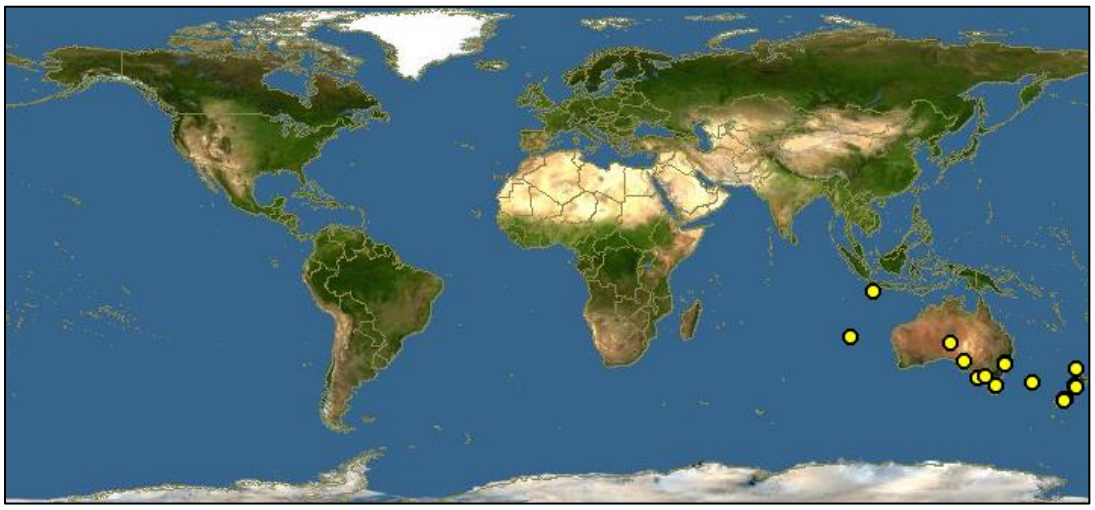

Fig.3. Big-belly seahorse worldwide distribution[3]

Seahorse aquaculture has emerged as a solution to fulfill the rising consumer demand while conserving wild seahorse populations. The big-belly seahorse is an ideal candidate for commercial culture, having a large, smooth-skinned body, and has been successfully cultured (Woods, 2000). Nevertheless, large-scale commercial seahorse production is challenging due to poor breeding, low juvenile survival, inadequate diet, poor rearing environments, high sensitivity towards varying water quality or culture conditions, and especially frequent disease outbreaks (Aurélio et al., 2013; Chang and Southgate, 2001; Zhang et al., 2011). Seahorses reared in captivity are highly susceptible to pathogenic infections by bacteria (e.g., *Vibrio* spp., *Mycobacterium*

[3] https://www.discoverlife.org/mp/20m?r=0.2&la=3&lo=48&kind=Hippocampus+abdominalis

hippocampi) (Alcaide et al., 2001; Balcázar et al., 2014), fungi (e.g., *Exophiala pisciphila*), parasites (e.g., *Glugea heraldi* and *Uronema marinum*), and viruses (Fioravanti and Florio, 2017). The common diseases affecting seahorse aquaculture include skin ulcers, tail rot disease, gas bubble disease, swim bladder inflation, scuticociliatosis, and hemorrhages (Lin et al., 2016). Therefore, a better understanding of the innate defense mechanisms of big-belly seahorses is essential for disease prevention, improving their health as well as survival rate, and fostering sustainable seahorse aquaculture.

1.3.Red-spotted grouper (*Epinephelus akaara*)

The red-spotted grouper, *Epinephelus akaara*, also known as the Hong Kong grouper is a protogynous hermaphrodite marine bony fish in the Serranidae family. It has been listed as endangered in the Red List of the International Union for Conservation of Nature (IUCN) since 2003 due to pollution and overexploitation (Sadovy et al., 2018).

The red-spotted grouper is an excellent candidate for extensive aquaculture and it has been widely cultured in several Southeast Asian countries including China, Taiwan, South Korea, and Japan because of its rapid growth, high nutritional value, efficient feed conversion, and high market demand (Yang et al., 2021). It has been used for sex determination and differentiation studies as a research model for developmental and reproduction schemes (Zhou and Gui, 2010). Red-spotted grouper has gained great commercial value as one of the most expensive fish among the other Serranidae

species, particularly in China market, due to its unique red color (Yang et al., 2021). Commercial grouper aquaculture has emerged with rapid growth to answer the rising market demand and the constant decrease in wild capture over the late two decades.

Fig.4. Red-spotted grouper (*Epinephelus akaara*)[4]

Grouper aquaculture production has been afflicted by several drawbacks such as poor culture conditions and intensive farming practices that may lead to crowding stress causing disease outbreaks easily. In addition to bacterial and parasitic infections, the frequent outbreaks of viral diseases, such as iridovirus, chloriridovirus, ranavirus, lymphocystis virus, and megalocytivirus, have been creating a huge economic loss in grouper aquaculture (Lee, 1995; Yeh et al., 2008). These disease occurrences can be combatted through effective disease management strategies. However, the existing knowledge on the grouper defense mechanisms against pathogens is limited. Therefore, further studies are required to determine the immune responses, expression profiles, and molecular mechanisms of red-spotted grouper.

[4] https://www.fishbase.se/summary/348

CHAPTER 1

Molecular characterization of two cystatins (Cystatin B and Cystatin C) from big-belly seahorse and their implications in host immune defense mechanisms

2.1. Introduction

Proteolytic enzymes, such as cysteine proteases, have numerous functions in organisms by catalyzing the hydrolytic cleavage of peptide bonds in target proteins. Their functions extend from routine protein digestion to more specific processes, such as proenzyme activation, the release of active peptides and hormones from precursors, protein translocation across membranes, gene expression, differentiation, blood coagulation, and cell death (Neurath, 1984). The lysosomal cysteine proteases serve as important biomarkers owing to their involvement in several autoimmune and inflammatory disorders, for instance, rheumatoid arthritis, multiple sclerosis, atherosclerosis, and malignancy (Berdowska, 2004). Despite the physiological functions of proteases, their proteolytic activity is tightly regulated by an array of activators, cellular receptors, and inhibitors to prevent aberrant protein degradation under normal physiological conditions (Skrzydlewska et al., 2005). To maintain the delicate balance in the body, their multi-faceted proteolytic activity is solidly regulated by a group of endogenous cysteine protease inhibitors known as cystatins.

Cystatins are a protein superfamily of lysosomal cysteine protease inhibitors that are ubiquitously present in plants as well as animals and are devoted to modulating cellular protein breakdown (Turk and Bode, 1991a). Cystatins reversibly form tight complexes with papain-like cysteine proteases, for instance, plant-based papain and some lysosomal cathepsins, thereby inhibiting their proteolytic activity (Bode and Huber, 2000; Pol and Björk, 1999). The cystatin superfamily consists of three types of

evolutionarily related (homologous) proteins classified based on their structural differences, designated types I (stefins), II (cystatins), and III cystatins (kininogens). Type I cystatins are primarily expressed intracellularly and lack signal peptides and disulfide bonds, whereas type II cystatins are predominantly expressed extracellularly and comprise signal peptides and disulfide bonds. Type III cystatins are large multidomain plasma proteins generally present in extracellular fluids (Turk et al., 2002).

Cystatin B (CSTB), also known as stefin B, is an endogenous cysteine protease inhibitor of the stefin family abundant in the cytosol, nucleus, and mitochondria of various cell types (Shamsi and Bano, 2017). Stefins are single-chain polypeptides that lack disulfide bonds and carbohydrate groups (Turk and Bode, 1991a). CSTB was initially found as a cathepsin B inhibitor in humans and was present in extracellular fluids, although it is an intracellular protein (Turk and Bode, 1991a). In addition to its anti-proteolytic activity, the roles of CSTB in host immune responses and neurodegenerative diseases have been identified (Giaimo et al., 2002; Takahashi et al., 1994). Several proteomic and transcriptomic analyses have been conducted in teleosts under immune challenge to elucidate the immunological functions of CSTB (Rajan et al., 2011; Wynne et al., 2008). To date, CSTB has been identified and studied in different teleost species, including *Scophthalmus maximus* (Xiao et al., 2010), *Oplegnathus fasciatus* (Premachandra et al., 2012b), and *Sebastes schlegelii* (Wickramasinghe et al., 2020).

Cystatin C (CSTC) is an extracellular cysteine protease inhibitor in the type II cystatin family, abundantly expressed and present in various organisms. Growing evidence suggests the immune response activity of CSTC against different exogenous and endogenous antigens regardless of its protease inhibitory activity. In addition to host protease inhibition, CSTC also acts on the cysteine proteases of pathogens that are essential for pathogen invasion and degradation of the extracellular matrix of the host cell (Coombs and Mottram, 1997; Frendéus et al., 2009). Recent studies have shown that CSTC is associated with critical steps of the inflammatory and immunomodulatory processes, from pathogen invasion to antigen elimination (Werle et al., 2003). Varying concentrations of CSTC have been shown to modulate the immune responses, including antigen presentation and the release of various inflammatory mediators such as cytokines and nitric oxide (NO) under pathological conditions in monocytes, macrophages, antigen-presenting cells, and tumor cells. (Zi and Xu, 2018). In addition, CSTC can, either directly or indirectly, control the proliferation, differentiation, and expression of the co-stimulatory secondary signal molecule in T cells, which are crucial to the acquired immune system (Vray et al., 2002). Moreover, CSTC has exhibited an inhibitory effect against certain viruses such as coronavirus (Collins and Grubb, 1991), poliovirus (Korant et al., 1985), herpes simplex virus (Gu et al., 1995), and adenovirus (Ruzindana-Umunyana and Weber, 2001) either by blocking their replication or suppressing their virulence. Thus far, several studies have elucidated the immune function of CSTC in various teleost species,

including chum salmon (*Oncorhynchus keta*) (Yamashita and Konagaya, 1996), rainbow trout (*Oncorhynchus mykiss*) (Li et al., 1998), large yellow croaker (*Pseudosciaena crocea*) (Li et al., 2009), spinyhead croaker (*Collichthys lucidus*) (Song et al., 2016), and orange-spotted grouper (*Epinephelus coioides*) (Wei et al., 2019).

Although extensive research on the function of Cystatins as biomarkers or immunomodulators in mammals has been carried out under various immune-related and pathological situations, it is essential to comprehend its role in teleost immune systems against pathogenic infections (Andrade, 2014; Kopitar-Jerala, 2006). To this end, the current study identified and described two Cystatin homologs (CSTB and CSTC) from big-belly seahorses (designated as HaCSTB and HaCSTC respectively). *HaCSTB* and *HaCSTC* expressions in different tissues under normal physiological and immune-stimulated conditions were analyzed. In addition, the *in vitro* cysteine protease inhibitory activity of recombinant HaCSTB and HaCSTC were evaluated. The expression profile of viral transcripts, pro-inflammatory cytokines, pro- and anti-apoptotic genes, and apoptosis were analyzed following viral hemorrhagic septicemia virus (VHSV) infection in HaCSTB- and HaCSTC-overexpressing fathead minnow cells (FHM).

2.2. Materials and methodology

2.2.1. Identification and bioinformatics analysis of *HaCSTB* and *HaCSTC*

The coding sequences of *HaCSTB* and *HaCSTC* were acquired from the big-belly seahorse transcriptome library created by Jeju National University, the Republic of Korea (Oh et al., 2016), and the sequence was verified using the Basic Local Alignment Tool (BLAST) on the National Center for Biotechnology Information (NCBI) website (https://blast.ncbi.nlm.nih.gov/Blast.cgi). Different *in-silico* analysis tools were used to describe the identified sequences. The open reading frame (ORF) and deduced amino acid sequence of HaCSTB and HaCSTC were obtained using CLC Main Workbench software v.7.7.1 (http://www.clcbio.com). The physicochemical properties were predicted using the ExPASy ProtParam online tool (https://web.expasy.org/protparam/). The putative domains and catalytic sites were deduced using the NCBI conserved domain (https://www.ncbi.nlm.nih.gov/Structure/cdd/wrpsb.cgi) and ExPASy PROSITE databases (https://prosite.expasy.org/), respectively. Signal peptides and *N*-linked glycosylation sites were determined using SignalP 4.1 (http://www.cbs.dtu.dk/services/SignalP/) and NetNGlyc 1.0 servers (http://www.cbs.dtu.dk/services/NetNGlyc/), respectively. The tertiary structure of HaCSTB and HaCSTC were predicted using the SWISS-MODEL ExPASy tool (https://swissmodel.expasy.org/) with the protein data bank (PDB) template and illustrated using PyMOL Molecular Graphics System v.2.3.1 (https://pymol.org/2/).

HaCSTB and HaCSTC were aligned with other known orthologous sequences of Cystatins to obtain pairwise identity and similarity using MatGAT software (Campanella et al., 2003) and multiple sequence alignments using the Clustal Omega online tool (https://www.ebi.ac.uk/Tools/msa/clustalo/). The multiple sequence alignment was visualized using the Color Align Conservation (https://www.bioinformatics.org/sms2/color_align_cons.html) online tool. An unrooted phylogenetic tree was constructed using MEGA software version X with the neighbor-joining method (5,000 bootstraps) (Tamura et al., 2021).

2.2.2. Experimental fish, tissue distribution, and immune challenge experiments

Healthy big-belly seahorses with an average body weight of 8 ± 0.25 g were obtained from the ornamental fish breeding center on Jeju Island, South Korea. They were kept for an acclimatization period of 1 week before the experiments start in 300-L tanks with aerated seawater at a temperature of 18 ± 2 °C and salinity of 34 ± 0.6‰ practical salinity units at the Fish Vaccine Research Center, Jeju National University, Republic of Korea. The seahorses were fed twice daily with mysis shrimp during the acclimatization period. All experimental procedures were carried out in accordance with the instructions set by the Animal Experiment Ethics Committee of Jeju National University.

For tissue distribution six healthy, unchallenged seahorses (3 males and 3 females) with an average body weight of 8 ± 0.25 g were dissected to collect 14 different tissues, including ovaries, pouch, gills, testis, spleen, brain, intestine, stomach, skin, blood,

heart, liver, kidney, and muscle for tissue-specific *HaCSTC* expression analysis. Blood was obtained by cutting the edge of the tails, and peripheral blood cells (PBCs) were isolated by centrifugation at 3,000 × *g* and 4 °C for 10 min. All tissue samples were instantly frozen in liquid nitrogen and stored at −80 °C.

To perform the immune challenge, seahorses weighing an average of 3 ± 0.25 g were placed into 5 groups of 35 individuals per group. Each experimental group of seahorses was injected intraperitoneally (IP) with 100 μL of sterile phosphate-buffered saline (PBS control), lipopolysaccharides (LPS) (1.25 μg/μL; Sigma-Aldrich, St. Louis, MO, USA), polyinosinic: polycytidylic acid (poly I: C) (1.5 μg/μL; Sigma-Aldrich), and cell suspensions of *Edwardsiella tarda* (5×10^3 CFU/μL) or *Streptococcus iniae* (1×10^5 CFU/μL) prepared in PBS. After injection, the seahorses were transferred to five different tanks corresponding to the type of immune stimulus, and PBCs were collected from five seahorses from each experimental group at 0, 3, 6, 12, 24, 48, and 72 h post-injection. Seahorses were not fed during immune challenge experiments.

2.2.3. Total RNA isolation and cDNA synthesis

Total RNA was isolated from the collected tissue samples using RNAiso Plus total RNA extraction reagent (Takara Bio Inc., Shiga, Japan), and the extracted RNA was purified using an RNeasy Mini Kit (Qiagen, Hilden, Germany). RNA purity and concentration were measured using a Multiscan™ GO Microplate Spectrophotometer (Thermo Fisher Scientific, Waltham, MA, USA). Agarose gel electrophoresis (1%) was used to determine RNA integrity. First-strand cDNA was synthesized in a 20-μL

reaction mixture using 2.5 μg of RNA as the template and a PrimeScript™ II First-strand cDNA Synthesis Kit (Takara Bio Inc.). The synthesized cDNA samples were 40-fold diluted with nuclease-free water and stored at −80 °C.

2.2.4. Analysis of spatial and temporal expression by quantitative real-time PCR (qPCR)

To analyze the transcriptional expression of *HaCSTB* and *HaCSTC* in different healthy and immune-challenged tissues, qPCR was performed using a Thermal Cycler Dice Real-Time System III (Takara Bio Inc.). Seahorse 40S ribosomal protein S7 gene (GenBank Accession no: KP780177) was used as an internal control gene in the qPCR assay. qPCR primers were designed using the PrimerQuest Tool from the IDT online server (https://sg.idtdna.com/Primerquest/Home/Index) according to the guidelines of minimum information for publication of quantitative real-time PCR experiments (MIQE) [33], as included in Table 1. qPCR was performed in a reaction mixture consisting of 1 μL nuclease-free water, 3 μL template cDNA, 0.4 μL of each primer (10 pmol/μL), and 5 μL of 2× Takara Ex Taq™ SYBR premix (Takara Bio Inc.), under the following thermal cycler conditions: an initial cycle of 95 °C for 10 min, 45 cycles of 95 °C for 5 s, 58 °C for 10 s, 72 °C for 20 s, and a final cycle of 95 °C for 15 s, 60 °C for 30 s, and 95 °C for 15 s. The internal control gene expression was used to normalize *HaCSTB* and *HaCSTC* expression. All reactions were carried out in triplicate. The relative expression of *HaCSTB* and *HaCSTC* were analyzed using the Livak $2^{-\Delta\Delta CT}$ method (Livak and Schmittgen, 2001). For spatial expression analysis,

normalized Ct values of *HaCSTB* and *HaCSTC* were expressed as fold values against the basal level. The lowest expressed tissue was selected as the basal level.

For temporal expression analysis, the Ct values of *HaCSTB* and *HaCSTC* were expressed as fold values against the untreated control after normalizing it to both the internal and PBS-injected controls at each time point. Data were analyzed using Student's *t*-test at a significance level of $p < 0.05$.

2.2.5. Cloning and construction of *HaCSTB* and *HaCSTC* expression vectors

Cloning primers with corresponding restriction recognition sites were designed using the IDT oligo analyzer tool (https://sg.idtdna.com/calc/analyzer) as listed in Table 1. The coding regions of *HaCSTB* and *HaCSTC* were amplified by PCR using the pre-designed primers and cDNA template from the PBCs of *H. abdominalis* under the following cycling conditions: initial denaturation at 94 ℃ for 4 min, followed by 35 cycles of 30 s at 94 ℃ (denaturation), 30 s at 58 ℃ (annealing), and 25 s at 72 ℃ (extension), and then 10 min at 72 ℃ (final extension). The amplified sequences were cloned into the pMAL-c5X (New England Biolabs, Ipswich, MA, USA) and pcDNA™ $3.1^{(+)}$ (Invitrogen, Waltham, MA, USA) vectors using the restriction sites *Eco*RV/*Eco*RI and *Kpn*I/*Eco*RI respectively. Briefly, restriction digestion was performed on purified PCR products and vectors using the respective restriction enzymes (Takara Bio Inc.), followed by ligation using a DNA Ligation Mix (Takara Bio Inc.) at 16 ℃ for 30 min according to the manufacturer's protocol. Subsequently, the recombinant plasmids were transformed into *Escherichia coli* DH5α competent

cells (Enzynomics Inc., Daejeon, Korea) using the heat-shock method. The successful transformants were identified by colony PCR and separated by plasmid extraction using an AccuPrep® Plasmid Mini Extraction Kit (Bioneer, Daejeon, Korea). The *HaCSTB* and *HaCSTC* clones were confirmed by sequencing (Macrogen, Seoul, Korea). Sequence-confirmed recombinant plasmids were again transformed into DH5α cells, and plasmids for cell assays were extracted using a Qiagen® Plasmid Midi Kit (Qiagen).

Table 1: Details of the gene-specific primers used in this study

Primer sequence (5′-3′)	Description	Melting Temperature	GenBank Accession
TGTGGCTGGGACCAACTACTTCA	HaCSTB qPCR-F	60 ºC	OL870960
ATGGCATCGGCATGTGTCTTGG	HaCSTB qPCR-R	60 ºC	OL870960
GGCGTCAAGTACTACATCACCGTCAA	HaCSTC qPCR-F	60 ºC	OP009439
CATAGGCGGCTCCACACAATGAATG	HaCSTC qPCR-R	60 ºC	OP009439
ACTCTGGAACTGGCAGAGGAAGAC	Seahorse 40S ribosomal S7 qPCR-F	60 ºC	KP780177
TGAAGTCATTCATGTTGGTGGCCTGTA	Seahorse 40S ribosomal S7 qPCR-R	60 ºC	KP780177
GAGAGAgatatcATGATATGCGGAGGACTTACAG ATGGTAC	HaCSTB Cloning-F (*Eco*RV)	59.2 ºC	OL870960
GAGAGAgaattcTCAGAAGAACTCAATGGCATCG GC	HaCSTB Cloning-R (*Eco*RI)	59.5 ºC	OL870960
GAGAGAggtaccATGATATGCGGAGGACTTACAG ATGGTAC	HaCSTB pEGFP – F (*Kpn*I)	59.2 ºC	OL870960

GAGAGAgggcccAGAAGAACTCAATGGCATCGGCAT	HaCSTB pEGFP – R (*Apa*I)	59.0 ºC	OL870960
GAGAGAggtaccATGATATGCGGAGGACTTACAGATGGTAC	HaCSTB pcDNA Cloning-F (*Kpn*I)	59.2 ºC	OL870960
GAGAGAgggcccTCAGAAGAACTCAATGGCATCGGC	HaCSTB pcDNA Cloning- R (*Apa*I)	59.5 ºC	OL870960
GAGAGAgatatcATGATTTTGAAGGTAGTCTTCATTTTTCTTGGGGTC	HaCSTC Cloning-F (*Eco*RV)	60.2 ºC	OP009439
GAGAGAgaattcCTAGCAGTCCCTTGGCTCTTGC	HaCSTC Cloning-R (*Eco*RI)	60.0 ºC	OP009439
GAGAGAggtaccATGGTTTTGAAGGTAGTCTTCATTTTTCTTGGGGTC	HaCSTC pcDNA Cloning-F (*Kpn*I)	60.2 ºC	OP009439
GAGAGAgaattcCTAGCAGTCCCTTGGCTCTTGC	HaCSTC pcDNA Cloning- R (*Eco*RI)	60.0 ºC	OP009439
TCTCCACTTGTCCTTCGC	VHSV-NV qPCR-F	61.0 ºC	AGS83381
TCTCGAAGAAGTCTGTAGCG	VHSV-NV qPCR-R	61.0 ºC	AGS83381

TGTCTCAGATCAGTGGGAAGTACGC	VHSV-N qPCR-F	60.0 ºC	AGS83377
GGACCTCAGCGACAAGTTCGG	VHSV-N qPCR-R	60.0 ºC	AGS83377
CTGGTTCGCCTATTCCAGAGTGC	VHSV-M qPCR-F	60.0 ºC	AGS83379
GGTCCAGGTAAGTGGCCTTTGC	VHSV-M qPCR-R	60.0 ºC	AGS83379
CAAGTGCGGACACGATCAATCCC	VHSV-RdRp qPCR-F	60.0 ºC	AGS83382
TGAGGAAAGGGCAACCATTCGC	VHSV-RdRp qPCR-R	60.0 ºC	AGS83382
TGGGACTGTTTGCCTTCG	FHM BCl2 qPCR-F	55.4 ºC	XP039532112.1
TCTGCCGCTGCATCTTTT	FHM BCl2 qPCR-R	55.2 ºC	XP039532112.1
TGGCACTGTTTCACCTCG	FHM BAX qPCR-F	55.3 ºC	XP039542657.1
ATCCTCCTTGCTGTCTGATC	FHM BAX qPCR-R	54.1 ºC	XP039542657.1
TCGCTTTGCTGTGCGTGACAT	FHM EF1α qPCR-F	60.0 ºC	AY643400
GGCAGCCTTCTGTGCAGACTTT	FHM EF1α qPCR-R	60.0 ºC	AY643400

2.2.6. Overexpression and purification of recombinant HaCSTB (rHaCSTB) and HaCSTC (rHaCSTC) proteins

After confirming the sequence, recombinant plasmids (HaCSTB-c5X and HaCSTC-c5X) were transformed into *E. coli* BL21 (DE3) cells (Novagen®; Merck, Darmstadt, Germany) to express recombinant protein. Inoculating recombinant plasmids containing *E. coli* BL21 cells into Luria-Bertani (LB) broth with 100 g/mL ampicillin yielded a seed culture. Thereafter, 5 mL of seed culture was added to 500 mL LB-rich ampicillin broth (enriched with 2% glucose and 100 g/mL ampicillin) and incubated at 37 °C and 200 rpm until the optical density at 600 nm (OD_{600}) reached 0.5. Protein expression was induced by adding 0.5 mM isopropyl-β-thiogalactopyranoside (IPTG; Promega, Madison, WI, USA) and further incubation at 20 °C and 200 rpm for 8 h. After the incubation period, the cells were harvested by centrifugation at 3,500 × *g* for 20 min at 4 °C, and the resulting pellet was resuspended in a 15-mL column buffer (20 mM Tris-HCl, pH 7.4, and 200 mM NaCl) and stored at −20 °C overnight. On the next day, a crude extract was obtained upon cell lysis through cold sonication of the pre-thawed resuspension, followed by centrifugation at 20,000 × *g* and 4 °C for 30 min to obtain the soluble fraction of the supernatant (Kim et al., 2020). Later, recombinant proteins (rHaCSTB and rHaCSTC) were obtained as fusion proteins of maltose-binding protein (MBP) after purification via affinity chromatography according to the pMAL-c5X fusion protein purification protocol (New England Biolabs). A Thermo Scientific NanoDrop 2000c (Thermo Fisher Scientific) was used to measure the protein

concentration, and a 12% sodium dodecyl sulfate-polyacrylamide gel electrophoresis (SDS-PAGE) was run to confirm the protein banding patterns.

2.2.7. Maintenance of FHM cell line and transfection

FHM cells were cultured in Leibovitz's L-15 medium (Sigma, USA) containing 10% Fetal Bovine Serum (FBS; Sigma, USA), 1% Gibco™ Penicillin-Streptomycin (Thermo Fisher Scientific, USA) at 25 °C. The cells were transfected with recombinant eukaryotic expression vectors according to the standard protocol using X-tremeGENE™ 9 (Roche, Germany).

2.2.8 Subcellular localization of HaCSTB

FHM cells were seeded into 6-well plates at a density of 5×10^5 cells/mL and incubated for 24 h at 25 °C. Then, the cells were transfected with the pEGFP-N1 vector harboring the HaCSTB construct (pEGFP-HaCSTB) or the pEGFP-N1 vector as a control, followed by incubation for 48 h. Subsequently, the transfected live cells were stained with 250 nM MitoTracker (Invitrogen, USA) and incubated for 10–20 min at 25 °C. The cells were fixed with 4% formaldehyde and washed twice with 1× PBS. The fixed cells were then stained with 4,6-diamidino-2-phenylindole solution (DAPI; Invitrogen, USA) following the manufacturer's protocol and incubated for 20 min at 25 °C. The subcellular localization of HaCSTB was observed using a fluorescence microscope at 400× magnification (Leica Microsystems, Germany). Images of HaCSTB localization were processed and merged using Leica Application Suite X software version 3.7.4.

2.2.9. Functional assays

2.2.9.1. Papain inhibitory activity assay

To determine the papain inhibitory activity of recombinant proteins (rHaCSTB and rHaCSTC), the papain inhibition assay was carried out as previously described with a few modifications (Yu et al., 2018). Briefly, the activating agent for the assay was freshly prepared by dissolving 50 mM L-cysteine (Sigma-Aldrich) and 20 mM ethylenediaminetetraacetic acid (EDTA) in Tris buffer (50 mM, pH 7.4). For the assay, a reaction mixture of 10 μL of recombinant protein (at final concentrations of 0, 0.08, 0.16, 0.32, 0.48, 0.64, and 0.80 μg/μL), 32 μL of papain (0.5 μg/μL; Sigma-Aldrich), and 8 μL of a freshly prepared activating agent were incubated at 28 °C for 15 min in a 96-well plate. At the initiation of the reaction, 50 μL of 0.5% (w/v) azocasein (Sigma-Aldrich) was added to the reaction mixture, followed by an incubation period at 37 °C for 30 minutes. Next, 120 μL of 5% (w/v) trichloroacetic acid (TCA) was added and chilled on ice for 5 min to terminate the reaction. Subsequently, the supernatant was collected by centrifugation at 2,000 × g for 3 min, and its absorbance was measured at 440 nm using a Multiskan SkyHigh Microplate Spectrophotometer (Thermo Fisher Scientific). The relative inhibition percentage (%) was calculated as follows:

$$100 \times \left(1 - \frac{A_{440} of\ rHaCSTB/C}{A_{440} of\ positive\ control}\right).$$

A similar assay was performed by replacing rHaCSTB/C protein with 10 μL of Tris buffer (50 mM, pH 7.4) as the positive control under the same conditions. In

addition, under the same conditions, MBP was used to investigate its effect on rHaCSTB/C activity. All assays were conducted in triplicate.

2.2.9.2. Determination of pH and temperature effect on papain inhibitory activity

To assess the effect of pH, rHaCSTB (0.28 μg/μL) was incubated with assay buffers of different pH values (pH 3, 4, 5, 6, 7, 8, 9, 10, and 11) for 30 min at 37 ℃. To investigate the effect of temperature, rHaCSTB was incubated with assay buffer (pH 8) at different temperatures, including 25, 35, 45, 55, 65, 75, and 85 ℃. The papain inhibitory activities of the mixtures were determined as described in section 2.9.1.

2.2.9.3. Determination of the cell survival rate via WST-1 assay after viral hemorrhagic septicemia virus infection

To determine the protective effect of HaCSTB and HaCSTC, a cell viability assay was performed using WST-1 (Takara Bio Inc.) according to the manufacturer's protocol after the VHSV infection of HaCSTB- or HaCSTC-overexpressing FHM cells. Briefly, FHM cells were seeded into 24-well plates at a cell concentration of 5×10^5 cells/mL and kept for 24 h at 25 ℃. The cells were then transfected with the pcDNA™ 3.1(+) vector harboring the HaCSTB construct (pcDNA-HaCSTB), HaCSTC constructs (pcDNA-HaCSTC) or the empty pcDNA™ 3.1(+) vector as the control, followed by 24 h incubation at 25 ℃. Afterward, FHM cells were infected with 1×10^{-4} multiplicity of infection (MOI) of VHSV (FWando05) (Priyathilaka et al., 2018) and incubated at 20 ℃ for 24 h. After a mild cytopathic effect was observed under a

microscope (Leica Microsystems, Wetzlar, Germany), WST-1 reagent was added to the cells, incubated for 10 min, and absorbance was measured using a Multiskan SkyHigh Microplate Spectrophotometer (Thermo Fisher Scientific) at 440 nm with 690 nm as the reference wavelength.

2.2.9.4. Determination of viral and downstream genes expression of HaCSTB- and HaCSTC-overexpressing FHM cells after VHSV infection

FHM cells were seeded into 12-well plates and incubated at 25 °C for 24 h. Thereafter, the cells were transfected with the pcDNA™ $3.1^{(+)}$ vector harboring the HaCSTB construct (pcDNA-HaCSTB), HaCSTC constructs (pcDNA-HaCSTC), or the empty pcDNA™ $3.1^{(+)}$ vector as the control. Next, FHM cells were infected with 1×10^{-4} MOI of VHSV as described in section 2.2.9.3 and incubated at 20 °C for 24 h, after which the cells were harvested at 0, 24, and 48 h post-infection (p.i.). Afterward, RNA was extracted using an RNeasy Mini Kit (Qiagen), followed by cDNA synthesis using a PrimeScript™ 1^{st} strand cDNA Synthesis Kit. Subsequently, qPCR was performed to analyze the VHSV genes such as non-virion protein (*VHSV NV*), nucleoprotein (*VHSV N*), matrix protein (*VHSV M*), and RNA-dependent RNA polymerase (*VHSV RdRp*). Further, downstream expression of FHM cell apoptosis-related genes, including anti-apoptotic B-cell lymphoma 2 (*FHM Bcl-2*), and pro-apoptotic Bcl-2-associated X (*FHM Bax*) was analyzed. mRNA expression profiles were determined using the corresponding primers as listed in Table 1 under the qPCR conditions described in section 2.2.4. FHM elongation factor 1 alpha (*FHM EF1α*) was used as the internal

control gene. Relative gene expression was evaluated using the Livak $2^{-\Delta\Delta CT}$ method. The Ct values were expressed as fold values after normalizing them to both the internal and non-transfected controls at each time point. Data were analyzed using Student's t-test at a significance level of $p < 0.05$. In addition, the Bax/Bcl-2 fold-induction ratio was measured to identify the effect of HaCSTB and HaCSTC in FHM cells on VHSV-induced apoptosis.

2.2.9.5. Morphological observation of cell apoptosis via Hoechst 33342 staining

Hoechst 33342 staining was performed to determine the effects of HaCSTB and HaCSTC on apoptosis induced by VHSV infection in FHM cells. FHM cells in 24-well plates were transfected with expression vectors and infected with VHSV, as mentioned in section 2.2.9.3. Twenty-four hours after VHSV infection, the cells were stained with Hoechst 33342 stain (Invitrogen) according to the manufacturer's protocol, and the morphological differences in cell nuclei were observed using a fluorescence microscope (Leica Microsystems) at 200× magnification. Leica Application Suite X software version 3.7.4 (Leica Microsystems) was used to process the images of staining results.

2.2.9.6. Flow cytometry analysis of apoptotic cell percentage

Flow cytometry analysis was conducted to quantitatively evaluate the effects of HaCSTB and HaCSTC on VHSV-induced apoptosis using propidium iodide (PI) according to a previously established method (Piao et al., 2022). FHM cells transfected

with the expression vectors were infected with VHSV, as described in 2.2.9.3 Twenty-four hours after VHSV infection, the cells were centrifuged (1000×*g*, 10 min, 10 °C) and fixed in 70 % ethanol. The cells were washed twice with 2 mM EDTA solution and stained for 30 min with PI (100 μg/mL). Eventually, the apoptotic cell percentage (percentage of sub-G1 cells) was analyzed by BD FACSCalibur™ flow cytometer (Becton Dickinson, San Jose, CA, USA) and CellQuest and ModFit Software (Becton Dickinson, SanJose, CA, USA).

2.3. Results

2.3.1. Identification and bioinformatics analysis of *HaCSTB* and *HaCSTC*

The cDNA sequences of *HaCSTB* and *HaCSTC* consisted of ORFs of 297-bp and 390-bp length, encoding polypeptides of 98 and 129 amino acids with estimated molecular weights of 10.8 kDa and 14.29 kDa respectively. Their isoelectric points were 6.89 and 5.73 respectively. The identified sequences were submitted under accession numbers OL870960 and OP009439 to the NCBI GenBank database. Amino acid sequence analysis revealed that both HaCSTB and HaCSTC harbored a cystatin domain with cysteine protease inhibitor features, such as a conserved glycine residue at the *N*-terminal, a conserved QXVXG pentapeptide motif in the middle, and a variant of proline–tryptophan motif at the *C*-terminal, which indicates that it belongs to the cystatin superfamily (Figure 5). HaCSTB does not contain signal peptides, carbohydrate groups, or disulfide bonds linked to the protein whereas HaCSTC protein

contains disulfide bonds, a signal peptide with a cleavage site at 18/19 residues, which helps secretion outside the cells, and a predicted N-linked glycosylation site at the 82nd amino acid residue (Figure 5). Altogether, *in silico* analysis suggested the identified *HaCSTB* and *HaCSTC* homologs are members of the cystatin family 1 and the cystatin family 2 respectively.

The 3D structure of HaCSTB comprised a five-turn α-helix core surrounded by a four-stranded antiparallel β-sheet that resembled the main feature of the cystatin fold (Figure 2B). As shown in Figure 2B, the highly conserved pentapeptide motif (QXVXG) is in the first β-hairpin loop from the *N*-terminal, and the second β-hairpin loop contains the PW motif variant, where a tyrosine amino acid substitutes a tryptophan. Both β-hairpin loops and the *N*-terminus, containing conserved regions, form a wedge-shaped structure (Figure 5B).

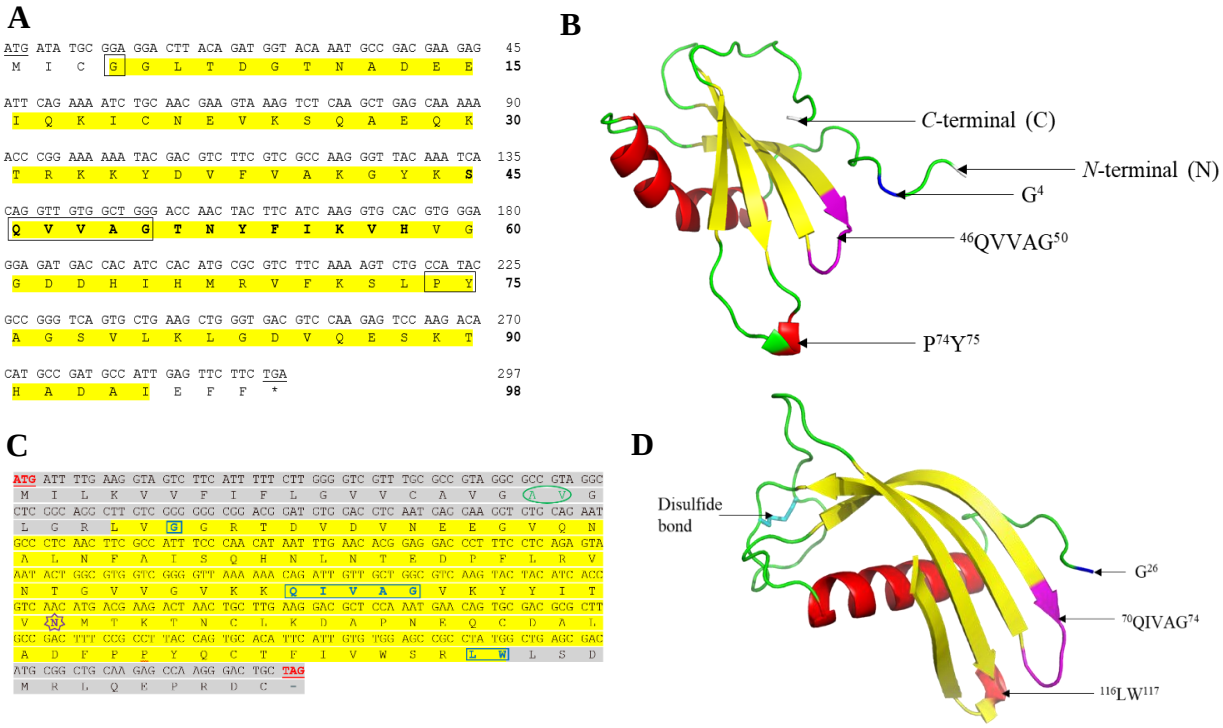

Fig.5. Nucleotide and deduced amino acid sequences of **(A).** HaCSTB and **(C)** HaCSTC.

The cystatin domain is shaded in yellow color, and the cysteine protease inhibitor signature is denoted in boldface. The conserved glycine residue (G4), QXVXG pentapeptide motif (46QVVAG50), and P74Y75 motif are denoted using boxes. Predicted three-dimensional structure of (B). HaCSTB and (D). HaCSTC based on human stefin B (P04080). Five turn α-helix, four-stranded antiparallel β-pleated sheets, and loops are shown in red, yellow, and green colors, respectively. C-terminal (C), N-terminal (N), conserved G, QXVXG, and PY motifs are indicated with arrowheads in the figure.

The predicted 3D structure of HaCSTC is a monomer that resembles a cystatin fold with four antiparallel β-sheets surrounding the four-turn α-helix core (Figure 5D). The

wedge-shaped active site of the protein is formed by an *N*-terminal glycine residue, a QXVXG motif in the 1st β-hairpin loop, and an LW motif in the 2nd β-hairpin loop (Figure 5D). The disulfide bond in the structure is typical of the cystatin family 2 (Figure 5D).

Pairwise sequence alignment of HaCSTB with other CSTB orthologs showed the highest homology with *Hippocampus comes* with 93.9% identity, and 98.0% similarity (Table 2), whereas that of HaCSTC showed 87.6% sequence identity, and 90.7% similarity with *H. comes* (Figure 6). Multiple sequence alignments of CSTB and CSTC orthologs showed conservation of the *N*-terminal glycine residue (G), QXVXG motif, and *C*-terminal proline-tryptophan (PW) motif (Figure 6). The phylogenetic tree revealed three distinct groups of cystatins where HaCSTB and HaCSTC were clustered with the teleost group in cystatin families 1 and 2 respectively, exhibiting evolutionary proximity to *H. comes* (Figure 7).

Table.2. Pairwise identity (I%) and similarity (S%) of the big-belly seahorse HaCSTB protein with selected orthologs at the amino acid level.

No	Scientific Name	NCBI Accession Number	Identity %	Similarity%	Gap%	Amino Acid
1	*Hippocampus comes*	XP_019727384.1	93.9	98.0	0.0	98
2	*Sygnathus acus*	XP_037104283.1	74.5	87.8	0.0	98
3	*Paralichthys olivaceus*	ACC86114.1	54.1	72.4	0.0	98
4	*Oncorhynchus mykiss*	NP_001117971.1	56.1	74.5	0.0	98
5	*Salmo salar*	ACI69028.1	54.1	73.5	0.0	98
6	*Mus musculus*	AAC52851.1	44.9	62.2	0.0	98
7	*Homo sapiens*	AAF44059.1	49	66.3	0.0	98
8	*Oryctolagus cuniculus*	BAA75920.1	49	63.3	0.0	98
9	*Taeniopygia guttata*	NP_001232786.1	52	68.4	0.0	98
10	*Anas platyrhynchos*	XP_027305525.1	54.1	66.3	0.0	98
12	*Gallus gallus*	NP_001185577.1	51.0	68.4	0.0	98
13	*Varanus komodoensis*	KAF7238113.1	50	64.3	0.0	98
14	*Xenopus tropicalis*	NP_001106571.1	37.8	60.2	0.0	98

A

Similarity percentage	Identity percentage													
	1	2	3	4	5	6	7	8	9	10	11	12	13	14
1. *Hippocampus comes*		87.6	61.9	53.2	51.9	49.2	47.7	32	30.7	31.2	31.5	31.1	29.8	34.3
2. *Hippocampus abdominalis*	90.7		59.7	51.9	51.1	46.3	46.3	31.5	31.9	30.7	29.5	30.9	28.3	31.9
3. *Syngnathus acus*	76.2	69.8		52.4	54.3	47.7	48.9	31.5	29.8	32.6	29.5	32.5	30.5	34.5
4. *Melanotaenia boesemani*	69.8	65.1	70.4		65.6	57.4	58.5	32	36.2	34	34.5	33.6	32.2	35.3
5. *Micropterus salmoides*	71.7	69	74.8	76.4		65.6	72.9	32.9	33.6	33.6	33.8	37.7	35.8	37
6. *Paralichthys olivaceus*	69	65.9	71.4	72.2	85		56.2	30.1	34	29.3	29.7	33.8	32.5	32.6
7. *Epinephelus coioides*	69.8	67.4	72.1	72.9	88.4	79.8		33.3	32.6	31.9	34.9	36.6	34.2	37
8. *Homo sapiens*	50	49.3	51.4	56.8	52.1	51.4	55.5		70.5	67.8	66	39	40.3	49.3
9. *Rattus norvegicus*	49.3	50.7	53.6	60	52.9	52.9	55	84.2		87.1	59.1	42.5	44.2	49.7
10. *Mus musculus domesticus*	50.7	49.3	53.6	55.7	50.7	49.3	52.9	82.2	95.7		60.4	39.2	40.5	47.5
11. *Bos taurus*	50.7	48.6	54.1	57.4	52.7	49.3	52.7	79.7	73	75		43.4	44.7	52
12. *Gallus gallus*	47.7	49	48.3	52.3	55.6	53.6	58.3	61.6	61.6	60.3	63.6		88.7	51.7
13. *Numida meleagris*	49	49	49.7	53	55	53	56.3	64.9	64.9	63.6	66.2	92.7		52.3
14. *Mauremys mutica*	54.4	54.4	58.8	57.4	59.6	52.2	62.5	66.4	69.3	66.4	66.9	68.9	68.9	
15. *Chelonia mydas*	55.9	54.4	60.3	58.8	61.8	55.1	63.2	68.5	70.7	69.3	68.9	70.9	71.5	94.1

B

C

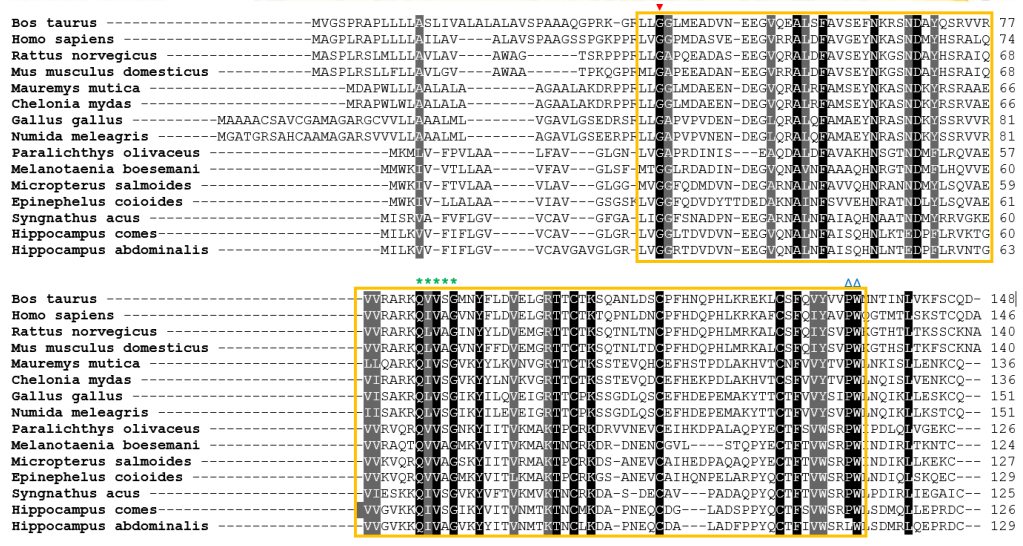

Fig.6. Multiple sequence alignment of **(A).** HaCSTB and **(B).** HaCSTC with known cystatin orthologs in other species.

The identical residues among sequences are indicated by the black-colored background, and the gray-colored background indicates similar residues. The cystatin domain is marked with a yellow-colored box. The conserved G, QxVxG, and PW motifs are indicated with the (▼), (*), and (Δ) symbols, respectively.

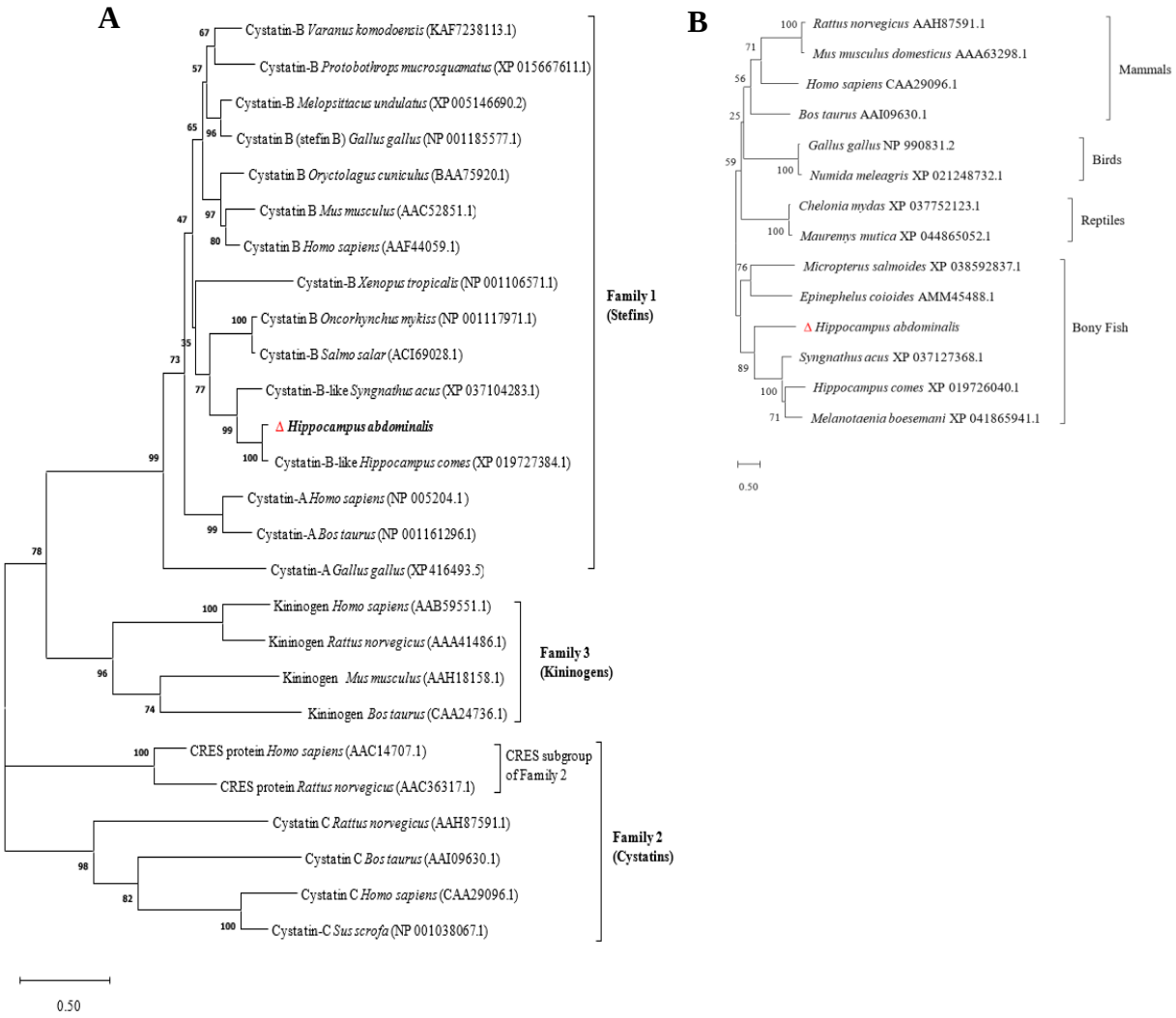

Fig.7. The phylogenetic tree of **(A).** cystatin superfamily members and **(B).** cystatin family 2 members from different species

2.3.2. Spatial and temporal expression analysis of *HaCSTB* and *HaCSTC*

To determine the normal physiological function of cystatin in the big-belly seahorse, the spatial *HaCSTB* and *HaCSTC* expression levels in different seahorse tissues were analyzed (Figure 8). Both *HaCSTB* and *HaCSTC* were generally expressed in all tested tissues. The highest *HaCSTB* expression was observed in PBCs, with a fold value of

32.4, followed by the testes (29.4-fold) and pouch (22.5-fold). The highest *HaCSTC* expression was observed in in ovaries, with a fold value of 29.3, followed by the spleen (22.5-fold) and brain (17.0-fold). The lowest expression was found in the gills.

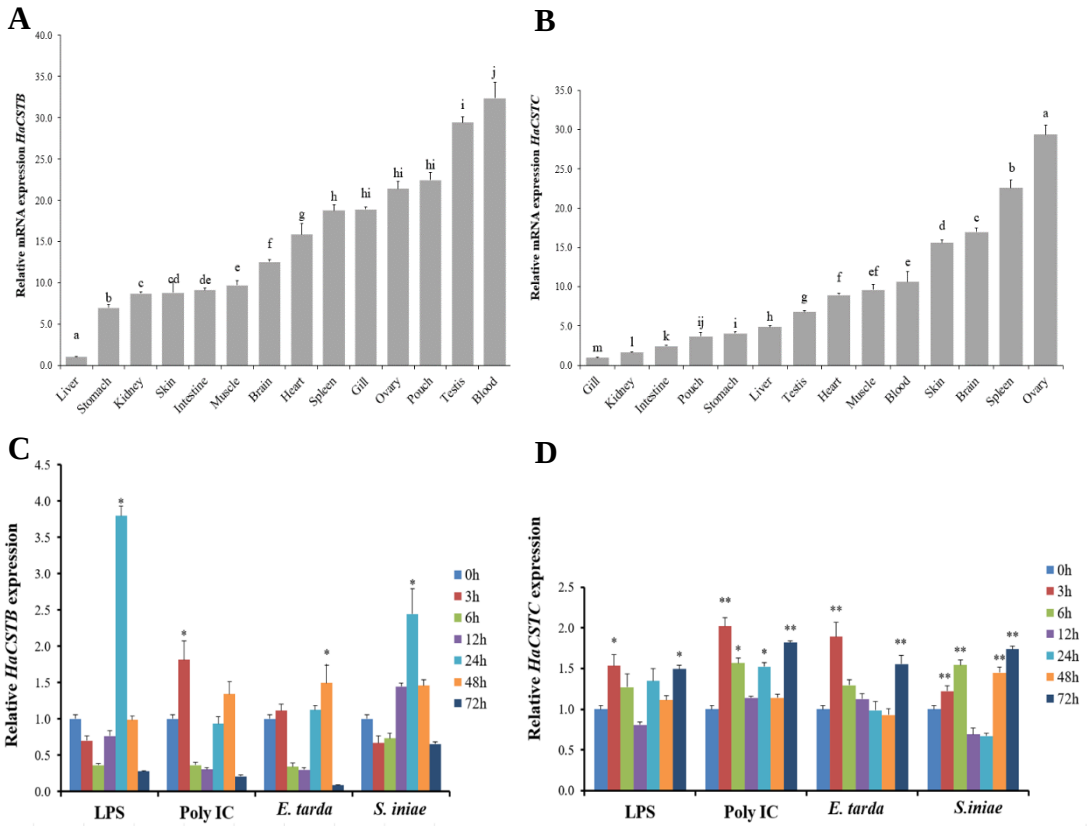

Fig.8. Tissue-specific mRNA expression of **(A).** HaCSTB and **(B).** HaCSTC in different tissues and temporal mRNA expression of **(C).** HaCSTB and **(D).** HaCSTC in the blood after immune challenge.

All experiments were performed in triplicate (n = 3). The error bars represent the standard deviation (SD). Statistical analysis of tissue expression data was performed using one-way analysis of variance (ANOVA), and significant differences ($p < 0.05$) were indicated by different lowercase letters. Comparisons for the immune challenge

data were carried out using the Student's t-test, and significant differences compared to the 0 h control were denoted with an asterisk ("*", $p < 0.05$) or a double asterisk ("**", $p < 0.01$).

To determine the immune role of cystatins in the big-belly seahorse, temporal mRNA expression levels of both *HaCSTB* and *HaCSTC* in PBCs were analyzed upon immune stimulation with LPS (bacterial wall component), poly I:C (double-stranded viral mimic), Gram-negative *E. tarda*, and Gram-positive *S. iniae* at several time points (Figure 8). The results revealed a noticeable variation of *HaCSTB* expression in PBCs in response to LPS, Poly I:C, and live bacteria. Upon LPS immune stimulation, *HaCSTB* mRNA expression was significantly upregulated at 24 h post-injection (p.i.) by 3.8-fold compared to basal levels (Figure 8C). Furthermore, *HaCSTB* exhibited an early response upon Poly I:C (a double-stranded RNA viral mimic) at 3 h p.i. with a significant ($p < 0.01$) upregulation (1.8-fold). *E. tarda* stimulation resulted in 1.5-fold upregulation ($p < 0.05$) of *HaCSTB* at 48 h p.i. compared to its basal level (0 h p.i.). The immune challenge with *S. iniae* upregulated the *HaCSTB* transcript levels at 12 h, 24 h, and 48 h p.i. compared with those at 0 h p.i. Upon immune stimulation, *HaCSTC* mRNA expression was significantly ($p < 0.01$) upregulated by 1.5, 2.0, 1.9, and 1.2-folds at 3 h p.i. for LPS, poly I:C, *E. tarda*, and *S. iniae* immune stimulants, respectively (Figure 8D). Furthermore, following an oscillating pattern, *HaCSTC* mRNA expression was significantly ($p < 0.05$) upregulated at 72 h p.i for all immune stimulants.

2.3.3. Overexpression and protein purification

The ORFs of *HaCSTB* and *HaCSTC* were cloned into the pMAL-c5X vector and overexpressed in *E. coli* BL21 cells to produce the recombinant fusion proteins (rHaCSTB and rHaCSTB) with maltose-binding protein (MBP). The 12% SDS-PAGE gel analysis revealed that rHaCSTB and rHaCSTC were present in the soluble fraction in which single protein bands appeared at approximately 53.3 kDa (42.5 kDa MBP + 10.8 kDa of rHaCSTB) and 56.3 kDa (42.5 kDa MBP + 13.8 kDa of rHaCSTC) respectively (Figure 9A, B).

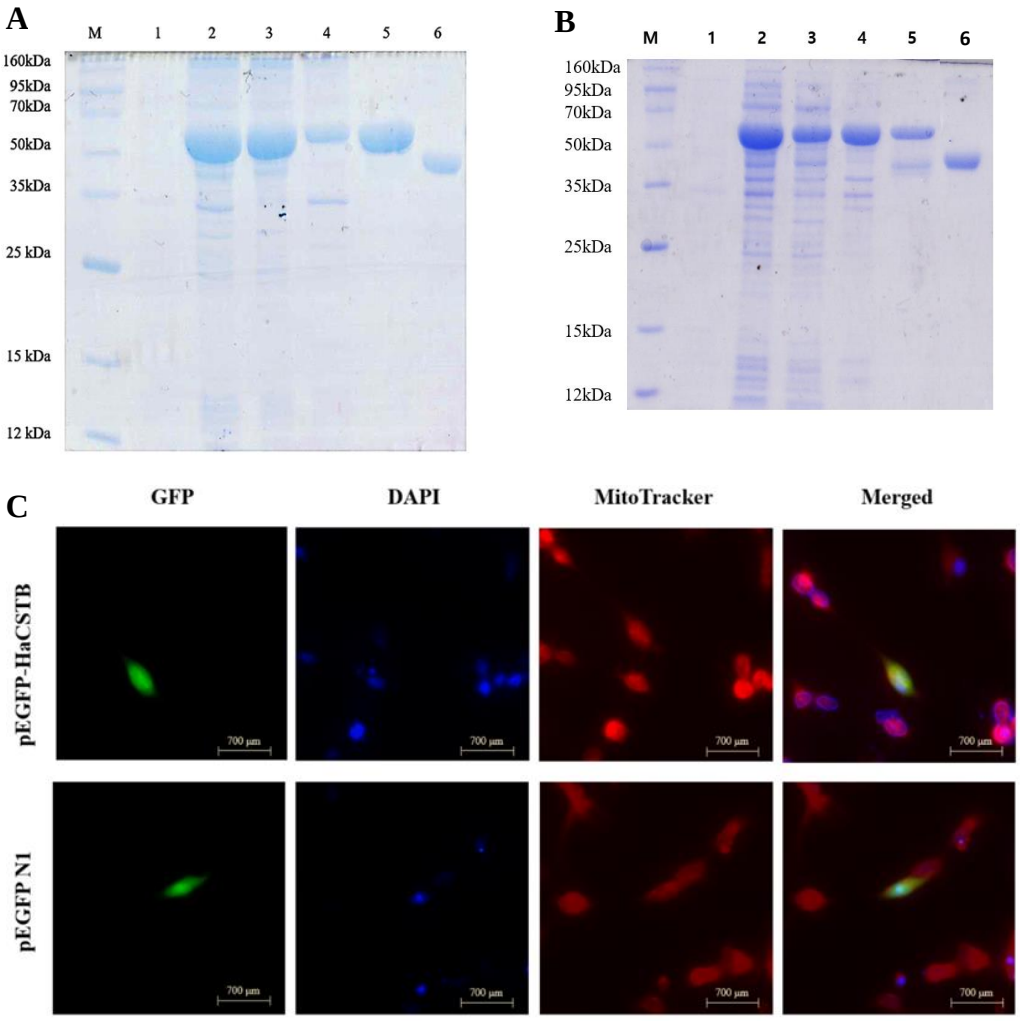

Fig.9. Analysis of purified MBP fused rHaCSTB (A) and rHaCSTC (B) protein by SDS PAGE

M: Unstained protein marker (Enzynomics); 1: Crude extraction of uninduced cells; 2: lysate; 3: Supernatant; 4: pellet; 5: purified fusion protein (rHaCSTB-MBP or rHaCSTC-MBP); 6: MBP (C) Subcellular localization of HaCSTB in FHM cells. Fluorescence images of FHM cells, transfected with the pEGFP-HaCSTB in the first row and the pEGFP-N1 control vector in the second row. Images in the first, second, third, and fourth columns show the GFP (green)-tagged protein, DAPI (blue)- stained

nuclei, Mitotracker (red)-stained mitochondria, and merged images of the first three columns, respectively.

2.3.4. Subcellular localization of HaCSTB

The subcellular localization of HaCSTB was determined in FHM cells based on the green fluorescence emitted by the EGFP-HaCSTB protein. DAPI-stained nuclei in FHM cells were observed in blue, whereas Mitotracker-stained mitochondria appeared red under the fluorescence microscope (Figure 9C). Images revealed that HaCSTB localized to the cytoplasm, nuclei, and mitochondria. However, a subcellular localization assay was not performed for HaCSTC because it is an extracellular protein according to the *in silico* analysis.

2.3.5. Functional assays

2.3.5.1 Papain inhibitory activity assay

To investigate their protease inhibitory activities, both rHaCSTB and rHaCSTC recombinant proteins were allowed to react with the papain enzyme *in vitro* at increasing concentrations, and residual papain enzyme activity was measured based on the estimation of TCA-soluble, digested products with small molecular weights. Both rHaCSTB and rHaCSTC inhibited papain in a concentration-dependent manner (Figure 10A). The highest inhibitory percentage was exhibited as 82 % by rHaCSTB and 25 % by rHaCSTC at 0.8 μg/μL of protein concentration. The assay was performed for MBP alone as a control to verify its effect.

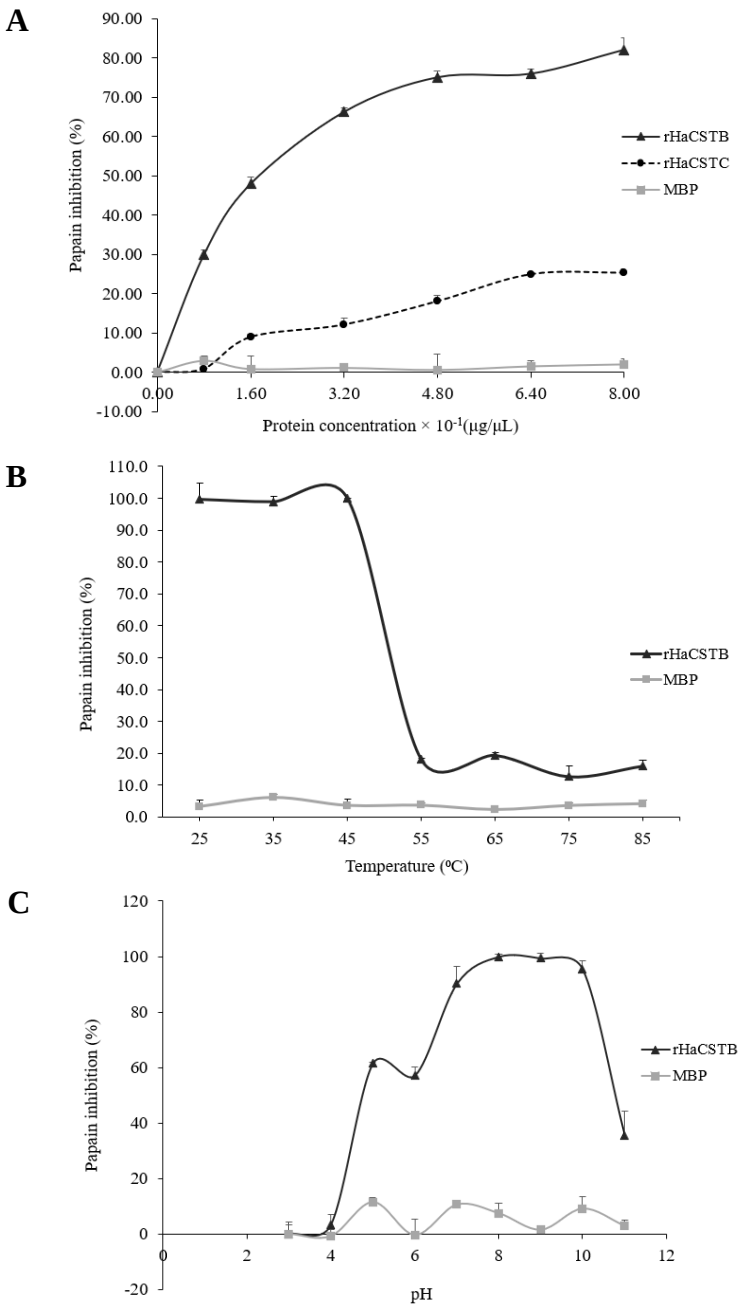

Fig.10. *In vitro* papain inhibitory activity of rHaCSTB and rHaCSTC at different **(A)**. protein concentrations, **(B)**. temperature, and **(C)**. pH.

Azo-casein was used as a substrate for the papain enzyme, and MBP was used as a control. Error bars represent the SD (n = 3).

2.3.5.2. Effect of pH and temperature effect on papain inhibitory activity

To determine the effect of pH and temperature on the inhibitory activity of rHaCSTB, a papain inhibition assay was conducted at a pH range of 3–11 and a temperature range of 25–85 °C. The assay was performed for MBP alone as a control to verify its effect. rHaCSTB exhibited the highest inhibitory activity against papain within the temperature range of 25–45 °C, indicating a plateau in the graph, and the inhibitory activity suddenly decreased after 55 °C (Figure 10B). The inhibitory activity of rHaCSTB varied under different pH conditions and the maximum inhibitory activity was observed at pH 8 (Figure 10C). Furthermore, the graph showed a plateau within the pH range of 8–10, and the inhibitory activity suddenly decreased at pH 11.

2.3.5.3. HaCSTB and HaCSTC overexpression protects FHM cells against VHSV infection

The WST-1 assay was employed to determine the effect of HaCSTB and HaCSTC on FHM cell viability against VHSV infection. Cell viability was significantly reduced after VHSV infection in pcDNA™ 3.1$^{(+)}$ vector-transfected FHM cells ($p < 0.05$) (Figure 11). This result illustrated that the cell survival percentage of both HaCSTB- and HaCSTC-overexpressing FHM cells (HaCSTB- pcDNA™3.1$^{(+)}$ and HaCSTC-pcDNA™3.1$^{(+)}$) were significantly higher than that of pcDNA™ 3.1$^{(+)}$ vector-transfected FHM cells 24 h post-VHSV infection ($p < 0.05$) (Figure 11).

2.3.5.4. HaCSTB and HaCSTC overexpression suppresses VHSV gene expression

The relative expression profile of VHSV transcripts was analyzed in both HaCSTB- and HaCSTC- pcDNA™3.1$^{(+)}$-overexpressing FHM cells at 0, 24, and 48 h post-VHSV infection. Based on qPCR analysis, VHSV transcripts of *VHSV NV*, *N*, *M*, and *RdRp* genes were significantly downregulated at 24 and 48 h p.i. compared with that of pcDNA™3.1$^{(+)}$-overexpressing cells and 0-h controls ($p < 0.05$) (Figure 12).

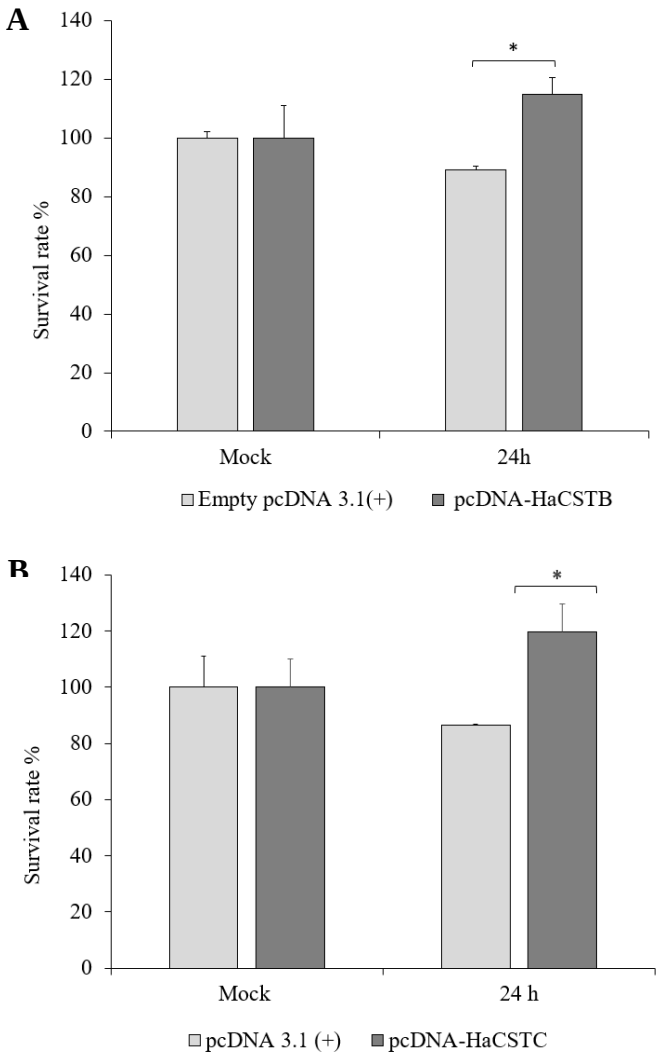

Fig.11. (A) The effect of **(A).** HaCSTB and **(B).** HaCSTC overexpression on FHM epithelial cell viability 24 h after VHSV (1×10^{-4} MOI) infection in empty pcDNA™ 3.1(+) and HaCSTB- or HaCSTC- pcDNA™ 3.1(+) transfected FHM cells.

Experiments were carried out in triplicate (n = 3), and error bars represent the SD. Asterisks indicate significant differences ("*," $p < 0.05$; Student's t-test). MOI, multiplicity of infection; VHSV, viral hemorrhagic septicemia virus; FHM, fathead minnow.

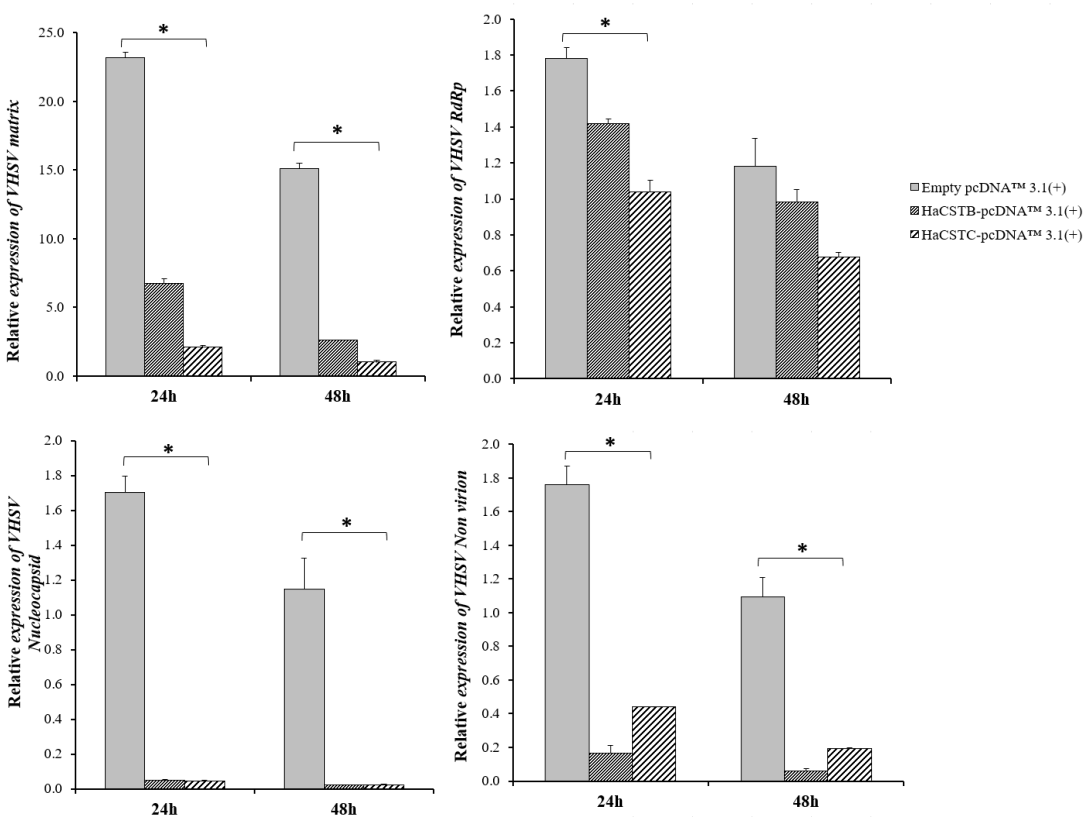

Fig.12. The relative mRNA expression levels of VHSV genes VHSV_NV, VHSV_N, VHSV_M and VHSV_RdRp at 24 and 48 h after VHSV (1×10^{-4} MOI) infection in empty pcDNA™ 3.1(+) and HaCSTB- or HaCSTC- pcDNA™ 3.1(+) transfected FHM cells.

Experiments were carried out in triplicate (n = 3), and error bars represent the SD. Asterisks indicate significant differences ("*," $p < 0.05$; Student's t-test). MOI, multiplicity of infection; VHSV, viral hemorrhagic septicemia virus; FHM, fathead minnow.

2.3.5.5. HaCSTB and HaCSTC overexpression reduces VHSV-induced apoptosis

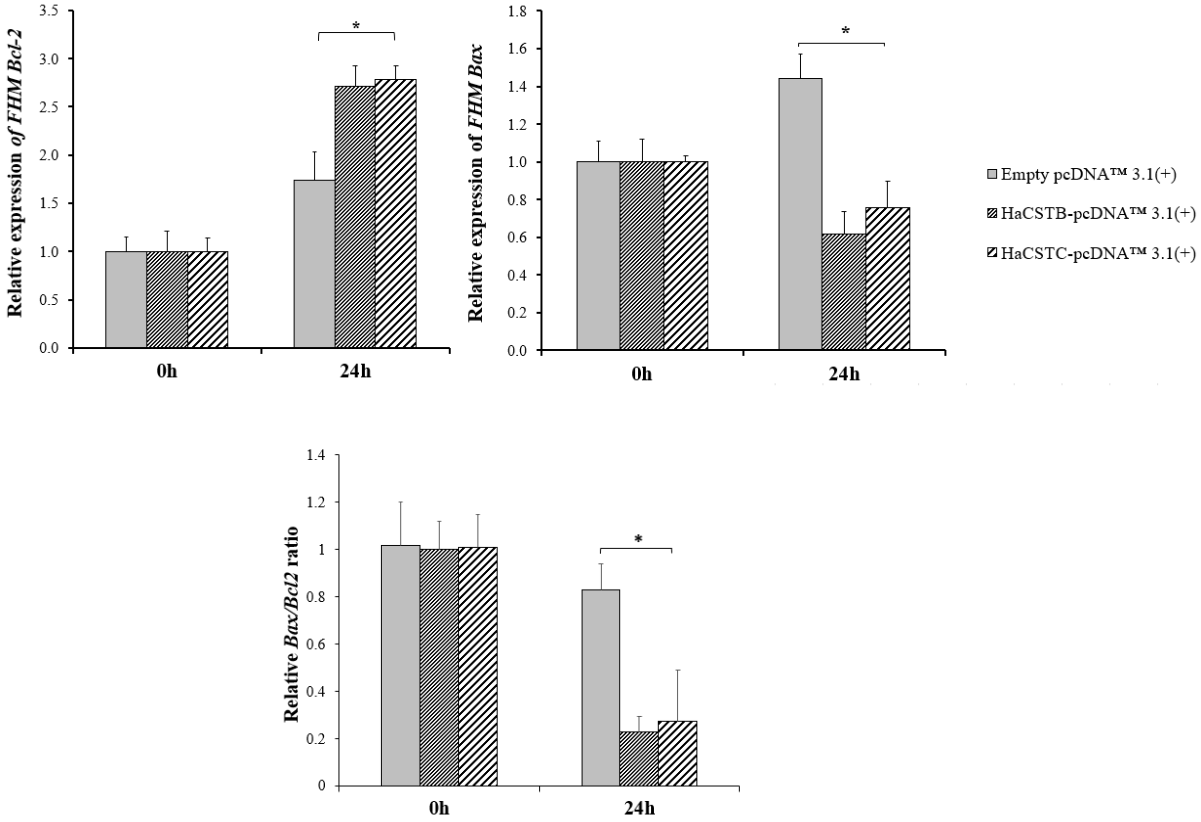

Fig. 13. The relative mRNA expression levels of FHM_Bcl2, FHM_Bax, and the ratio of Bax/Bcl-2 expression levels at 24 and 48 h after VHSV (1×10^{-4} MOI) infection in empty pcDNA™ $3.1^{(+)}$ or HaCSTB- and HaCSTC- pcDNA™ $3.1^{(+)}$ transfected FHM cells.

Experiments were carried out in triplicate and error bars represent the SD (n = 3). Asterisks indicate significant differences ("*", $p < 0.05$, "**," $p < 0.01$; Student's t-test). MOI, multiplicity of infection; FHM, fathead minnow; VHSV, viral hemorrhagic septicemia virus.

To determine the effect of HaCSTB and HaCSTC on VHSV-induced apoptosis, the relative transcriptional expression of anti-apoptotic *Bcl-2* and pro-apoptotic *Bax* and

in HaCSTB- and HaCSTC- pcDNA™3.1$^{(+)}$-overexpressing FHM cells was analyzed following VHSV infection. Results showed that both HaCSTB and HaCSTC significantly increased the mRNA expression of *Bcl-2* and decreased *Bax* after VHSV infection ($p < 0.05$) (Figure 13). Moreover, the ratio of *Bax/Bcl-2* was quantified, and it was significantly lower in both HaCSTB- and HaCSTC-overexpressing FHM cells than that in the empty pcDNA™ 3.1$^{(+)}$ vector-transfected FHM cells 24 h post-VHSV infection ($p < 0.05$) (Figure 13).

The transcriptional analysis results of apoptotic genes were confirmed by staining the nuclei of FHM cells using the cell-permeable nucleic acid dye Hoechst 33342 after VHSV infection. Apoptotic nuclei with nuclear condensation and fragmentation were stained more brightly with light-blue fluorescence, whereas live intact nuclei appeared less bright with blue fluorescence and an oval shape (Figure 14A). Apoptotic bodies were drastically increased 24 h post-VHSV infection in empty pcDNA™3.1$^{(+)}$-transfected FHM cells (Figure 14A). Both HaCSTB- and HaCSTC- pcDNA™3.1$^{(+)}$-overexpressing FHM cells showed fewer apoptotic bodies than the empty pcDNA™ 3.1$^{(+)}$-transfected cells 24 h post-VHSV infection. These findings suggested that overexpression of both HaCSTB and HaCSTC significantly decreased VHSV-induced cellular apoptosis 24 h p.i.

Flow cytometry analysis quantitatively demonstrated that the apoptotic cell percentage of both HaCSTB- and HaCSTC- pcDNA™3.1(+)-overexpressing FHM cells was

significantly lower than the empty pcDNA™ 3.1(+) vector-transfected cells after VHSV infection (Figure 14B), confirming the previous Hoechst staining results.

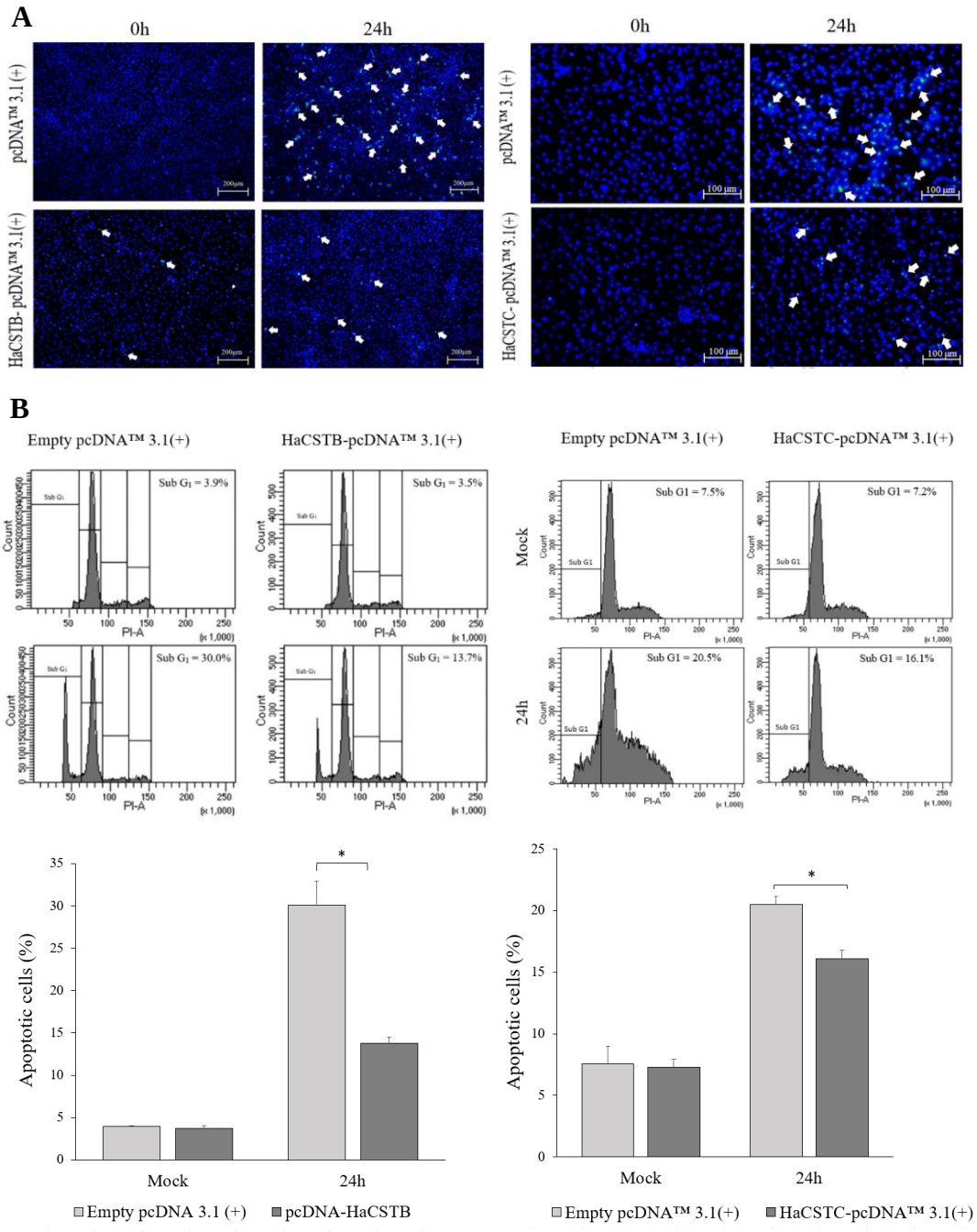

Fig.14. **(A)** Morphological changes in the nuclei of Hoechst 33342-stained FHM cells 24 h post-VHSV infection; **(B)** Flow cytometry analysis of apoptotic cells at 24 h post-VHSV infection.

FHM cells were transfected with empty pcDNA™ 3.1(+) or HaCSTB- pcDNA™ 3.1(+) and HaCSTC- pcDNA™ 3.1(+) vectors and apoptosis was induced after VHSV (1 × 10-4 MOI) infection. White arrows indicate apoptotic bodies or condensed nuclei. Experiments were carried out in triplicate and error bars represent the SD (n = 3). Asterisks indicate significant differences ("*", $p < 0.05$, "**," $p < 0.01$; Student's t-test). MOI, multiplicity of infection; FHM, fathead minnow; VHSV, viral hemorrhagic septicemia virus.

2.4. Discussion

Mounting evidence suggests immune regulatory functions of cystatins in vertebrates, which are either dependent or independent of its putative cysteine protease inhibitory activity (Gauthier et al., 2011; Holloway et al., 2018; Levy et al., 2006; Li et al., 2009). The serum CSTC level is considered an important biomarker for the prognosis of various diseases, owing to its relatively low molecular weight (Séronie-Vivien et al., 2008). However, the molecular mechanism behind the immunomodulatory functions of cystatin in teleosts is enigmatic. Therefore, in the current study, we comprehensively demonstrated the immune response of CSTB and CSTC from *H. abdominalis* against bacterial and viral infections.

According to the bioinformatics analysis, HaCSTB belongs to cystatin family 1, possessing characteristic cysteine protease inhibitor features, including three cystatin motifs (G, QXVXG, and PW) whereas HaCSTC belongs to the type 2 cystatin family since it possesses the characteristic cystatin domain with three conserved catalytic

motifs (G, QXVXG, and LW), a signal peptide, and a disulfide bond at the carboxyl terminus (Josiah Ochieng and Gautam Chaudhuri, 2010). There were tyrosine substitution (PY) of tryptophan and leucine substitution (LW) of proline in the conserved PW motif of HaCSTB and HaCSTC respectively, similar to that in zebrafish (*Danio rerio*) and Chinese sturgeon (*Acipenser sinensis*) (Bai et al., 2006), unlike in other teleost homologs such as large yellow croaker, olive flounder (*Paralichthys olivaceus*), and orange-spotted grouper (Ahn et al., 2013; Li et al., 2009; Wei et al., 2019). This replacement might not significantly alter the inhibitory function of CSTC because both proline and leucine are hydrophobic amino acids with similar isoelectric points.

Cystatin reversibly blocks the active site of cysteine proteases to impede their proteolytic activity by tightly binding to them without forming covalent bonds, which in turn does not cause any conformational changes to either of the interacting proteins (Pemberton, 2006). The 3D structure of HaCSTB complied with the models for cystatin fold from previous studies, comprising a core of a five-turn α-helix, surrounded by a four-stranded antiparallel β-sheet, and together forming a hydrophobic wedge-shape that is highly matching to the active site of cysteine proteases (Turk and Bode, 1991a). The predicted three-dimensional structure of HaCSTC conforms to the characteristic cystatin fold, with a four-turn α-helix core enveloped by a four-stranded antiparallel β-sheet, generating a hydrophobic wedge shape, compatible with the cysteine protease active site (Turk and Bode, 1991b). The

N-terminal glycine (G) is crucial for properly orienting the active site region towards the cysteine protease, having QXVXG and LW motifs in the first and second hairpin loops (Henskens et al., 1996). The cystatin superfamily consists of three main subfamilies: type 1 (stefins), type 2 (cystatins), and type 3 (kininogens). Family 1 are intracellular, unglycosylated proteins with an approximate molecular weight of 11 kDa that lack signal sequence and disulfide linkages. In contrast, family 2 are extracellular proteins with a molecular weight of 13–14 kDa, comprised of a signal sequence and disulfide linkages at the carboxyl terminus. Family 3 are glycosylated with a comparatively higher molecular weight, approximately 88–114 kDa (Josiah Ochieng and Gautam Chaudhuri, 2010).

Cystatins are implicated in a broad range of processes, including protein catabolism, hormonal regulation, bone resorption, inflammation, antigen presentation, T cell-dependent immune reaction, and immune defense against infectious pathogens (Henskens et al., 1996; Pierre and Mellman, 1998). CSTB is ubiquitously distributed in epithelial cells, lymphocytes, monocytes, the placenta, liver, and spleen, suggesting its general protective role against unrestrained lysosomal proteolytic activity (Henskens et al., 1996). CSTC was once believed to be a housekeeping gene owing to its ubiquitous expression in various tissues and body fluids without any tissue-specificity (Bobek and Levine, 1992). CSTC is produced at a consistent rate and released into body fluids such as urine, plasma, mucus, and cerebrospinal fluid (Tavéra et al., 1990). Among analyzed tissues, we observed the highest *HaCSTB* expression in

PBCs. Similarly, CSTB from disk abalone (*Haliotis discus discus*) and family 1 cystatin from the Chinese mitten crab (*Eriocheir sinensis*) exhibited higher transcript levels in hemocytes and hemolymph, which are the first-line innate immune tissues in invertebrates (Li et al., 2010; Premachandra et al., 2012a). Following its expressions in blood, *HaCSTB* expression was highest in the testes and brood pouch of the seahorse, indicating its ubiquitous expression across tissues. The seahorse brood pouch is a highly vascularized, sensitive organ, similar to the mammalian uterus, which bears a large number of fry in an enclosed environment that requires high immune protection (Tang et al., 2021). Our study found that *HaCSTC* is expressed at elevated levels in the ovaries, spleen, and brain of healthy big-belly seahorses in order. The functions of cystatins are intertwined with those of their target cysteine proteases. Proteases and their inhibitors are found abundantly in tissues with a high protein turnover (Cole et al., 1989). The main component of the ovary is hormone-producing stromal cells, and ovarian function is linked to protein metabolism because of the routine production and release of oocytes and hormones required for female reproduction (Yu et al., 2015). Proteases break down the extracellular matrix between the oocyte and follicular layer during ovulation in mammals and fish (Curry et al., 1989). To protect ovarian tissues from injury, ovulatory follicles generate corresponding inhibitors for each protease. As a result, both proteases and their inhibitors are abundant in ovarian fluid (Tsai et al., 1996). Similarly, protease inhibitory family 2 cystatin homologs are abundant in carp ovarian fluid (Tsai et al., 1996). Furthermore, human transcriptome analysis

demonstrated that 67% of total human proteins are expressed in the ovary, and the ovary has the most enriched genes in common with the brain and testis (Yu et al., 2015). Similar studies reported the spatial expression of *CSTC* homologs in the spleen and brain at elevated levels (Wei et al., 2019).

Moreover, the involvement of CSTB in the immune response against pathogenic bacteria in leech (Theromyzon tessulatum), turbot (Scophthalmus maximus), and Chinese mitten crab (Eriocheir sinensis) has been previously established (Lefebvre et al., 2004; Li et al., 2010; Xiao et al., 2010). CSTC is involved in inflammatory and immune responses at every crucial step, from pathogen invasion to elimination of later immune disorders. A previous study suggested CSTC level in body fluids as a biomarker for diagnosing various inflammatory and immune-related diseases (Werle et al., 2003). In the current study, we investigated the temporal mRNA expression of *HaCSTB* and *HaCSTC* in PBCs of big-belly seahorses against different external immune stimulants. PBCs play a key role in the homeostasis of the fish immune system through the modulation of immune-related gene expression following different immune stimuli (Puente-Marin et al., 2019; Shen et al., 2018). Moreover, white blood cells are involved in innate and acquired immunity (Abbas et al., 2005). Our study demonstrated that *HaCSTB* and *HaCSTC* transcript levels in blood were elevated in sudden response to all tested immune stimulants, including bacterial cell wall component LPS, viral mimic double-stranded RNA poly I:C, live gram-negative bacteria *E. tarda*, and live gram-positive bacteria *S. iniae* 3 h p.i., suggesting the

involvement of cystatins in the immune response. In line with our findings, similar studies showed elevated mRNA expression of *CSTC* in *P. olivaceus* and *P. crocea* in response to immune challenge with LPS, peptidoglycan, poly I:C, and inactivated bacterial vaccines (Li et al., 2009; Yu et al., 2019). Furthermore, CSTC has been reported to prevent certain viruses from replication (Björck et al., 1990; Collins and Grubb, 1991). For instance, the Singapore grouper iridovirus (SGIV) significantly raised the level of *CSTC* transcripts in the spleen of the orange-spotted grouper (Wei et al., 2019). It has also been observed that synthesized peptide derivatives of CSTC block bacterial growth by inhibiting bacterial proteases (Björck et al., 1989). LPS is an endotoxic cell wall component of gram-negative bacteria, potentially used to induce inflammation in higher animals through their interactions with receptors on leukocytes, thus activating signal transduction pathways (Suzuki et al., 2000). Several other teleost species exhibited an upregulation in *CSTB* mRNA expression upon bacterial immune challenge (Premachandra et al., 2012b; Wickramasinghe et al., 2020). In accordance, our study showed increased *HaCSTB* transcripts levels in response to live bacterial infections with *E. tarda and S. iniae* which are primary bacterial pathogens, can cause fatal hemorrhagic septicemia in fish (Li et al., 2012). In addition to bacterial immune stimuli, we also observed upregulated *HaCSTB* mRNA expression in response to viral mimic Poly I:C, suggesting that HaCSTB could perform a specific role in the immune response against both attacking viruses and bacteria in big-belly seahorse. Poly I:C is an immunostimulant that acts as a ligand for toll-like receptor (TLR) 3 and is widely

used to study viral disease-related immune reactions (Zhou et al., 2014). The indispensable contribution of CSTB against viral infections such as Ectromelia virus (ECTV), H-1 parvovirus, and white spot syndrome virus (WSSV) has been described in previous studies (Bossowska-Nowicka et al., 2019; Di Piazza et al., 2007; Zou and Liu, 2020). In line with the present findings, the immune challenge with Poly I:C significantly upregulated the mRNA expression of cystatin C in Japanese flounder (*Paralichthys olivaceus*) (Yu et al., 2019). It has also been shown that Singapore grouper iridovirus (SGIV) viral infection significantly upregulated the CSTB transcripts level in the spleen of orange-spotted grouper (*Epinephelus coioides*) (Wei et al., 2022). By contrast, CSTB is a profound inhibitor of antimicrobial proteases such as cathepsins B, H, L, and S (Pol and Björk, 2001). Moreover, the upregulation of cathepsins is essential for infection or immune stimulation, but excessive activation often leads to pathological conditions (Kagitani-Shimono et al., 2002). These results indicated that CSTB could regulate the host proteases at immune stimulation or infection. Therefore, the magnitude of upregulation or downregulation of CSTB could indirectly but critically affect the host immune responses.

At the subcellular level, CSTB generally localizes to the nuclei of proliferating cells or the cytosol, mitochondria, and nuclei of differentiated cells (Riccio et al., 2001). Maher *et al*. proposed that CSTB translocates into the mitochondria to maintain mitochondrial integrity under LPS stimulation (Maher et al., 2014). In our study, microscopic observation revealed CSTB subcellular localization in the cytosol,

mitochondria, and nuclei. CSTB colocalizes with cathepsin B in the cell-matrix and nuclear scaffold of differentiated cells while existing in separate cell compartments in proliferating cells (Riccio et al., 2001).

Papain family proteases such as cathepsins play important roles in normal cellular functions, such as protein catabolism, antigen presentation (Hsing and Rudensky, 2005), zymogen and prohormone activation, and bone remodeling (Turk et al., 2001). Apart from cystatins, other natural protease inhibitors, such as thyrophins and serpins, also maintain the balance in proteolytic activity (Lenarčič and Bevec, 1998; Turk et al., 1997). CSTB plays a pivotal role in controlling the proteolytic activities of cathepsins within the nucleus to protect protein molecules, such as transcriptional factors, from proteolytic degradation (Ceru et al., 2010). In our study, both rHaCSTB and rHaCSTC exhibited potent protease inhibitory activity. Similarly, CSTB from rock bream and CSTC from *P. olivaceus* showed concentration-dependent papain inhibition (Premachandra et al., 2012b). Further analysis revealed that the inhibitory activity of rHaCSTB is affected by pH and temperature, consistent with previous findings on CSTB from *Schistosoma japonicum* (Yang et al., 2014). In contrast to our findings, a previous study reported that recombinant cystatin from black rockfish (*Sebastes schlegelii*) exhibited significant thermal stability at 90 ºC for one hour (Wickramasinghe et al., 2020).

Cystatins might suppress the replication of some viruses by inhibiting the cysteine proteases, which are crucial for viral replication, thus highlighting the

potential of cystatins as antiviral agents (Björck et al., 1990; Collins and Grubb, 1998). Interestingly, we observed that overexpression of both HaCSTB and HaCSTC in FHM cells increased cell viability and reduced the expression of viral transcripts after viral infection unfolding its immune response against viral infections in seahorses. These findings are consistent with a recent study, which reported that the overexpression of CSTC from *E. coioides* suppressed the replication of SGIV and viral-induced apoptosis in grouper spleen cells (Wei et al., 2019). In addition, previous research revealed the antiviral effect of CSTC against several viruses, including hepatitis C virus, human immunodeficiency virus, and feline immunodeficiency virus (Bandivdekar et al., 2015; Behairy et al., 2012; Ghys et al., 2016). Furthermore, chicken cystatin has been proven to inhibit poliovirus replication in human cells [9] partially. A short peptide derivative resembling part of the proteinase-binding site of human CSTC could suppress cysteine proteases that are exclusive for the growth of a group of streptococci, inhibiting their proliferation (Björck et al., 1989). Likewise, recombinant human CSTC inhibits the proliferation of the herpes simplex virus and human coronaviruses (Björck et al., 1990).

Apoptosis plays an essential role in the immune system. It involves numerous immunological functions, including eliminating infected and tumor cells, self-reactive lymphocytes, and activated immune cells to prevent unnecessary immune reactions after clearing infections [29]. Apoptosis is typically characterized by cell shrinkage, membrane blebbing, and DNA condensation due to hydrolytic enzymes (Wyllie, 1980).

Cathepsins released by lysosomes might trigger apoptosis by damaging cytoskeletal and nuclear proteins, DNA repair enzymes, or DNA through activation of caspases (Vancompernolle et al., 1998). CSTC demonstrated an anti-apoptotic effect by inhibiting cathepsin B-induced DNA fragmentation via endonucleases and by inhibiting cathepsin C-mediated pro-granzyme cleavage (Zi and Xu, 2018). The regulatory role of CSTC in apoptosis is quite controversial because numerous studies have reported both anti- and pro-apoptotic functions of CSTC (Zi and Xu, 2018). CSTC also promotes apoptosis by decreasing anti-apoptotic Bcl-2 expression and increasing pro-apoptotic Bid expression, which in turn causes the mitochondrial release of Cyc (Liang et al., 2011). On the contrary, our study showed an anti-apoptotic effect of HaCSTC. HaCSTC caused higher VHSV-induced anti-apoptotic *Bcl-2* expression, reduced pro-apoptotic *Bax* and *Cyc* expression, and resulted in a lower *Bax/Bcl2* ratio, indicating an anti-apoptotic effect since a higher *Bax/Bcl2* ratio is critical in determining apoptotic pathway activation.

Bcl-2 and Bax are essential Bcl-2-like family proteins that regulate intrinsic apoptosis, exerting anti- and pro-apoptotic effects, respectively (Cui and Placzek, 2018). Pro-apoptotic Bax oligomerization causes the release of Cyc from the mitochondrial intermembrane space to the cytosol to induce apoptosome formation and subsequent caspase-3 activation to continue cell death in the intrinsic apoptotic pathway. At the same time, Bcl-2 protein is suppressed (Li et al., 1997).

To confirm our findings, we observed nuclear condensation, DNA fragmentation, and apoptotic body formation in Hoechst-stained VHSV-infected FHM cells. Consistent with our study, previous research demonstrated that Rhabdovirus- and Iridovirus-induced apoptosis in fish cell lines is suppressed by cystatins by blocking cathepsin B and its downstream caspases to protect cells from death (Björklund et al., 1997; Wei et al., 2019). CSTC suppressed SGIV-induced apoptosis and reduced caspase-3 activity in FHM cells, suggesting that it regulates SGIV-induced apoptosis (Wei et al., 2019). Thus, CSTC could be a promising target molecule for treating inflammatory autoimmune disorders by modifying its dual roles in apoptosis in different cell types under different conditions.

2.5. Conclusion

In conclusion, CSTB and CSTC homologs (HaCSTB and HaCSTC), in the big-belly seahorse were identified and described to highlight their involvement in host immunological defense. HaCSTB showed evolutionary proximity to CSTB homologs from teleosts, whereas HaCSTC showed evolutionary proximity to CSTC teleostean homologs, both containing all conserved catalytic motifs typical of type I and type II cystatin family. Both *HaCSTB* and *HaCSTC* were upregulated in response to LPS, Gram-positive and -negative bacteria, and viral analogs. Both rHaCSTB and rHaCSTC displayed dose-dependent, strong *in vitro* papain inhibitory activity. Furthermore, HaCSTB and HaCSTC overexpression exhibited potent antiviral effects by increasing the FHM cell viability and downregulating the expression of the viral transcripts after

VHSV infection. In addition, overexpression of HaCSTB and HaCSTC in FHM cells reduced the viral-induced apoptosis. These findings may shed light on the involvement of CSTB and CSTC in the immunological response of seahorses to harmful viruses and bacteria.

CHAPTER 2

Molecular characterization of Cyclooxygenase 2 from Red-spotted grouper (*Epinephelus akaara*) & its involvement in host immune defense mechanism

3.1. Introduction

Prostaglandins are lipid-based signaling molecules that exert a multitude of pathophysiological functions including inflammation, mediating pain, cardiovascular homeostasis, reproduction, angiogenesis, and carcinogenesis by signaling through G-protein coupled cellular receptors (Wun et al., 2004). Cyclooxygenases (COX), prostaglandin H synthases, or prostaglandin-endoperoxide synthases are the rate-limiting enzymes that biosynthesize the prostaglandins from arachidonic acid in nuclear and plasma membranes at the first step (Wun et al., 2004). There are two isoforms of cyclooxygenases such as constitutive COX-1 and inducible COX-2. COX-1 is constitutively expressed in various tissues and cells, by contrast, COX-2 is dramatically upregulated in response to various stimuli including mitogens, cytokines, and growth factors (Williams et al., 1997; Wun et al., 2004). In addition, COX-2 has been implicated in the development of several ailments such as inflammation, atherosclerosis, diabetic nephropathy, and tumor growth (Hua et al., 2015). COX-2 is a target of non-steroidal anti-inflammatory drugs (NSAIDs) therapies, for example, COX-2 selective inhibitors (COXIBs), treating different ailments such as pain, fever, rheumatoid arthritis, osteoarthritis, and cancer (Turini and DuBois, 2002).

COX-2, as an immediate-early response gene, is induced by bacterial lipopolysaccharides, and cytokines such as interleukin IL-1, IL-2, and tumor necrosis factor TNF-α which are associated with inflammation (Vane et al., 1998). Various pathogens use their virulence strategies to induce the COX-2 transcription via JNKs

and p38 MAPK-dependent NF-κ B and AP-1 activation and thereby COX-2 derived prostaglandins are released in large quantities during primary infection (Hua et al., 2015).

Although COX-2 is a comprehensively studied mammalian dioxygenase, its molecular mechanism behind the teleost immune defense system should be further disclosed. COX-2 expression was reported to be induced during parasitic infections by *Myxobolus cerebralis*, *Tetracapsuloides bryosalmonae*, and *Gyrodactylus derjavini* in some fish species, rainbow trout (*Oncorhynchus mykiss*) and sea bream (*Sparus aurata*) (Lindenstrøm et al., 2004; Severin and El-Matbouli, 2007). Immune stimulation with LPS was linked with the upregulation in COX-2 expression in fish cell lines from goldfish (*Carassius auratus*) (ZOU et al., 1999), Atlantic cod (*Gadus morhua*) (Holen and Olsvik, 2016), rainbow trout (*Oncorhynchus mykiss*) (Chettri et al., 2011), and zebrafish (*Danio rerio*) (Hwang et al., 2016; Ryu et al., 2015). It indicates that COX-2 might contribute to enhancing inflammation during the early stages of infection by producing prostaglandins and both COX-2 and its metabolite, prostaglandin play a key role in the immune system.

In the current study, COX-2 homolog, designated as EaCOX2, was identified and characterized from the red-spotted grouper, *Epinephelus akaara*, unveiling its potent immune role. *EaCOX2* transcription profiles were analyzed under both healthy and immune-challenged conditions in red-spotted grouper. The effect of EaCOX2 overexpression in fathead minnow cells (FHM) cell was determined on cell viability.

Moreover, the pro-inflammatory effect of EaCOX2 overexpression in murine macrophages (RAW264.7) was analyzed by determining the NO production and macrophage polarization.

3.2. Materials and methods

3.2.1. Identification and *in-silico* analysis of EaCOX2

The coding sequence of putative *EaCOX2* was deduced from an established grouper transcriptome database, using the Basic Local Alignment Search Tool (BLAST) program curated at the National Center for Biotechnology Information (NCBI) (McGinnis and Madden, 2004). The deduced amino acid sequence for the EaCOX2 open reading frame (ORF) and the protein domains were obtained using Unipro UGENE software (Okonechnikov et al., 2012) and the ExPASy Prosite (Sigrist et al., 2013) respectively. The ExPASy ProtParam tool was used to analyze the physicochemical properties of the EaCOX2 protein. Pairwise and multiple sequence alignments were created with orthologous EaCOX2 protein sequences to compare the identity and similarity using the EMBOSS needle (Rice et al., 2000) and the ClustalW2 programs (Larkin et al., 2007), respectively. A phylogenetic tree was constructed using the MEGA7.0.26 software with the neighbor-joining method (Kumar et al., 2016). Five thousand bootstrap replications were taken to assess nodal support.

3.2.2. Fish husbandry

Healthy red-spotted grouper fish, with an average body weight of 68 g, were obtained from the Marine Science Institute, Jeju National University, South Korea Seahorses (NCBI taxonomy: 215347). The fish were acclimatized in 300 L aerated seawater tanks at 26 ± 2 °C and 34 ± 0.6 g/L of salinity and fed a commercial fish feed once per day for one week before the investigation. The approved guidelines by the Animal Care and Use Committee of Jeju National University were adopted during the experiment.

3.2.3. Immune challenge experiment and tissue collection

To analyze the spatial expression of *EaCOX2*, five unchallenged, healthy fish were taken. Altogether, 12 types of tissues were collected including the head kidney, spleen, gill, trunk kidney, intestine, stomach, heart, brain, liver, muscle, and skin. Blood was harvested from the caudal vein of the fish and peripheral blood cells were collected by centrifugation at 3000×g at 4 °C for 10 min. After the tissue collection, they were snap-frozen in liquid nitrogen for storage at -80 °C.

For the challenge experiment, healthy fish were separated into four groups of 35 individuals. For the control group, 100 μL of PBS was injected intraperitoneally. The other three groups of fish were intraperitoneally administered with 100 μL of the bacterial endotoxin LPS (5 μg/g; Sigma-Aldrich, St. Louis, MO, USA), poly(I:C) (5 μg/g; Sigma), and a live form of nervous necrosis virus (NNV; 1×10^6 $TCID_{50}$/mL) separately. Afterward, blood samples were collected at 0, 6, 12, 24, 48, 72, and 120h

post-injection (p.i.) from five individuals per group, and frozen in liquid nitrogen for storage at -80 °C.

3.2.4. RNA isolation and cDNA synthesis

Total RNA was extracted with RNAiso plus reagent (TaKaRa, Japan). The extracted RNA was purified using the RNeasy spin column (Qiagen, USA). The RNA purity and concentration were measured with a Multiscan™ GO Microplate Spectrophotometer (Thermo Fisher Scientific, Waltham, MA, USA) and the integrity of RNA was verified by 1.5 % agarose gel electrophoresis. The cDNA was synthesized using the PrimerScript™ II 1st strand cDNA Synthesis Kit (TaKaRa, Japan) from 2.5 μg of total RNA. Following, the synthesized cDNAs were diluted to 40-fold and stored at -20 ºC for further use.

3.2.5. EaCOX2 transcription analysis by quantitative real-time PCR (qPCR)

The *EaCOX2* transcription profile was analyzed in healthy and immune-challenged red-spotted groupers by qPCR using synthesized cDNA samples as a template and a thermal cycler Dice™ TP950 (TaKaRa). All gene-specific qPCR primers (Table 3) were constructed using the IDT Primer Quest online Tool (https://sg.idtdna.com/Primerquest/Home/Index) according to the MIQE guidelines (Owczarzy et al., 2008). The qPCR mixture (10 μL) contained 3 μL of cDNA template, 5 μL of TaKaRa 2 × Ex Taq™ SYBR premix, 0.4 μL of each forward and reverse primer (10 pmol/μL), and 1.2 μL of nuclease-free water. Triplicate runs were

performed for each experiment and the following qPCR parameters were used; single cycle at 95 °C for 10 s, followed by 45 cycles at 95 °C for 10 s, 58 °C for 10 s, and 72 °C for 20 s, and a melting cycle at 95 °C for 15 s, 60 °C for 30 s, and 95 °C for 15 s. The elongation factor 1-β (Genbank accession number- MZ747613) was used as the housekeeping gene to normalize the *EaCOX2* expression using the Livak $2^{-\Delta\Delta CT}$ method (Livak and Schmittgen, 2001).

For spatial expression analysis, normalized Ct values of *EaCOX2* were expressed as fold values against the lowest expression level, obtained for a particular tissue.

For temporal expression analysis, the Ct values of *EaCOX2* were expressed as fold values against the 0 h control group after normalizing it to the corresponding PBS-injected controls at each time point. Data were analyzed using Student's *t*-test at a significance level of $p < 0.05$.

3.2.6. Construction of recombinant *EaCOX-2* expression vectors, cell culture, and transfection

Cloning primers with corresponding restriction recognition sites were designed using the IDT oligo analyzer tool (https://sg.idtdna.com/calc/analyzer) as listed in Table 3. The ORF of *EaCOX-2* was amplified by PCR using the pre-designed primers and cDNA template under the following PCR protocol: initial denaturation at 94 ºC for 5 min; 30 cycles of amplification at 94 ºC for 30 s, 58 ºC for 30 s, 72 ºC for 1 min, and a final extension at 72 º C for 7 min. The reaction mixture (50 μL) contained 50 ng of template, 4 μL of 2.5 mM dNTPs, 5 μL of 10 × ExTaq buffer, 4 μL of 10 pmol of

each primer, and 0.2 μL of 3 units of ExTaq polymerase. The amplified *EaCOX-2* sequence was cloned into the pcDNA™ 3.1$^{(+)}$ (Invitrogen, Waltham, MA, USA) vector using the restriction sites *BamHI*/*Apa*I (Table 3). For that, the PCR product and the pcDNA™ 3.1$^{(+)}$ vector were digested using bands at the desired molecular size and were cut and purified using the Accuprep® gel purification kit (Bioneer Co., Korea). Ligation was carried out at 16 °C for 30 min with Ligation Mighty Mix (5.0 μL; TaKaRa Bio Inc.) and incubated overnight at 4 °C. By using the heat-shock method, the ligated product was transformed into *Escherichia coli* (*E. coli*) DH5α competent cells, and the successful clones were confirmed by sequencing and plamids were purified using the QIAfilter™ Plasmid Midi Kit (Qiagen, Germany).

FHM cells were grown in Leibovitz's L-15 medium (Sigma-Aldrich) containing 10% fetal bovine serum (FBS; Sigma-Aldrich) and 1% Gibco™ Penicillin-Streptomycin (Thermo Fisher Scientific) at 25 °C.

RAW264.7 murine macrophage cells were cultured in complete Dulbecco's modified Eagle's medium (DMEM; Sigma, USA) with 5% FBS (Sigma, USA) and 1% penicillin, and incubated at 37 °C and 5% CO2.

After the cells reached 80% confluence, the cells were transfected with EaCOX2-pcDNA™ 3.1$^{(+)}$ and Empty-pcDNA™ 3.1$^{(+)}$ expression vectors according to the standard protocol using X-tremeGENE™ 9 (Roche Diagnostics GmbH, Mannheim, Germany).

Table 3: Sequences of primers used in this study

Name	Sequence (5′- 3′)	Purpose	
EaCOX2-4-cF	GAGAGAggatccATGATGAACAGATTCACATT TGCGGTTTTCC	Cloning	
EaCOX2-cR	GAGAGAgggcccTTAGAGCTCAGTAGTCCTTT TTTTCAAAATGACTGTG	Cloning	
EaCOX2-qF	TGGCACCCTCTGATGCCTGATA	qPCR	
EaCOX2-qR	ACCCGTCCAGCAATCTGCTTTG	qPCR	
Elongation factor 1-β (EF1-β)	CCACATCAAATCCTACCAGAGCCAGA	qPCR reference	internal
Elongation factor 1-β (EF1-β)	GTCGTCGTCCTCCTCGTCATCTTT	qPCR reference	internal

3.2.7. Functional assays

3.2.7.1. Determination of cell viability by WST-1 assay

To determine the protective effect of EaCOX2, a cell viability assay was performed using WST-1 (Takara Bio Inc.) according to the manufacturer's protocol after the treatment with lipopolysaccharide (LPS; 1 μg/mL) (10μg/mL). Briefly, FHM cells were seeded into 24-well plates at a cell concentration of 5×10^5 cells/mL and kept for 24 h at 25 °C. The cells were then transfected with the EaCOX2-pcDNA™ $3.1^{(+)}$ expression and empty pcDNA™ $3.1^{(+)}$ vectors (control) and incubated at 25 °C for 24 h. Afterward, FHM cells were treated with LPS (10 μg/mL) and incubated at 25 °C for 24 h. After a mild cytopathic effect was observed under a microscope (Leica Microsystems, Wetzlar, Germany), WST-1 reagent was added to the cells, incubated for 10 min, and absorbance was measured using a Multiskan SkyHigh Microplate Spectrophotometer (Thermo Fisher Scientific) at 440 nm with 690 nm as the reference wavelength.

3.2.7.2. Flowcytometry assay

Flow cytometry analysis was conducted to quantitatively evaluate the effect of EaCOX2 overexpression on cell apoptosis using propidium iodide (PI) according to a previously established method (Piao et al., 2022). FHM cells were transfected with EaCOX2-pcDNA™ 3.1(+) expression and empty pcDNA™ 3.1(+) vectors (control) and incubated at 25 °C for 24 h. Afterward, the cells were centrifuged (100g, 10 min, 10 °C) and fixed in 70 % ethanol. Then, the cells were washed twice with 2 mM EDTA solution and stained for 30 min with PI (100 μg/mL). Eventually, the apoptotic cell percentage (percentage of sub-G1 cells) was analyzed by BD FACSCalibur™ flow cytometer (Becton Dickinson, San Jose, CA, USA) and CellQuest and ModFit Software (Becton Dickinson, SanJose, CA, USA).

3.2.7.3. Determination of macrophage polarization

RAW264.7 murine macrophage cells were cultured in Nunc®Lab-Tek® chamber slide (1×10^5 cells/mL) and transfected with EaCOX2-pcDNA™ 3.1(+) expression and empty pcDNA™ 3.1(+) vectors (control), followed by 24 h incubation at 37 °C and 5% CO2. To determine the effect of EaCOX2 overexpression on macrophage polarization, the cells were then fixed with 3% formaldehyde and stained with Cytopainter Phalloidine–iFluor 594 staining kit (Abcam, UK)according to the manufacturer's protocol. The nucleus of the fixed cells were stained with NucBlue™ Fixed Cell Ready Probes™ Reagent (DAPI) (Invitrogen, USA). Fluorescent images of the cells (400 ×) were obtained using the Leica DM 6000B imaging system.

3.2.7.4. Nitric oxide (NO) production assay

NO production was determined using the Griess reagent (Udayantha et al., 2021). RAW264.7 cells were seeded into 96-well plates at a cell density of 1×10^5 cells/mL using the same conditions described in section 2.7.1. Then, they were transfected with recombinant EaCOX2-pcDNA™ $3.1^{(+)}$ expression vector and the empty pcDNA™ $3.1^{(+)}$ vector. (control). After 24 h of incubation, the cells were treated with LPS (0.1 μg/mL) to induce NO production. Subsequently, Griess reagent (1: 1 ratio of 1% sulfanilamide in 30% acetic acid and 0.1% N-(1-naphthyl) ethylenediamine dihydrochloride in 60% acetic acid) was added and incubated for 10 minutes at dark conditions in room temperature. Finally, the absorbance was measured at 540 nm using a Multiskan SkyHigh Microplate Spectrophotometer (Thermo Fischer Scientific, USA).

3.2.10. Statistical analysis

All experiments were performed in triplicate, and the data are presented as the mean ± standard deviation (SD). The statistical significance of spatial expression and immune stimulation experiment was analyzed using one-way analysis of variance (ANOVA) using Duncan's test and student's t-test respectively ($p < 0.05$).

3. 3. Results

3.3.1. Identification and sequence characterization of EaCOX2

The cDNA sequence of the *EaCOX2* gene was identified by searching the cDNA library of *E. akaara*. The cDNA sequence is 1827 bp in length, encoding a polypeptide chain of 608 amino acids with a combined molecular weight of 70 kDa. The estimated isoelectric point (p*I*) was 6.91. This protein is an extracellular protein with signal peptides. According to the NCBI-conserved domain database, the EaCOX2 protein contains two conserved domains, a membrane-binding domain (prostaglandin-endoperoxide synthase) and a catalytic domain (calcium-binding EGF-like domain) (Figure 15A). The amino terminus of the protein contains a single epidermal growth factor (EGF) module. The catalytic domain has two distinct active sites; cyclooxygenase and peroxidase. The center of the catalytic domain contains heme-binding sites which are anchored by the active site of the enzyme (Figure 1). The predicted 3D structure of EaCOX2 is a homodimer and the catalytic domain consists of alpha-helical structures (Figure 15B). The protein contains five glycosylation sites at N56, N93, N133, N399, and N584 which are essential for protein folding and stability.

According to the pairwise sequence alignment, EaCOX2 showed the highest sequence identity (99.0 %) and similarity (99.0 %) with *Epinephelus lanceolatus.* The multiple sequence alignment showed its high conservation among vertebrates with slight differences in the dimerization, membrane-binding, and substrate-binding

domains among other COX2 orthologs (Fig.16A). A phylogenetic tree was constructed based on the protein sequence and the results revealed that EaCOX2 was clustered in the fish group of COX2 homologs showing evolutionary proximity to *E. lanceolatus* (Fig. 16B.).

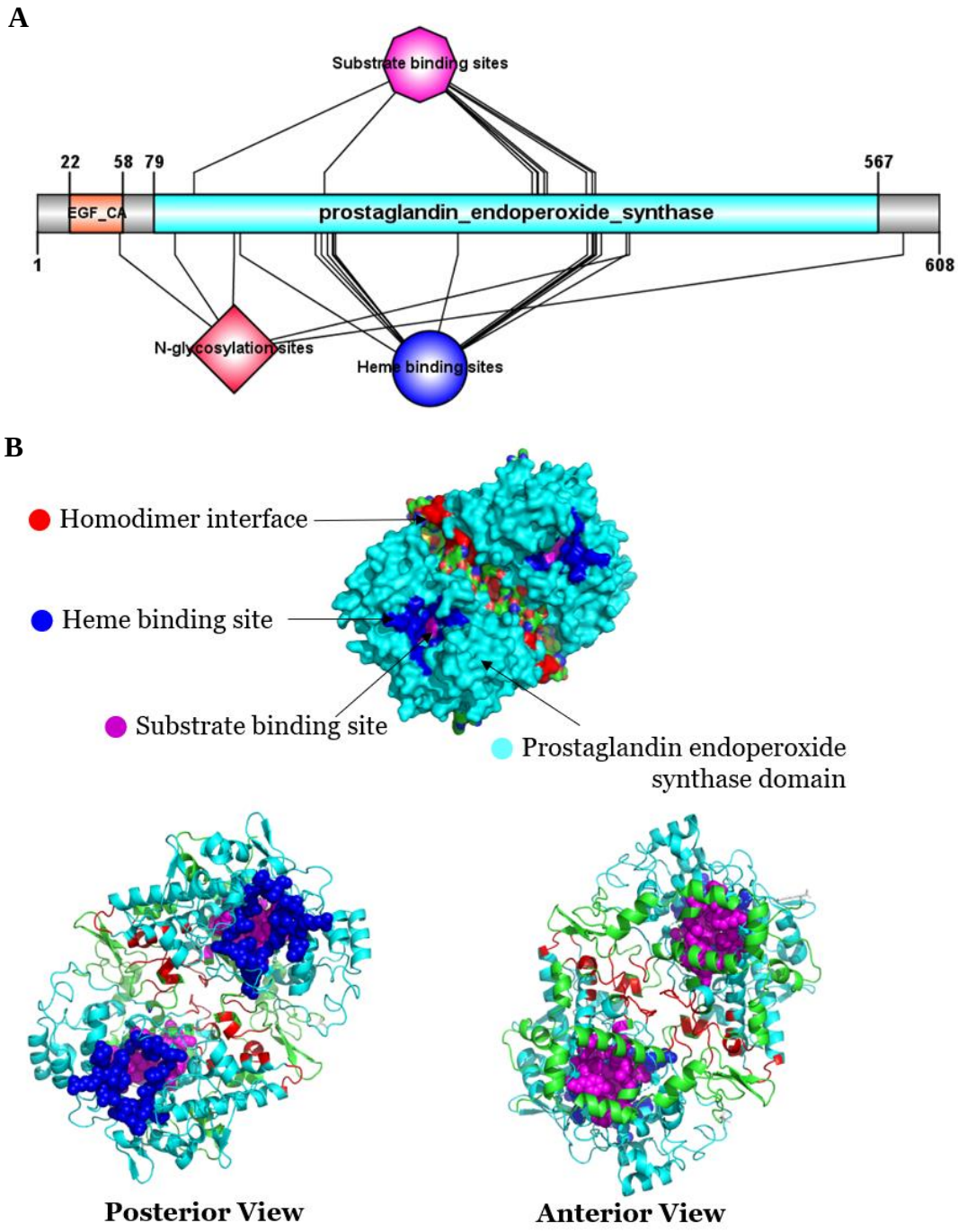

Fig.15. (A). EaCOX2 protein domain architecture, **(B).** the predicted three-dimensional structure of EaCOX2 protein.

The catalytic domain, heme binding sites, substrate binding sites, and homodimer interface are indicated in light blue, dark blue, pink, and red respectively.

A

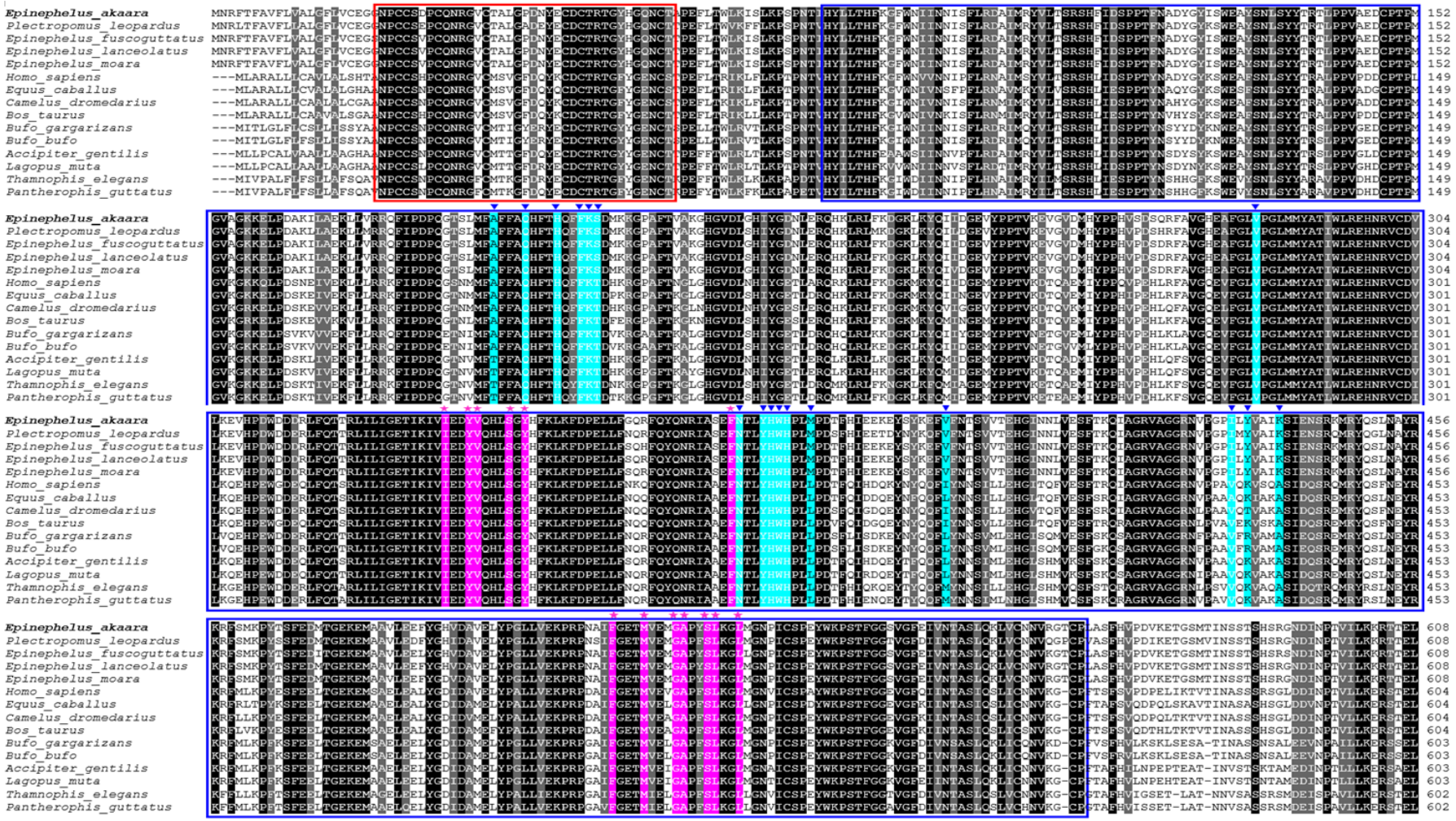

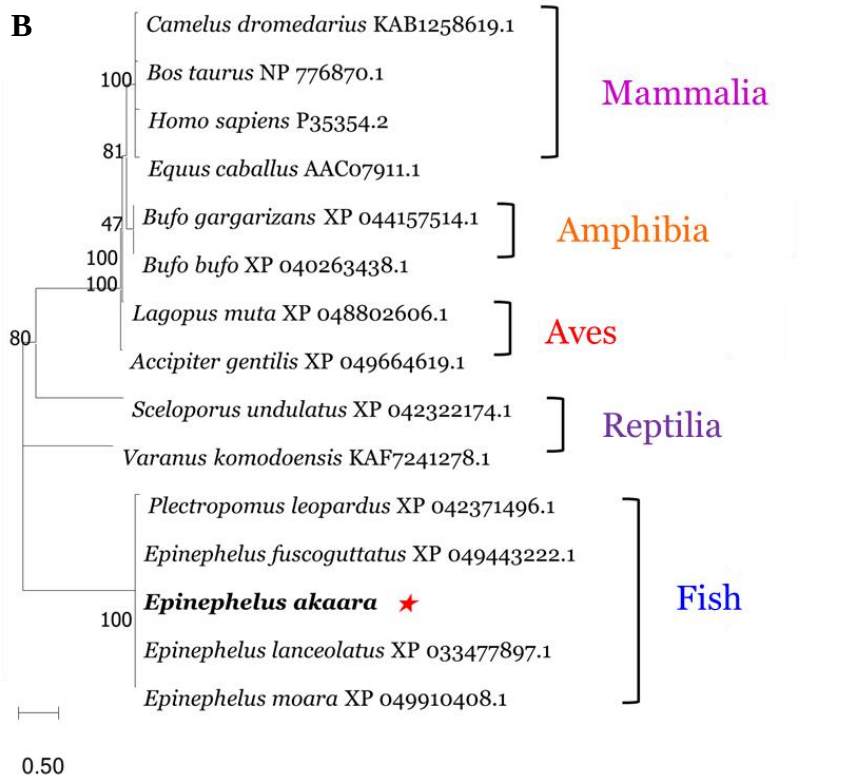

Fig.16. (A). Multiple sequence alignment of EaCOX2 with other vertebrate orthologs. **(B).** The phylogenetic tree of EaCOX2 and other COX2 orthologs.

Amino acids highlighted in black, and grey indicates fully and partially conserved regions of the sequences, respectively. Calcium binding EGF-like domain (membrane-binding) and Prostaglandin endoperoxide synthase domain are indicated in red and blue colored boxes respectively. Substrate binding sites and heme-binding sites are indicated with "★" and "▼" symbols.

3.3.2. Spatial expression pattern of *EaCOX2*

The expression of the mRNA transcript of *EaCOX2* in different tissues was analyzed using qPCR. The tissue-specific distribution revealed that *EaCOX2* showed significantly the highest expression (p <0.05) in gills (~ 265.2 fold) followed by the

skin (~ 91.6 fold) and kidney (~ 62.1 fold). While the liver contained the lowest mRNA level and it was defined as the basal level (Fig. 17.).

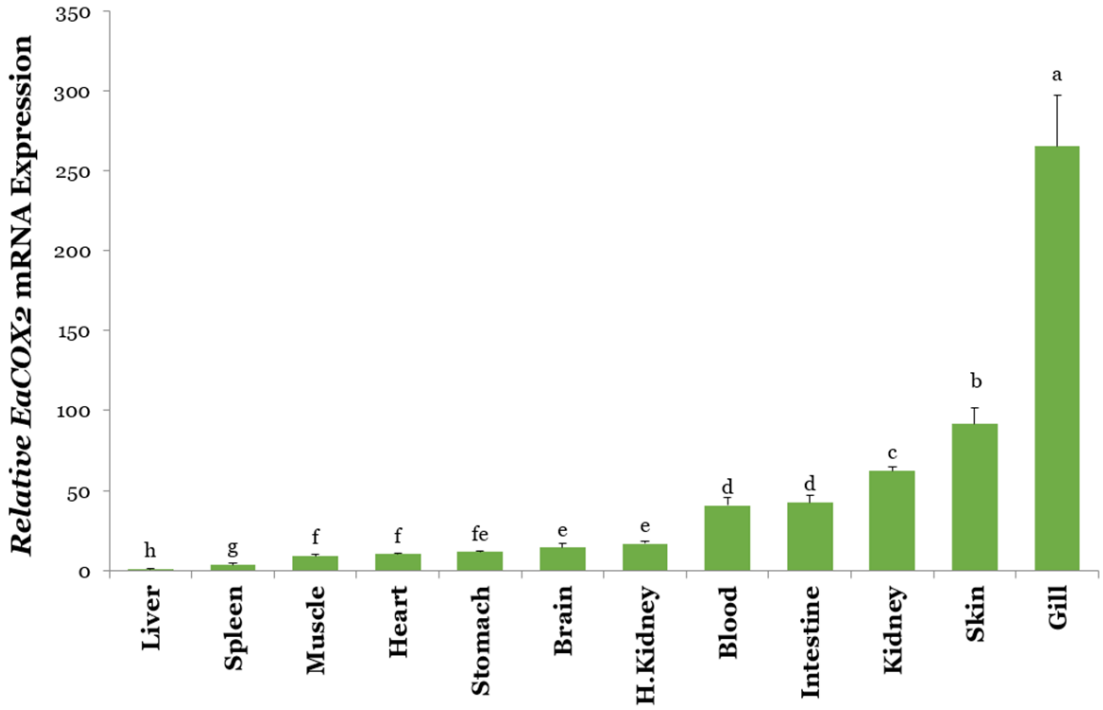

Fig.17. The spatial transcriptional analysis of *EaCOX2* in different tissues of *E. akaara.*

Ct values were normalized to the internal control and expressed as fold values against values from the tissue with the lowest expression. Statistical analysis of tissue expression data was performed using one-way analysis of variance (ANOVA), and significant differences ($p < 0.05$) were indicated by different lowercase letters.

3.3.3. Temporal expression of *EaCOX2* after immune challenge

Temporal mRNA expression patterns of EaCOX2 in gills were determined in response to the immune challenge with LPS (bacterial wall component), Poly I: C (double-stranded viral mimic), and the live NNV relative to the PBS-treated control. *EaCOX2*

transcripts were significantly upregulated (p <0.05) at 12 h and 24 h post-infection (p.i) after immune challenge with LPS, poly I: C, and live NNV, followed by recuperation (Figure 18).

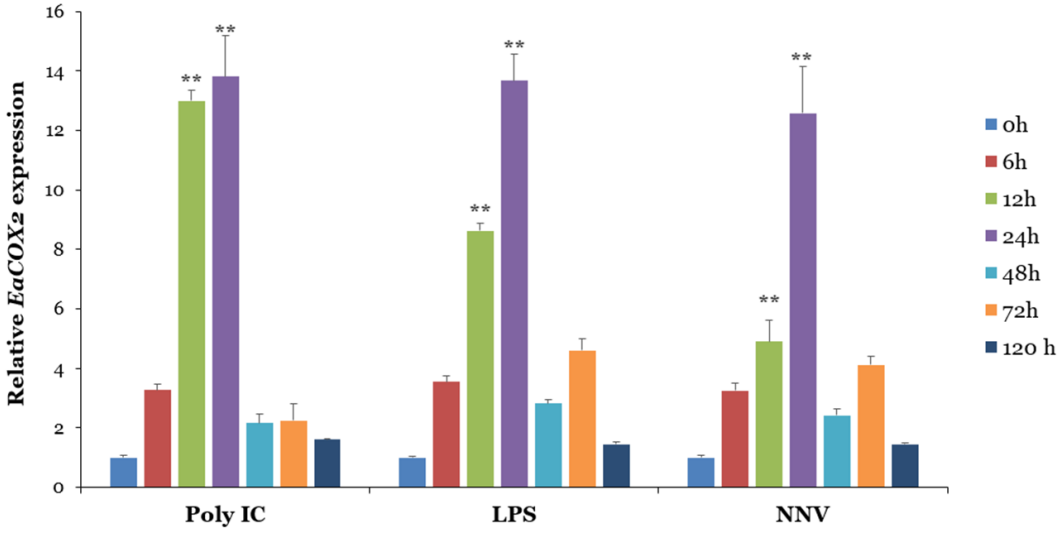

Fig.18 Temporal expression of *EaCOX2* in gills of *E. akaara*, upon immune stimulation.

Ct values were normalized to both the internal control and PBS-injected control at each time point and expressed as fold values with respect to the 0 h control. Comparisons for the immune challenge data were carried out using the Student's t-test, and significant differences compared to the 0h control were denoted with a double asterisk ("**", $p < 0.01$).

3.3.4. the effect of EaCOX2 overexpression on FHM cell viability

WST-1 assay was performed to determine the effect of EaCOX2 on the FHM cell viability. The result disclosed that the survival cell percentage is significantly lower in

EaCOX2 overexpressing FHM cells (EaCOX2-pcDNA™3.1(+)) compared to the pcDNA™ 3.1(+) vector-transfected counterparts both with and without the LPS treatment (10μg/mL) ($p < 0.05$) (Figure 19).

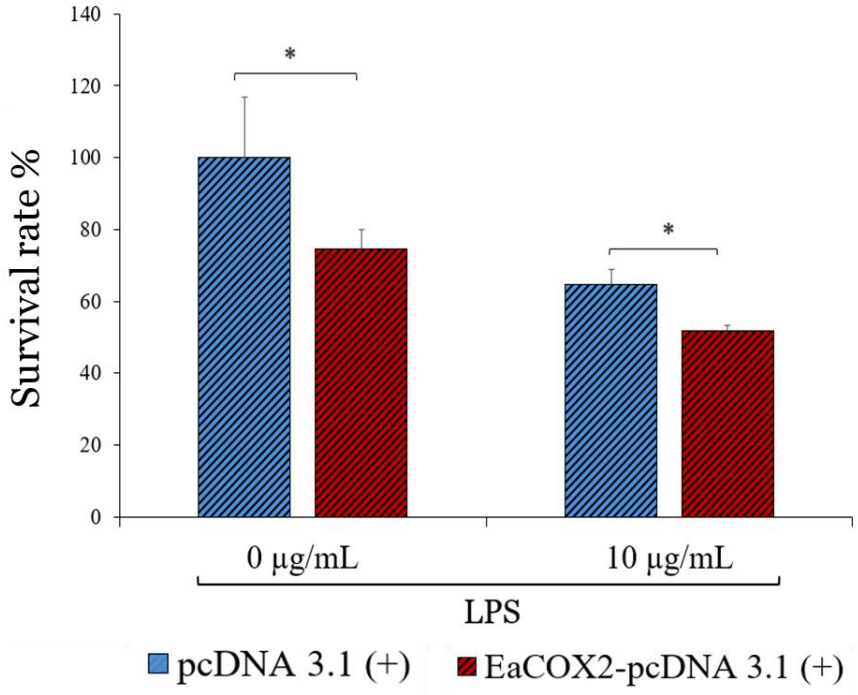

Fig.19. The cell survival rate of FHM cells transfected with EaCOX2-pcDNA and pcDNA 3.1(+) after 24 h lipopolysaccharide (LPS)-treatment.

Error bars represent the means ± SD (n = 3).). Asterisks indicate significant differences ("*", $p < 0.05$ or "**", $p < 0.01$) compared to the respective pcDNA control (Student's t-test).

3.3.5. The effect of EaCOX2 overexpression on apoptosis

The effect of EaCOX2 overexpression on the FHM cell apoptosis was quantitively evaluated by flow cytometry analysis using the PI stain. Flow cytometry analysis

demonstrated that the apoptotic cell percentage of EaCOX2-overexpressing FHM cells was significantly higher than the pcDNA™ 3.1(+) vector-transfected counterparts (Figure 20).

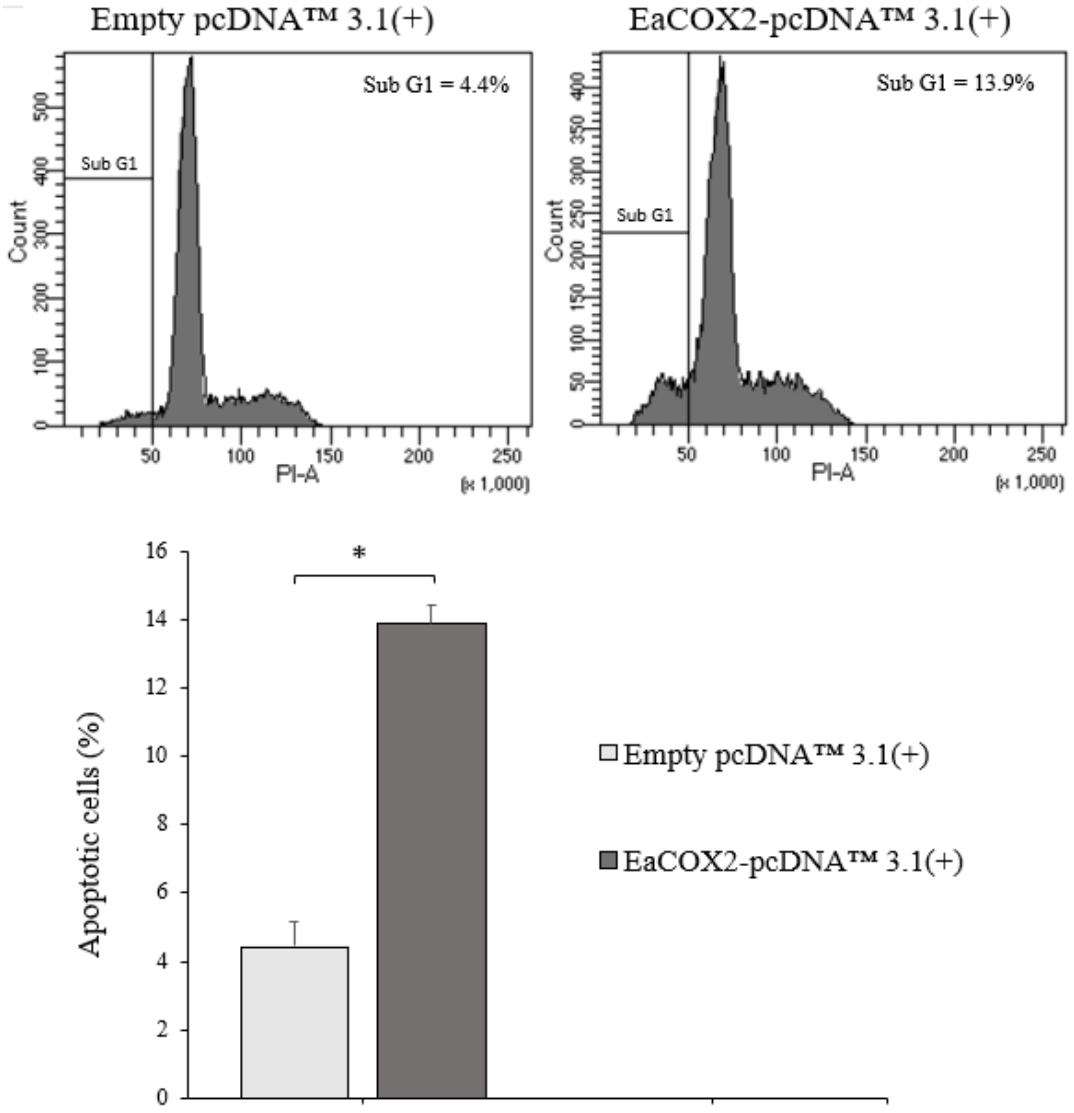

Fig.20. Flow cytometry analysis of apoptotic cells percentage.

Asterisks indicate significant differences ("*", $p < 0.05$) compared to the respective pcDNA control (Student's t-test).

3.3.6. The effect of EaCOX2 overexpression on macrophage polarization

The effect of EaCOX2 on macrophage polarization was observed using fluorescent microscopy in EaCOX2 overexpressing RAW264.7 cells (Figure 21). EaCOX2 overexpressing macrophages (EaCOX2-pcDNA™3.1(+)) exhibited classical M1 type macrophage polarization. M1 polarized cells are more elongated, stretched, or dendritic in morphology compared to the pcDNA™3.1(+) vector-transfected counterparts which are more rounded or circular (Figure 21).

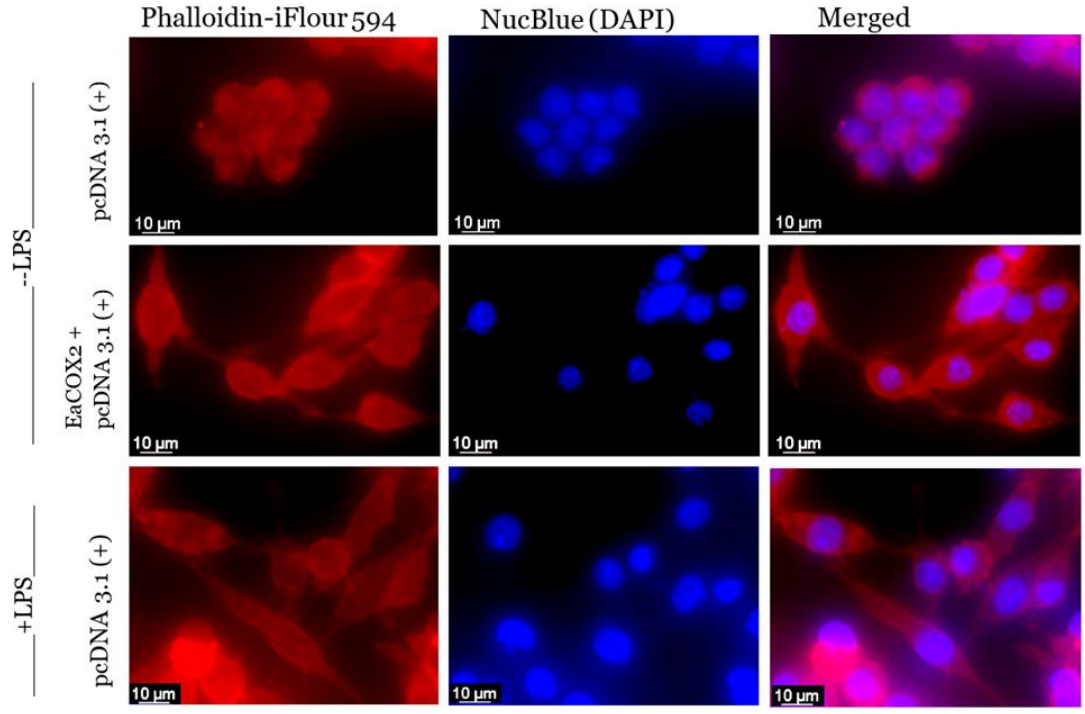

Fig.21. Fluorescent microscopy images of RAW 264.7 cells transfected with EaCOX2-pcDNA and pcDNA 3.1(+).

3.3.7. The effect of EaCOX2 overexpression on NO production

Griess assay was performed to determine the effect of EaCOX2 on the NO production in RAW264.7 cells after treatment with LPS (0.1 µg/mL). The results disclosed that

after 12 h of LPS stimulation, NO production is significantly increased in both empty pcDNA™3.1(+) (control) and EaCOX2-pcDNA™3.1(+) transfected RAW264.7 cells ($p < 0.05$) (Figure 7A). Nevertheless, NO production is significantly higher in EaCOX2 overexpressing cells compared to that in the control cells ($p < 0.05$) (Figure 22).

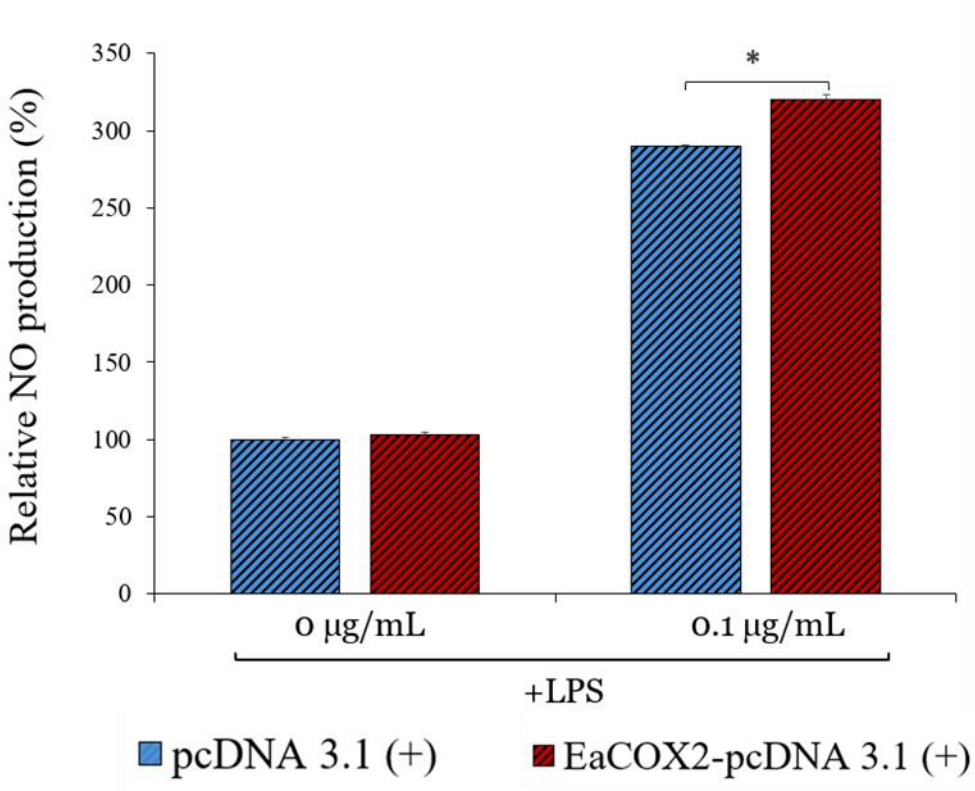

Fig.22. NO production by empty pcDNA™3.1(+) (control) and EaCOX2-pcDNA™3.1(+) transfected RAW264.7 cells after 12 h lipopolysaccharide (LPS)-treatment.

Error bars represent the means ± SD (n = 3).). Asterisks indicate significant differences ("*", $p < 0.05$ compared to the respective pcDNA control (Student's t-test).

3.4. Discussion

COX-2 is a comprehensively studied and well-explained mammalian cyclooxygenase that is the primary target of anti-inflammatory drug therapies such as COX-2-selective inhibitor celecoxib to treat rheumatoid arthritis, atherosclerosis, osteoarthritis, Alzheimer's disease, and cancer (McCormack et al., 2011). Notwithstanding, comprehension of teleostean COX2 is still dawning compared to mammalian COX-2. The current study was undertaken to comprehend the molecular and functional properties of the teleostean homolog of COX-2 from *E. akaara*.

Cyclooxygenases are members of the myeloperoxidase superfamily which catalyze the rate-limiting step of the biosynthesis of prostaglandins, lipid mediators involved in inflammatory responses (Daiyasu and Toh, 2000). As with all other COX-2 orthologs, EaCOX2 encodes a polypeptide chain of around 600 amino acids with approximately 70 kDa molecular weight (Michael Garavito et al., 2002) COXs are highly conserved with slight changes in the membrane-binding and catalytic domains and amino-terminal signal peptides among other organisms (Chandrasekharan et al., 2002). There are two types of COX isomers; constitutively expressed COX-1 and inducible COX-2 which share a 60% of sequence similarity (Fitzpatrick, 2004). According to the sequence analysis, COX-2 was highly conserved among vertebrates and EaCOX2 showed evolutionary proximity to teleosts. Studies on mammals disclosed that COX-2 protein harbors three conserved domains, an epidermal growth factor-like domain, a membrane-binding domain, and a catalytic domain that contains peroxidase and

cyclooxygenase active sites, flanking a central heme group (Chandrasekharan and Simmons, 2004). COX-2 are homodimers and monotopic membrane proteins which are aimed at the luminal membrane of the endoplasmic reticulum. COX-2 is glycosylated on asparagine in all species (Chandrasekharan and Simmons, 2004).

COX-2 is a prostaglandin-synthesizing enzyme, which plays a profound role in the inflammation in teleost. The expression of this enzyme is regulated both transcriptionally and post-transcriptionally at numerous levels (Sheppe and Edelmann, 2021). COX-1 is constitutively expressed as a house-keeping gene, on the contrary, COX2 is expressed at low levels in the resting cells whereas their expression is noticeably boosted in response to the pro-inflammatory mediators, such as IL-1β and TNF-α (Dinarello, 2009) and other mitogenic stimuli (Chettri et al., 2011). According to our results, COX2 transcripts were highly expressed in the gill in healthy red-spotted grouper and significantly upregulated upon all tested types of immune stimulation with Gram-negative bacterial toxin; LPS, a viral mimic synthetic analog of double-stranded RNA; poly I: C, and live NNV. Similary, previous study reports the highest COX-2 expression in the gill tissue of *Larmichthys crocea* (Wang et al., 2016). Gill is the primary defense against external pathogens in teleosts (Gomez et al., 2013). That indicates the potential inflammatory role of COX2 in innate immunity against both bacterial and viral infections. The previous study reports that Gram-negative bacteria such as *Salmonella typhimurium, S.flexneri,* and *E. coli* alter the COX-2 expression either by toll-like receptor 4-dependent signaling pathway or by virulence factors

secreted through a type three secretion system (Sheppe and Edelmann, 2021). Later, COX-2-derived prostaglandins exert a crucial role during pathogen infections by enhancing the inflammasome activation, causing the formation of pore-induced traps, thereby, trapping the bacteria from escaping the dying cells (Sheppe and Edelmann, 2021).

COX-2 overexpression is reported to be associated with several inflammatory disorders (Redondo et al., 2011). In the current study, we evaluated the effect of EaCOX2 overexpression on FHM cell viability and apoptosis. Our results disclosed that overexpression of EaCOX2 caused decreased FHM cell viability and increased cell apoptosis. Supporting our findings, COX-2 was found to be involved in programmed cell death through PGE2-mediated activation of the inflammasome. Further, pharmaceutical inhibition or genetic knockdown of COX-2 caused a reduction in pro-inflammatory IL-β secretion and programmed cell death (Hua et al., 2015). COX-2-derived prostaglandins are secreted in large amounts during the inflammations (Greenhough et al., 2009). Thus, overexpression of COX-2 plays a crucial role in the development and progression of inflammation. In the current study, a pro-inflammatory effect was observed after visualizing the Phalloidine–iFluor 594 stained EaCOX2 overexpressing macrophages RAW 264.7. It showed classical pro-inflammatory M1-type polarization with a more elongated, dendritic-like morphology upon EaCOX2 overexpression contrary to more circular and confluent naive macrophages. M1 polarized macrophages show pro-inflammatory effects by

producing several inflammatory cytokines and reactive nitrogen or oxygen species with a bactericidal effect whereas alternative M2 polarized macrophages mitigate inflammation with a poor bactericidal effect (Mills et al., 2000; Rao Muvva et al., 2020). M2 polarized cells which are more circular compared to M1, show anti-inflammatory effects, promoting cell proliferation and tissue repair (Mills et al., 2000).

3.5. Conclusion

In this study, the cDNA of Cyclooxygenase 2 was identified and functionally characterized from *E. akaara*. It showed high conservation and evolutionary proximity with the other vertebrate COX-2 homologs. The highest level of *EaCOX2* mRNA expression was observed in the gill tissue of healthy *E. akkara*, through qPCR analysis. Immune stimulation with both bacteria and virus caused significant upregulation of *EaCOX2* transcripts level at 12 h and 24 h post-infection in the gills of *E. akaara*. EaCOX2 overexpression demonstrated a proinflammatory effect by reducing FHM cell viability, and M1-type macrophage polarization and by triggering reactive NO production. Collectively, the findings of this research suggest the profound role of *EaCOX2* in the teleost immune and inflammatory responses.

References

Abbas, A.R., Baldwin, D., Ma, Y., Ouyang, W., Gurney, A., Martin, F., Fong, S., van Lookeren Campagne, M., Godowski, P., Williams, P.M., Chan, A.C., Clark, H.F., 2005. Immune response in silico (IRIS): Immune-specific genes identified from a compendium of microarray expression data. Genes Immun. 6, 319–331. https://doi.org/10.1038/sj.gene.6364173

Ahn, S.J., Bak, H.J., Park, J.H., Lee, J.Y., Kim, N.Y., Han, J.W., Jo, H.I., Chung, J.K., Lee, H.H., 2013. Olive Flounder (*Paralichthys olivaceus*) Cystatin C: Cloning, mRNA Expression, and Enzymatic Characterization of Olive Flounder Cystatin C. Appl. Biochem. Biotechnol. 170, 1216–1228. https://doi.org/10.1007/s12010-013-0248-5

Alcaide, E., Gil-Sanz, C., Sanjuán, E., Esteve, D., Amaro, C., Silveira, L., 2001. *Vibrio harveyi* causes disease in seahorse, Hippocampus sp. J. Fish Dis. https://doi.org/10.1046/j.1365-2761.2001.00297.x

Andrade, M.J., 2014. Cystatin C: An underexplored biomarker that goes beyond renal function. Rev. Port. Cardiol. https://doi.org/10.1016/j.repc.2014.07.001

Aurélio, M., Faleiro, F., Lopes, V.M., Pires, V., Lopes, A.R., Pimentel, M.S., Repolho, T., Baptista, M., Narciso, L., Rosa, R., 2013. Physiological and behavioral responses of temperate seahorses (*Hippocampus guttulatus*) to environmental warming. Mar. Biol. 160, 2663–2670. https://doi.org/10.1007/s00227-013-2259-8

Bai, J., Ma, D., Lao, H., Jian, Q., Ye, X., Luo, J., Xong, X., Li, Y., Liang, X., 2006. Molecular cloning, sequencing, expression of Chinese sturgeon cystatin in yeast *Pichia pastoris* and its proteinase inhibitory activity. J. Biotechnol. 125, 231–241. https://doi.org/10.1016/j.jbiotec.2006.02.023

Balcázar, J.L., Planas, M., Pintado, J., 2014. *Mycobacterium hippocampi* sp. nov., a rapidly growing scotochromogenic species isolated from a seahorse with tail rot. Curr. Microbiol. 69, 329–333. https://doi.org/10.1007/s00284-014-0588-6

Bandivdekar, A., Vernekar, V., Velhal, S., 2015. Evaluation of cystatin C activities against HIV. Indian J. Med. Res. 141, 423. https://doi.org/10.4103/0971-5916.159282

Baum, J.K., Meeuwig, J.J., Vincent, A.C.J., 2003. Bycatch of lined seahorses (*Hippocampus erectus*) in a Gulf of Mexico shrimp trawl fishery. Fish. Bull. 101, 721–731.

Behairy, B.E., Saber, M.A., Elhenawy, I.A., Abou-Zeinah, S.S., El-Sharawy, A.A., Sira, M.M., 2012. Serum cystatin C correlates negatively with viral load in treatment-naïve children with chronic hepatitis C. J. Pediatr. Gastroenterol. Nutr. 54, 364–368. https://doi.org/10.1097/MPG.0b013e31823e98c2

Berdowska, I., 2004. Cysteine proteases as disease markers. Clin. Chim. Acta 342, 41–69. https://doi.org/10.1016/j.cccn.2003.12.016

Björck, L., Åkesson, P., Bohus, M., Trojnar, J., Abrahamson, M., Olafsson, I., Grubb, A., 1989. Bacterial growth blocked by a synthetic peptide based on the structure of a human proteinase inhibitor. Nature 337, 385–386. https://doi.org/10.1038/337385a0

Björck, L., Grubb, A., Kjellén, L., 1990. Cystatin C, a human proteinase inhibitor, blocks replication of herpes simplex virus. J. Virol. 64, 941–943. https://doi.org/10.1128/jvi.64.2.941-943.1990

Björklund, H. V, Johansson, T.R., Rinne, A., 1997. Rhabdovirus-induced apoptosis in a fish cell line is inhibited by a human endogenous acid cysteine proteinase inhibitor. J. Virol. 71, 5658–5662. https://doi.org/10.1128/jvi.71.7.5658-5662.1997

Bobek, L.A., Levine, M.J., 1992. Cystatins — Inhibitors of Cysteine Proteinases. Crit. Rev. Oral Biol. Med. 3, 307–332. https://doi.org/10.1177/10454411920030040101

Bode, W., Huber, R., 2000. Structural basis of the endoproteinase–protein inhibitor interaction. Biochim. Biophys. Acta - Protein Struct. Mol. Enzymol. 1477, 241–

252. https://doi.org/10.1016/S0167-4838(99)00276-9

Bossowska-Nowicka, M., Mielcarska, M.B., Romaniewicz, M., Kaczmarek, M.M., Gregorczyk-Zboroch, K.P., Struzik, J., Grodzik, M., Gieryńska, M.M., Toka, F.N., Szulc-Dąbrowska, L., 2019. Ectromelia virus suppresses expression of cathepsins and cystatins in conventional dendritic cells to efficiently execute the replication process. BMC Microbiol. 19, 92. https://doi.org/10.1186/s12866-019-1471-1

Boyd, C.E., McNevin, A.A., Davis, R.P., 2022. The contribution of fisheries and aquaculture to the global protein supply. Food Secur. 14, 805–827. https://doi.org/10.1007/s12571-021-01246-9

Bustin, S.A., Benes, V., Garson, J.A., Hellemans, J., Huggett, J., Kubista, M., Mueller, R., Nolan, T., Pfaffl, M.W., Shipley, G.L., Vandesompele, J., Wittwer, C.T., 2009. The MIQE guidelines: Minimum information for publication of quantitative real-time PCR experiments. Clin. Chem. 55, 611–622. https://doi.org/10.1373/clinchem.2008.112797

Campanella, J.J., Bitincka, L., Smalley, J., 2003. MatGAT: An application that generates similarity/identity matrices using protein or DNA sequences. BMC Bioinformatics 4, 1–4. https://doi.org/10.1186/1471-2105-4-29

Ceru, S., Konjar, S., Maher, K., Repnik, U., Krizaj, I., Bencina, M., Renko, M., Nepveu, A., Zerovnik, E., Turk, B., Kopitar-Jerala, N., 2010. Stefin B interacts with histones and cathepsin L in the nucleus. J. Biol. Chem. 285, 10078–10086. https://doi.org/10.1074/jbc.M109.034793

Chandrasekharan, N. V., Dai, H., Roos, K.L.T., Evanson, N.K., Tomsik, J., Elton, T.S., Simmons, D.L., 2002. COX-3, a cyclooxygenase-1 variant inhibited by acetaminophen and other analgesic/antipyretic drugs: Cloning, structure, and expression. Proc. Natl. Acad. Sci. 99, 13926–13931. https://doi.org/10.1073/pnas.162468699

Chandrasekharan, N. V., Simmons, D.L., 2004. The cyclooxygenases. Genome Biol.

https://doi.org/10.1186/gb-2004-5-9-241

Chang, M., Southgate, P.C., 2001. Effects of varying dietary fatty acid composition on growth and survival of seahorse, *Hippocampus* sp., juveniles. Aquarium Sci. Conserv. 3, 205–214. https://doi.org/10.1023/A:1011363807074

Chettri, J.K., Raida, M.K., Holten-Andersen, L., Kania, P.W., Buchmann, K., 2011. PAMP induced expression of immune relevant genes in head kidney leukocytes of rainbow trout (Oncorhynchus mykiss). Dev. Comp. Immunol. 35, 476–482. https://doi.org/10.1016/j.dci.2010.12.001

Cole, T., Dickson, P.W., Esnard, F., Averill, S., Risbridger, G.P., Gauthier, F., Schreiber, G., 1989. The cDNA structure and expression analysis of the genes for the cysteine proteinase inhibitor cystatin C and for beta2-microglobulin in rat brain. Eur. J. Biochem. 186, 35–42. https://doi.org/10.1111/j.1432-1033.1989.tb15174.x

Collins, A.R., Grubb, A., 1998. Cystatin D, a natural salivary cysteine protease inhibitor, inhibits coronavirus replication at its physiologic concentration. Oral Microbiol. Immunol. 13, 59–61. https://doi.org/10.1111/j.1399-302X.1998.tb00753.x

Collins, A.R., Grubb, A., 1991. Inhibitory effects of recombinant human cystatin C on human coronaviruses. Antimicrob. Agents Chemother. 35, 2444–2446. https://doi.org/10.1128/AAC.35.11.2444

Coombs, G.H., Mottram, J.C., 1997. Parasite proteinases and amino acid metabolism: Possibilities for chemotherapeutic exploitation. Parasitology 114, 61–80. https://doi.org/10.1017/s003118209700111x

Cui, J., Placzek, W., 2018. Post-Transcriptional Regulation of Anti-Apoptotic BCL2 Family Members. Int. J. Mol. Sci. 19, 308. https://doi.org/10.3390/ijms19010308

Curry, T.E., Dean, D.D., Sanders, S.L., Pedigo, N.G., Jones, P.B.C., 1989. The role of ovarian proteases and their inhibitors in ovulation. Steroids 54, 501–521.

https://doi.org/10.1016/0039-128X(89)90044-5

Daiyasu, H., Toh, H., 2000. Molecular Evolution of the Myeloperoxidase Family. J. Mol. Evol. 51, 433–445. https://doi.org/10.1007/s002390010106

Di Piazza, M., Mader, C., Geletneky, K., Herrero y Calle, M., Weber, E., Schlehofer, J., Deleu, L., Rommelaere, J., 2007. Cytosolic Activation of Cathepsins Mediates Parvovirus H-1-Induced Killing of Cisplatin and TRAIL-Resistant Glioma Cells. J. Virol. 81, 4186–4198. https://doi.org/10.1128/JVI.02601-06

Dinarello, C.A., 2009. Immunological and Inflammatory Functions of the Interleukin-1 Family. Annu. Rev. Immunol. 27, 519–550. https://doi.org/10.1146/annurev.immunol.021908.132612

Fioravanti, M.L., Florio, D., 2017. Common Diseases in Marine Ornamental Fishes. Mar. Ornam. Species Aquac. https://doi.org/10.1002/9781119169147.ch19

Fitzpatrick, F., 2004. Cyclooxygenase Enzymes: Regulation and Function. Curr. Pharm. Des. 10, 577–588. https://doi.org/10.2174/1381612043453144

Foster, S.J., Vincent, A.C.J., 2004. Life history and ecology of seahorses: Implications for conservation and management. J. Fish Biol. https://doi.org/10.1111/j.0022-1112.2004.00429.x

Frendéus, K.H., Wallin, H., Janciauskiene, S., Abrahamson, M., 2009. Macrophage responses to interferon-γ are dependent on cystatin C levels. Int. J. Biochem. Cell Biol. 41, 2262–2269. https://doi.org/10.1016/j.biocel.2009.05.005

Gauthier, S., Kaur, G., Mi, W., Tizon, B., Levy, E., 2011. Protective mechanisms by cystatin C in neurodegenerative diseases. Front. Biosci. - Sch. 3 S, 541–554. https://doi.org/10.2741/s170

Ghys, L.F., Paepe, D., Taffin, E.R., Vandermeulen, E., Duchateau, L., Smets, P.M., Delanghe, J., Daminet, S., 2016. Serum and urinary cystatin C in cats with feline immunodeficiency virus infection and cats with hyperthyroidism. J. Feline Med. Surg. 18, 658–665. https://doi.org/10.1177/1098612X15592343

Giaimo, R. Di, Riccio, M., Santi, S., Galeotti, C., Ambrosetti, D.C., Melli, M., 2002.

New insights into the molecular basis of progressive myoclonus epilepsy: A multiprotein complex with cystatin B. Hum. Mol. Genet. 11, 2941–2950. https://doi.org/10.1093/hmg/11.23.2941

Global fisheries and aquaculture at a glance [WWW Document], 2022. . Food Agric. Organ. United Nations. URL https://www.fao.org/3/cc0461en/online/sofia/2022/world-fisheries-aquaculture.html (accessed 12.19.22).

Gomez, D., Sunyer, J.O., Salinas, I., 2013. The mucosal immune system of fish: The evolution of tolerating commensals while fighting pathogens. Fish Shellfish Immunol. https://doi.org/10.1016/j.fsi.2013.09.032

Greenhough, A., Smartt, H.J.M., Moore, A.E., Roberts, H.R., Williams, A.C., Paraskeva, C., Kaidi, A., 2009. The COX-2/PGE2 pathway: key roles in the hallmarks of cancer and adaptation to the tumour microenvironment. Carcinogenesis 30, 377–386. https://doi.org/10.1093/carcin/bgp014

Gu, M., Haraszthy, G.G., Collins, A.R., Bergey, E.J., 1995. Identification of salivary proteins inhibiting herpes simplex virus 1 replication. Oral Microbiol. Immunol. 10, 54–59. https://doi.org/10.1111/j.1399-302X.1995.tb00118.x

Gudding, R., Van Muiswinkel, W.B., 2013. A history of fish vaccination. Fish Shellfish Immunol. 35, 1683–1688. https://doi.org/10.1016/j.fsi.2013.09.031

He, Q., Lu, G., Che, K., Zhao, E., Fang, Q., Wang, H., Liu, J., Huang, C., Dong, Q., 2011. Sperm cryopreservation of the endangered red spotted grouper, Epinephelus akaara, with a special emphasis on membrane lipids. Aquaculture 318, 185–190. https://doi.org/10.1016/j.aquaculture.2011.05.025

Henskens, Y.M.C., Veerman, E.C.L., Nieuw Amerongen, A. V., 1996. Review. Biol. Chem. Hoppe. Seyler. 377, 71–120. https://doi.org/10.1515/bchm3.1996.377.2.71

Holen, E., Olsvik, P.A., 2016. β-naphthoflavone interferes with cyp1c1, cox2 and IL-8 gene transcription and leukotriene B4 secretion in Atlantic cod (Gadus

morhua) head kidney cells during inflammation. Fish Shellfish Immunol. 54, 128–134. https://doi.org/10.1016/j.fsi.2016.03.043

Holloway, A.J., Yu, J., Arulanandam, B.P., Hoskinson, S.M., Eaves-Pyles, T., 2018. Cystatins 9 and C as a Novel Immunotherapy Treatment That Protects against Multidrug-Resistant New Delhi Metallo-Beta-Lactamase-1-Producing Klebsiella pneumoniae. Antimicrob. Agents Chemother. 62. https://doi.org/10.1128/AAC.01900-17

Hsing, L.C., Rudensky, A.Y., 2005. The lysosomal cysteine proteases in MHC class II antigen presentation. Immunol. Rev. https://doi.org/10.1111/j.0105-2896.2005.00310.x

Hua, K.-F., Chou, J.-C., Ka, S.-M., Tasi, Y.-L., Chen, A., Wu, S.-H., Chiu, H.-W., Wong, W.-T., Wang, Y.-F., Tsai, C.-L., Ho, C.-L., Lin, C.-H., 2015. Cyclooxygenase-2 Regulates NLRP3 Inflammasome-Derived IL-1β Production. J. Cell. Physiol. 230, 863–874. https://doi.org/10.1002/jcp.24815

Hwang, J.H., Kim, K.J., Ryu, S.J., Lee, B.Y., 2016. Caffeine prevents LPS-induced inflammatory responses in RAW264.7 cells and zebrafish. Chem. Biol. Interact. 248, 1–7. https://doi.org/10.1016/J.CBI.2016.01.020

Josiah Ochieng, Gautam Chaudhuri, 2010. Cystatin Superfamily. J. Health Care Poor Underserved 21, 51–70. https://doi.org/10.1353/hpu.0.0257

Kagitani-Shimono, K., Imai, K., Okamoto, N., Ono, J., Okada, S., 2002. Unverricht-Lundborg disease with cystatin B gene abnormalities. Pediatr. Neurol. 26, 55–60. https://doi.org/10.1016/S0887-8994(01)00336-8

Kim, G., Omeka, W.K.M., Liyanage, D.S., Lee, J., 2020. Molecular characterization, redox regulation, and immune responses of monothiol and dithiol glutaredoxins from disk abalone (*Haliotis discus discus*). Fish Shellfish Immunol. 107, 385–394. https://doi.org/10.1016/j.fsi.2020.10.025

Koldewey, H.J., Martin-Smith, K.M., 2010. A global review of seahorse aquaculture. Aquaculture. https://doi.org/10.1016/j.aquaculture.2009.11.010

Kopitar-Jerala, N., 2006. The role of cystatins in cells of the immune system. FEBS Lett. https://doi.org/10.1016/j.febslet.2006.10.055

Korant, B.D., Brzin, J., Turk, V., 1985. Cystatin, a protein inhibitor of cysteine proteases alters viral protein cleavages in infected human cells. Biochem. Biophys. Res. Commun. 127, 1072–1076. https://doi.org/10.1016/S0006-291X(85)80054-1

Kumar, S., Stecher, G., Tamura, K., 2016. MEGA7: Molecular Evolutionary Genetics Analysis Version 7.0 for Bigger Datasets. Mol. Biol. Evol. 33, 1870–1874. https://doi.org/10.1093/molbev/msw054

Kumaravel, K, Ravichandran, S., Balasubramanian, T., Sonneschein, L., 2012. Seahorses - A source of traditional medicine. Nat. Prod. Res. https://doi.org/10.1080/14786419.2012.662650

Kumaravel, K., Ravichandran, S., Balasubramanian, T., Sonneschein, L., 2012. Seahorses – A source of traditional medicine. Nat. Prod. Res. 26, 2330–2334. https://doi.org/10.1080/14786419.2012.662650

Larkin, M.A., Blackshields, G., Brown, N.P., Chenna, R., Mcgettigan, P.A., McWilliam, H., Valentin, F., Wallace, I.M., Wilm, A., Lopez, R., Thompson, J.D., Gibson, T.J., Higgins, D.G., 2007. Clustal W and Clustal X version 2.0. Bioinformatics 23, 2947–2948. https://doi.org/10.1093/bioinformatics/btm404

Lee, K.K., 1995. Pathogenesis studies on vibrio alginolyticus in the grouper, epinephelus malabaricus, bloch et schneider. Microb. Pathog. 19, 39–48. https://doi.org/10.1016/S0882-4010(85)90000-2

Lefebvre, C., Cocquerelle, C., Vandenbulcke, F., Hot, D., Huot, L., Lemoine, Y., Salzet, M., 2004. Transcriptomic analysis in the leech *Theromyzon tessulatum*: Involvement of cystatin B in innate immunity. Biochem. J. 380, 617–625. https://doi.org/10.1042/BJ20040478

Lenarčič, B., Bevec, T., 1998. Thyropins - new structurally related proteinase inhibitors. Biol. Chem.

Levy, E., Jaskolski, M., Grubb, A., 2006. The Role of Cystatin C in Cerebral Amyloid Angiopathy and Stroke: Cell Biology and Animal Models. Brain Pathol. 16, 60–70. https://doi.org/10.1111/j.1750-3639.2006.tb00562.x

Li, F., An, H., A. Seymour, T., Bradford, C.S., Morrissey, M.T., Bailey, G.S., Helmrich, A., Barnes, D.W., 1998. Molecular cloning, sequence analysis and expression distribution of rainbow trout (*Oncorhynchus mykiss*) cystatin C. Comp. Biochem. Physiol. Part B Biochem. Mol. Biol. 121, 135–143. https://doi.org/10.1016/S0305-0491(98)10074-3

Li, F., Gai, X., Wang, L., Song, L., Zhang, H., Qiu, L., Wang, M., Siva, V.S., 2010. Identification and characterization of a Cystatin gene from Chinese mitten crab *Eriocheir sinensis*. Fish Shellfish Immunol. 29, 521–529. https://doi.org/10.1016/J.FSI.2010.05.015

Li, M., Liu, Y., Wang, Q.-L., Chen, S.-L., Sha, Z.-X., 2012. BIRC7 gene in channel catfish (*Ictalurus punctatus*): Identification and expression analysis in response to *Edwardsiella tarda*, *Streptococcus iniae* and channel catfish Hemorrhage Reovirus. Fish Shellfish Immunol. 33, 146–153. https://doi.org/10.1016/j.fsi.2012.03.026

Li, P., Nijhawan, D., Budihardjo, I., Srinivasula, S.M., Ahmad, M., Alnemri, E.S., Wang, X., 1997. Cytochrome c and dATP-Dependent Formation of Apaf-1/Caspase-9 Complex Initiates an Apoptotic Protease Cascade. Cell 91, 479–489. https://doi.org/10.1016/S0092-8674(00)80434-1

Li, S., Ao, J., Chen, X., 2009. Molecular and functional characterization of a cystatin analogue in large yellow croaker (*Pseudosciaena crocea*). Mol. Immunol. 46, 1638–1646. https://doi.org/10.1016/j.molimm.2009.02.027

Liang, X., Nagai, A., Terashima, M., Sheikh, A.M., Shiota, Y., Mitaki, S., Kim, S.U., Yamaguchi, S., 2011. Cystatin C induces apoptosis and tyrosine hydroxylase gene expression through JNK-dependent pathway in neuronal cells. Neurosci. Lett. 496, 100–105. https://doi.org/10.1016/j.neulet.2011.03.091

Lin, T., Zhang, D., Liu, X., Xiao, D., 2016. Variations of immune parameters in the lined seahorse Hippocampus erectus after infection with enteritis pathogen of Vibrio parahaemolyticus. Fish Shellfish Immunol. 50, 247–254. https://doi.org/10.1016/j.fsi.2016.01.039

Lindenstrøm, T., Secombes, C.J., Buchmann, K., 2004. Expression of immune response genes in rainbow trout skin induced by Gyrodactylus derjavini infections. Vet. Immunol. Immunopathol. 97, 137–148. https://doi.org/10.1016/j.vetimm.2003.08.016

Livak, K.J., Schmittgen, T.D., 2001. Analysis of relative gene expression data using real-time quantitative PCR and the 2-ΔΔCT method. Methods 25, 402–408. https://doi.org/10.1006/meth.2001.1262

Luo, W., Wang, X., Qu, H., Qin, G., Zhang, H., Lin, Q., 2016. Genomic structure and expression pattern of MHC IIα and IIβ genes reveal an unusual immune trait in lined seahorse *Hippocampus erectus*. Fish Shellfish Immunol. 58, 521–529. https://doi.org/10.1016/j.fsi.2016.09.057

Maher, K., Kokelj, B.J., Butinar, M., Mikhaylov, G., Manček-Keber, M., Stoka, V., Vasiljeva, O., Turk, B., Grigoryev, S.A., Kopitar-Jerala, N., 2014. A role for stefin B (cystatin B) in inflammation and endotoxemia. J. Biol. Chem. 289, 31736–31750. https://doi.org/10.1074/jbc.M114.609396

McCormack, P.L., Lanas, A., McKenna, F., Patrignani, P., Simon, L.S., 2011. Celecoxib: A review of its use for symptomatic relief in the treatment of osteoarthritis, rheumatoid arthritis and ankylosing spondylitis. Drugs. https://doi.org/10.2165/11208240-000000000-00000

McGinnis, S., Madden, T.L., 2004. BLAST: At the core of a powerful and diverse set of sequence analysis tools. Nucleic Acids Res. 32, 20–25. https://doi.org/10.1093/nar/gkh435

Michael Garavito, R., Malkowski, M.G., DeWitt, D.L., 2002. The structures of prostaglandin endoperoxide H synthases-1 and -2. Prostaglandins Other Lipid

Mediat. 68–69, 129–152. https://doi.org/10.1016/S0090-6980(02)00026-6

Mills, C.D., Kincaid, K., Alt, J.M., Heilman, M.J., Hill, A.M., 2000. M-1/M-2 Macrophages and the Th1/Th2 Paradigm. J. Immunol. 164, 6166–6173. https://doi.org/10.4049/JIMMUNOL.164.12.6166

Neurath, H., 1984. Evolution of proteolytic enzymes. Science (80-.). https://doi.org/10.1126/science.6369538

Oh, M., Umasuthan, N., Elvitigala, D.A.S., Wan, Q., Jo, E., Ko, J., Noh, G.E., Shin, S., Rho, S., Lee, J., 2016. First comparative characterization of three distinct ferritin subunits from a teleost: Evidence for immune-responsive mRNA expression and iron depriving activity of seahorse (*Hippocampus abdominalis*) ferritins. Fish Shellfish Immunol. 49, 450–460. https://doi.org/10.1016/j.fsi.2015.12.039

Okonechnikov, K., Golosova, O., Fursov, M., Varlamov, A., Vaskin, Y., Efremov, I., German Grehov, O.G., Kandrov, D., Rasputin, K., Syabro, M., Tleukenov, T., 2012. Unipro UGENE: A unified bioinformatics toolkit. Bioinformatics 28, 1166–1167. https://doi.org/10.1093/bioinformatics/bts091

Owczarzy, R., Tataurov, A. V, Wu, Y., Manthey, J.A., McQuisten, K.A., Almabrazi, H.G., Pedersen, K.F., Lin, Y., Garretson, J., McEntaggart, N.O., Sailor, C.A., Dawson, R.B., Peek, A.S., 2008. IDT SciTools: a suite for analysis and design of nucleic acid oligomers. Nucleic Acids Res. 36, W163–W169. https://doi.org/10.1093/nar/gkn198

Pemberton, P.A., 2006. Proteinase Inhibitors: Cystatins, in: Encyclopedia of Respiratory Medicine, Four-Volume Set. Elsevier, pp. 511–517. https://doi.org/10.1016/B0-12-370879-6/00329-X

Piao, M.J., Han, X., Kang, K.A., Fernando, P.D.S.M., Herath, H.M.U.L., Hyun, J.W., 2022. The Endoplasmic Reticulum Stress Response Mediates Shikonin-Induced Apoptosis of 5-Fluorouracil-Resistant Colorectal Cancer Cells. Biomol. Ther. (Seoul). 30, 265–273. https://doi.org/10.4062/biomolther.2021.118

Pierre, P., Mellman, I., 1998. Developmental Regulation of Invariant Chain Proteolysis Controls MHC Class II Trafficking in Mouse Dendritic Cells. Cell 93, 1135–1145. https://doi.org/10.1016/S0092-8674(00)81458-0

Pol, E., Björk, I., 2001. Role of the single cysteine residue, Cys 3, of human and bovine cystatin B (stefin B) in the inhibition of cysteine proteinases. Protein Sci. 10, 1729–1738. https://doi.org/10.1110/ps.11901

Pol, E., Björk, I., 1999. Importance of the second binding loop and the C-terminal end of cystatin B (Stefin B) for inhibition of cysteine proteinases. Biochemistry 38, 10519–10526. https://doi.org/10.1021/bi990488k

Premachandra, H.K.A., Wan, Q., Elvitigala, D.A.S., Zoysa, M. De, Choi, C.Y., Whang, I., Lee, J., 2012a. Genomic characterization and expression profiles upon bacterial infection of a novel cystatin B homologue from disk abalone (*Haliotis discus discus*). Dev. Comp. Immunol. 38, 495–504. https://doi.org/10.1016/j.dci.2012.06.010

Premachandra, H.K.A., Whang, I., Lee, Y.D., Lee, S., De Zoysa, M., Oh, M.J., Jung, S.J., Lim, B.S., Noh, J.K., Park, H.C., Lee, J., 2012b. Cystatin B homolog from rock bream *Oplegnathus fasciatus*: Genomic characterization, transcriptional profiling and protease-inhibitory activity of recombinant protein. Comp. Biochem. Physiol. - B Biochem. Mol. Biol. 163, 138–146. https://doi.org/10.1016/j.cbpb.2012.05.012

Priyathilaka, T.T., Bathige, S.D.N.K., Lee, S., Lee, J., 2018. Molecular identification and functional analysis of two variants of myeloid differentiation factor 88 (MyD88) from disk abalone (*Haliotis discus discus*). Dev. Comp. Immunol. 79, 113–127. https://doi.org/10.1016/j.dci.2017.10.010

Puente-Marin, S., Thwaite, R., Mercado, L., Coll, J., Roher, N., Del Mar Ortega-Villaizan, M., 2019. Fish red blood cells modulate immune genes in response to bacterial inclusion bodies made of TNFα and a g-VHSV fragment. Front. Immunol. 10, 1055. https://doi.org/10.3389/fimmu.2019.01055

Rajan, B., Fernandes, J.M.O., Caipang, C.M.A., Kiron, V., Rombout, J.H.W.M., Brinchmann, M.F., 2011. Proteome reference map of the skin mucus of Atlantic cod (*Gadus morhua*) revealing immune competent molecules. Fish Shellfish Immunol. 31, 224–231. https://doi.org/10.1016/j.fsi.2011.05.006

Rao Muvva, J., Parasa, V.R., Lerm, M., Svensson, M., Brighenti, S., 2020. Polarization of Human Monocyte-Derived Cells With Vitamin D Promotes Control of Mycobacterium tuberculosis Infection. Front. Immunol. 10, 3157. https://doi.org/10.3389/FIMMU.2019.03157/BIBTEX

Redondo, S., Ruiz, E., Gordillo-Moscoso, A., Navarro-Dorado, J., Ramajo, M., Rodríguez, E., Reguillo, F., Carnero, M., Casado, M., Tejerina, T., 2011. Overproduction of cyclo-oxygenase-2 (COX-2) is involved in the resistance to apoptosis in vascular smooth muscle cells from diabetic patients: a link between inflammation and apoptosis. Diabetologia 54, 190–199. https://doi.org/10.1007/s00125-010-1947-x

Riccio, M., Di Giaimo, R., Pianetti, S., Palmieri, P.P., Melli, M., Santi, S., 2001. Nuclear localization of cystatin B, the cathepsin inhibitor implicated in myoclonus epilepsy (EPM1). Exp. Cell Res. 262, 84–94. https://doi.org/10.1006/excr.2000.5085

Rice, P., Longden, L., Bleasby, A., 2000. EMBOSS: The European Molecular Biology Open Software Suite. Trends Genet. 16, 276–277. https://doi.org/10.1016/S0168-9525(00)02024-2

Ruzindana-Umunyana, A., Weber, J.M., 2001. Interactions of human lacrimal and salivary cystatins with adenovirus endopeptidase. Antiviral Res. 51, 203–214. https://doi.org/10.1016/S0166-3542(01)00154-1

Ryu, S.J., Choi, H.S., Yoon, K.Y., Lee, O.H., Kim, K.J., Lee, B.Y., 2015. Oleuropein suppresses LPS-induced inflammatory responses in RAW 264.7 Cell and zebrafish. J. Agric. Food Chem. 63, 2098–2105. https://doi.org/10.1021/jf505894b

Sadovy, Y., 2001. The threat of fishing to highly fecund fishes. J. Fish Biol. 59, 90–108. https://doi.org/10.1111/j.1095-8649.2001.tb01381.x

Sadovy, Y., Liu, M., Amorim, P., Choat, J.H., Law, C., Ma, K., Myers, R., Rhodes, K., Samoilys, M., Suharti, S., To, A., 2018. Epinephelus akaara, Hong Kong Grouper [WWW Document]. IUCN Red List Threat. Species. URL https://www.iucnredlist.org/species/43974/100459934 (accessed 12.29.22).

Salin, K.R., Mohanakumaran, N.C., 2006. Resources and biodiversity of seahorses and the need for their conservation in India. Asia Aquac. 11, 3–8.

Séronie-Vivien, S., Delanaye, P., Piéroni, L., Mariat, C., Froissart, M., Cristol, J.-P., 2008. Cystatin C: current position and future prospects. Clin. Chem. Lab. Med. 46, 1664–1686. https://doi.org/10.1515/CCLM.2008.336

Severin, V.I.C., El-Matbouli, M., 2007. Relative quantification of immune-regulatory genes in two rainbow trout strains, Oncorhynchus mykiss, after exposure to Myxobolus cerebralis, the causative agent of whirling disease. Parasitol. Res. 101, 1019–1027. https://doi.org/10.1007/s00436-007-0582-z

Shamsi, A., Bano, B., 2017. Journey of cystatins from being mere thiol protease inhibitors to at heart of many pathological conditions. Int. J. Biol. Macromol. https://doi.org/10.1016/j.ijbiomac.2017.04.071

Shen, Y., Wang, D., Zhao, J., Chen, X., 2018. Fish red blood cells express immune genes and responses. Aquac. Fish. 3, 14–21. https://doi.org/10.1016/j.aaf.2018.01.001

Sheppe, A.E.F., Edelmann, M.J., 2021. Roles of Eicosanoids in Regulating Inflammation and Neutrophil Migration as an Innate Host Response to Bacterial Infections. Infect. Immun. 89. https://doi.org/10.1128/IAI.00095-21

Sigrist, C.J.A., De Castro, E., Cerutti, L., Cuche, B.A., Hulo, N., Bridge, A., Bougueleret, L., Xenarios, I., 2013. New and continuing developments at PROSITE. Nucleic Acids Res. 41, 344–347. https://doi.org/10.1093/nar/gks1067

Skrzydlewska, E., Sulkowska, M., Koda, M., Sulkowski, S., 2005. Proteolytic-antiproteolytic balance and its regulation in carcinogenesis. World J. Gastroenterol. https://doi.org/10.3748/wjg.v11.i9.1251

Song, W., Jiang, K.J., Zhang, F.Y., Zhao, M., Ma, L.B., 2016. Molecular cloning and gene expression analysis of cystatin C-like proteins in spinyhead croaker *Collichthys lucidus*. Genet. Mol. Res. 15. https://doi.org/10.4238/gmr.15017417

Suzuki, T., Hashimoto, S., Toyoda, N., Nagai, S., Yamazaki, N., Dong, H.-Y., Sakai, J., Yamashita, T., Nukiwa, T., Matsushima, K., 2000. Comprehensive gene expression profile of LPS-stimulated human monocytes by SAGE. Blood 96, 2584–2591. https://doi.org/10.1182/blood.V96.7.2584

Takahashi, M., Tezuka, T., Katunuma, N., 1994. Inhibition of growth and cysteine proteinase activity of *Staphylococcus aureus* V8 by phosphorylated cystatin α in skin cornified envelope. FEBS Lett. 355, 275–278. https://doi.org/10.1016/0014-5793(94)01196-6

Tamura, K., Stecher, G., Kumar, S., 2021. MEGA11: Molecular Evolutionary Genetics Analysis Version 11. Mol. Biol. Evol. 38, 3022–3027. https://doi.org/10.1093/molbev/msab120

Tang, L., Liu, Y.L., Qin, G., Lin, Q., Zhang, Y.H., 2021. Effects of tributyltin on gonad and brood pouch development of male pregnant lined seahorse (*Hippocampus erectus*) at environmentally relevant concentrations. J. Hazard. Mater. 408, 124854. https://doi.org/10.1016/j.jhazmat.2020.124854

Tavéra, C., Prévot, D., Girolami, J.P., Leung-Tack, J., Collé, A., 1990. Tissue and biological fluid distribution of cysteine proteinases inhibitor: rat cystatin C. Biol. Chem. Hoppe. Seyler. 371 Suppl, 187–92.

Tsai, Y.-J., Chang, G.-D., Huang, C.-J., Chang, Y.-S., Huang, F.-L., 1996. Purification and molecular cloning of carp ovarian cystatin. Comp. Biochem. Physiol. Part B Biochem. Mol. Biol. 113, 573–580. https://doi.org/10.1016/0305-0491(95)02070-5

Turini, M.E., DuBois, R.N., 2002. Cyclooxygenase-2: A Therapeutic Target. Annu. Rev. Med. 53, 35–57. https://doi.org/10.1146/annurev.med.53.082901.103952

Turk, B., Turk, D., Salvesen, G., 2002. Regulating Cysteine Protease Activity: Essential Role of Protease Inhibitors As Guardians and Regulators. Curr. Pharm. Des. 8, 1623–1637. https://doi.org/10.2174/1381612023394124

Turk, B., Turk, V., Turk, D., 1997. Structural and functional aspects of papain-like cysteine proteinases and their protein inhibitors. Biol. Chem.

Turk, V., Bode, W., 1991a. The cystatins: Protein inhibitors of cysteine proteinases. FEBS Lett. https://doi.org/10.1016/0014-5793(91)80804-C

Turk, V., Bode, W., 1991b. The cystatins: Protein inhibitors of cysteine proteinases. FEBS Lett. 285, 213–219. https://doi.org/10.1016/0014-5793(91)80804-C

Turk, V., Turk, B., Turk, D., 2001. Lysosomal cysteine proteases: Facts and opportunities. EMBO J. https://doi.org/10.1093/emboj/20.17.4629

Udayantha, H.M.V., Samaraweera, A.V., Nadarajapillai, K., Sandamalika, W.M.G., Lim, C., Yang, H., Lee, S., Lee, J., 2021. Molecular characterization and immune regulatory, antioxidant, and antiapoptotic activities of thioredoxin domain-containing protein 17 (TXNDC17) in yellowtail clownfish (*Amphiprion clarkii*). Fish Shellfish Immunol. 115, 75–85. https://doi.org/10.1016/j.fsi.2021.05.021

Vancompernolle, K., Van Herreweghe, F., Pynaert, G., Van de Craen, M., De Vos, K., Totty, N., Sterling, A., Fiers, W., Vandenabeele, P., Grooten, J., 1998. Atractyloside-induced release of cathepsin B, a protease with caspase-processing activity. FEBS Lett. 438, 150–158. https://doi.org/10.1016/S0014-5793(98)01275-7

Vane, J.R., Bakhle, Y.S., Botting, R.M., 1998. CYCLOOXYGENASES 1 AND 2. Annu. Rev. Pharmacol. Toxicol. 38, 97–120. https://doi.org/10.1146/annurev.pharmtox.38.1.97

Vray, B., Hartmann, S., Hoebeke, J., 2002. Immunomodulatory properties of

cystatins. Cell. Mol. Life Sci. 59, 1503–1512. https://doi.org/10.1007/s00018-002-8525-4

Wang, T., Yan, J., Xu, W., Ai, Q., Mai, K., 2016. Characterization of Cyclooxygenase-2 and its induction pathways in response to high lipid diet-induced inflammation in Larmichthys crocea. Sci. Rep. 6, 19921. https://doi.org/10.1038/srep19921

Wei, S., Cai, J., Wang, S., Yu, Y., Wei, J., Huang, Y., Huang, X., Qin, Q., 2019. Functional characterization of Cystatin C in orange-spotted grouper, *Epinephelus coioides*. Dev. Comp. Immunol. 96, 37–46. https://doi.org/10.1016/j.dci.2019.02.015

Wei, S., Han, H., Xu, S., Huang, Y., Wei, J., Qin, Q., 2022. Identification and functional characterization of Cystatin B in orange-spotted grouper, *Epinephelus coioides*. Dev. Comp. Immunol. 104383. https://doi.org/10.1016/j.dci.2022.104383

Werle, B., Sauckel, K., Nathanson, C.-M., Bjarnadottir, M., Spiess, E., Ebert, W., Abrahamson, M., 2003. Cystatins C, E/M and F in Human Pleural Fluids of Patients with Neoplastic and Inflammatory Lung Disorders. Biol. Chem. 384, 281–287. https://doi.org/10.1515/BC.2003.031

Wickramasinghe, P.D.S.U., Kwon, H., Elvitigala, D.A.S., Wan, Q., Lee, J., 2020. Identification and characterization of cystatin B from black rockfish, *Sebastes schlegelii*, indicating its potent immunological importance. Fish Shellfish Immunol. 104, 497–505. https://doi.org/10.1016/j.fsi.2020.05.068

Williams, C.S., Smalley, W., DuBois, R.N., 1997. Aspirin use and potential mechanisms for colorectal cancer prevention. J. Clin. Invest. 100, 1325–1329. https://doi.org/10.1172/JCI119651

Woods, C.M.C., 2000. Improving initial survival in cultured seahorses, *Hippocampus abdominalis* leeson, 1827 (Teleostei: Syngnathidae). Aquaculture 190, 377–388. https://doi.org/10.1016/S0044-8486(00)00408-7

Wun, T., McKnight, H., Tuscano, J.M., 2004. Increased cyclooxygenase-2 (COX-2): A potential role in the pathogenesis of lymphoma. Leuk. Res. 28, 179–190. https://doi.org/10.1016/S0145-2126(03)00183-8

Wyllie, A.H., 1980. Glucocorticoid-induced thymocyte apoptosis is associated with endogenous endonuclease activation. Nature 284, 555–556. https://doi.org/10.1038/284555a0

Wynne, J.W., O'Sullivan, M.G., Cook, M.T., Stone, G., Nowak, B.F., Lovell, D.R., Elliott, N.G., 2008. Transcriptome analyses of amoebic gill disease-affected atlantic salmon (Salmo salar) tissues reveal localized host gene suppression. Mar. Biotechnol. 10, 388–403. https://doi.org/10.1007/s10126-007-9075-4

Xiao, P.P., Hu, Y.H., Sun, L., 2010. *Scophthalmus maximus* cystatin B enhances head kidney macrophage-mediated bacterial killing. Dev. Comp. Immunol. 34, 1237–1241. https://doi.org/10.1016/j.dci.2010.07.008

Yamashita, M., Konagaya, S., 1996. Molecular cloning and gene expression of chum salmon cystatin. J. Biochem. 120, 483–487. https://doi.org/10.1093/oxfordjournals.jbchem.a021438

Yang, M., Wang, Q., Chen, J., Wang, Y., Zhang, Y., Qin, Q., 2021. Identification of candidate SNPs and genes associated with anti-RGNNV using GWAS in the red-spotted grouper, Epinephelus akaara. Fish Shellfish Immunol. 112, 31–37. https://doi.org/10.1016/j.fsi.2021.02.010

Yang, X., Liu, J., Yue, Y., Chen, W., Song, M., Zhan, X., Wu, Z., 2014. Cloning, expression and characterisation of a type II cystatin from *Schistosoma japonicum* which could regulate macrophage activation. Parasitol. Res. 113, 3985–3992. https://doi.org/10.1007/s00436-014-4064-9

Yeh, S.-P., Chang, C.-A., Chang, C.-Y., Liu, C.-H., Cheng, W., 2008. Dietary sodium alginate administration affects fingerling growth and resistance to Streptococcus sp. and iridovirus, and juvenile non-specific immune responses of the orange-spotted grouper, Epinephelus coioides. Fish Shellfish Immunol. 25,

19–27. https://doi.org/10.1016/j.fsi.2007.11.011

Yu, H., Si, Y., Liu, Y., Liu, J., Xu, X., Zhang, Q., Wang, X., 2018. Molecular characterization, expression and immune functions of cystatin B in Japanese flounder (*Paralichthys olivaceus*). Fish Shellfish Immunol. https://doi.org/10.1016/j.fsi.2018.07.054

Yu, H., Xu, X., Zhang, Q., Wang, X., 2019. Molecular characterization, expression and functional analysis of cystatin C in Japanese flounder (*Paralichthys olivaceus*). Fish Shellfish Immunol. 86, 695–701. https://doi.org/10.1016/j.fsi.2018.12.015

Yu, N.Y.-L., Hallström, B.M., Fagerberg, L., Ponten, F., Kawaji, H., Carninci, P., Forrest, A.R.R., Hayashizaki, Y., Uhlén, M., Daub, C.O., 2015. Complementing tissue characterization by integrating transcriptome profiling from the Human Protein Atlas and from the FANTOM5 consortium. Nucleic Acids Res. 43, 6787–6798. https://doi.org/10.1093/nar/gkv608

Zhang, D., Yin, F., Lin, J., 2011. Criteria for assessing juvenile quality of the lined seahorse, *Hippocampus erectus*. Aquaculture 322–323, 255–258. https://doi.org/10.1016/j.aquaculture.2011.10.008

Zhou, L., Gui, J.-F., 2010. Molecular mechanisms underlying sex change in hermaphroditic groupers. Fish Physiol. Biochem. 36, 181–193. https://doi.org/10.1007/s10695-008-9219-0

Zhou, Z.X., Zhang, B.C., Sun, L., 2014. Poly(I:C) induces antiviral immune responses in Japanese flounder (*Paralichthys olivaceus*) that require TLR3 and MDA5 and is negatively regulated by Myd88. PLoS One 9, e112918. https://doi.org/10.1371/journal.pone.0112918

Zi, M., Xu, Y., 2018. Involvement of cystatin C in immunity and apoptosis. Immunol. Lett. 196, 80–90. https://doi.org/10.1016/j.imlet.2018.01.006

ZOU, J., NEUMANN, N.F., HOLLAND, J.W., BELOSEVIC, M., CUNNINGHAM, C., SECOMBES, C.J., ROWLEY, A.F., 1999. Fish macrophages express a

cyclo-oxygenase-2 homologue after activation. Biochem. J. 340, 153–159. https://doi.org/10.1042/bj3400153

Zou, R. feng, Liu, Q. hui, 2020. Cloning and characterization of *Litopenaeus vannamei* cystainB-like in WSSV infection. Fish Shellfish Immunol. 105, 78–85. https://doi.org/10.1016/J.FSI.2020.07.008